UNIVERSITY OF TURKU

UV and Optical Properties of 27 Tidal Disruption Events and Nuclear Transients

MSc Thesis
University of Turku
Department of Physics and Astronomy
Astronomy
July 2023
BSc Louisa Arnell
Supervisors:
Docent Rubina Kotak,
Doctor Panagiotis Charalampopoulos
Examiners:
Docent Rubina Kotak
Professor Seppo Mattila

The originality of this thesis has been checked in accordance with the University of Turku quality assurance system using Turnitin Originality Check service.

UNIVERSITY OF TURKU
Department of Physics and Astronomy

Arnell, Louisa UV and Optical Properties of 27 Tidal Disruption Events and Nuclear Transients

MSc Thesis, 123 pages (+ 23 pages of appendices)
Astronomy
July 2023

I explore the UV/optical properties of 27 tidal disruption events (TDEs), TDE candidates and nuclear transients. Given their dependence on black holes, TDEs are expected to be able to probe quantities such as black hole mass and spin, as well as circumnuclear dust density. However, currently TDEs are not well-understood events, and there are only tens of confirmed TDEs. Before TDEs can be confidently implemented to probe such qualities, they must be better understood by the scientific community.

This thesis uses the properties of UV/optical TDEs such that masses of black holes and disrupted stars corresponding to TDEs can be inferred, and finds good agreement with literature values. It analyses the properties of TDEs in the sample, such as colour indices and post-peak decline to show that genuine tidal disruption events can be distinguished from interlopers, and to consider whether a TDE-origin is suitable for ambiguous events. It is essential to distinguish TDEs from non-TDE events such that we might have a larger sample at a time when there are few TDEs to study, and have a more complete understanding of their properties.

It is also key to separate total tidal disruptions from partial disruptions, as partial TDEs may often be mistaken for total TDEs. A more complete sample of partial disruptions will enable better constraining of the TDE rate. I explore the possibility of partial disruption for a number of events, and find that one event, AT2016fnl is consistent with a partial disruption.

Keywords: tidal disruption events, nuclear transients, UV, optical, black holes

Contents

1 Introduction **1**

2 Background **1**

2.1 Extragalactic Transients 1

2.2 Selection Requirements for Categorising TDEs 2

2.3 Kinematics of TDEs 3

2.4 X-Ray TDEs Vs. UV/optical TDEs 5

2.5 Spectroscopy 7

2.6 Spectral Type 8

2.7 Infrared TDEs 9

2.8 Radio TDEs 10

2.9 Relativistic TDEs 11

2.10 Neutrino-TDEs 11

2.11 Gamma Ray TDEs 12

2.12 TDEs in AGNs 12

2.13 Partial TDEs 13

2.14 Intermediate Mass Black Holes 15

2.15 Disruption Rate 15

3 Sample **16**

3.1 Sample Selection 16

3.2 Background Information on Transients in the Sample 17

3.2.1 AT2017bgt 17

3.2.2 AT2018zf 19

3.2.3 AT2018dyb 20

3.2.4 AT2018fyk 21

3.2.5 AT2018hyz 21

3.2.6 AT2019ahk 22
3.2.7 AT2019azh 22
3.2.8 AT2018cow 23
3.2.9 AT2018hco 25
3.2.10 AT2018iih 25
3.2.11 AT2019mha 25
3.2.12 AT2016fnl 26
3.2.13 AT2016ezh 26
3.2.14 AT2017eqx 28
3.2.15 AT2018zr 28
3.2.16 AT2018dyk 29
3.2.17 AT2018lna 30
3.2.18 AT2019avd 30
3.2.19 AT2019bhf 32
3.2.20 AT2019fdr 32
3.2.21 AT2019meg 34
3.2.22 AT2019lwu 34
3.2.23 AT2019pev 34
3.2.24 AT2019qiz 36
3.2.25 iPTF15af 36
3.2.26 OGLE16aaa 37
3.2.27 OGLE17aaj 38

4 Reductions **38**

4.1 Obtaining Flux Densities 38
4.2 Extinction Correction 41
4.3 Performing the Host-Subtraction 41

5 Findings **43**

5.1 Lightcurves . . . 43

5.2 Spectral Energy Distribution Fits . . . 45

5.3 Blackbody Radius, Blackbody Temperature and Bolometric Luminosity 50

5.4 Luminosity Power-Law Fits and Decay Rate . . . 51

5.5 Colour Indices . . . 62

5.6 Black Hole and Disrupted Star's Mass . . . 73

5.7 PTDE Candidates . . . 80

5.7.1 AT2016fnl . . . 83

5.7.2 AT2019qiz . . . 84

5.7.3 AT2018hyz . . . 85

5.7.4 AT2018fyk . . . 86

5.7.5 AT2016ezh . . . 86

5.7.6 AT2018zr . . . 87

5.7.7 iPTF15af . . . 88

5.7.8 AT2018dyb, AT2019ahk and AT2019azh . . . 88

5.8 Comparison with Other Transients . . . 89

6 Future Prospects **91**

7 Conclusions **94**

8 Acknowledgements **95**

1 Introduction

A star orbiting a black hole becomes 'tidally disrupted' if the tidal forces of the black hole are strong enough to overcome the star's own gravity. This scenario triggers a flare from the star as it is pulled apart. Approximately half of the star's mass is gravitationally bound to the the black hole (a fraction of which is accreted), while the other half escapes [1]. The defining features which set tidal disruption events (TDEs) apart from other transients are blue colours, little colour and temperature evolution, and a power-law post-peak luminosity decay[1]. Additionally, they are some of the brightest transient events, possibly reaching up to M=-23[2].

TDEs have been theorised since the 1970s [3] but it wasn't until 2002 when the first TDE candidates were discovered [4]. Since then, there have been $\sim$ 100 [1] TDE candidates discovered, with a current rate of $\sim$ 10 new events discovered per year [5].

This work analyses the photometric properties of 27 such UV/optical TDEs and TDE candidates, based on the Swift photometry detailed in Hinkle et al. (2021)[6]. It considers the objects' lightcurves, the evolution of their blackbody temperatures, radii and bolometric luminosities. It also explores their luminosity decline rates, colour indices and estimates the black hole (BH) and progenitor star masses associated with the TDEs.

2 Background

2.1 Extragalactic Transients

Transients are a class of objects which flare for a limited period of time (seconds to years), and then go quiet again. These flares may be in the form of electromagnetic radiation, the release of neutrinos [7], or in gravitational waves[8] . These events include supernovae, kilonovae and gamma-ray bursts among others [9]. TDEs also

have a home in this class of object[1]. Transients are discovered by time-domain surveys and follow-up observations [9] e.g. the Zwicky Transient Facility (ZTF) [10], the Panoramic Survey Telescope and Rapid Response System (Pan-STARRS) [11] and the All-Sky Automated Survey for Supernovae (ASSAS-N) [12].

When an object suddenly appears in a skymap, or a dim object suddenly brightens, it can be considered a transient. Transients are catalogued on the Transient Name Server (TNS), where they are usually given an 'AT' prefix to their name[1]. Transient type is usually classified by the object's spectra, though lightcurves can aid in classification[1].

2.2 Selection Requirements for Categorising TDEs

Some of the selection requirements for TDE candidates include being located within a certain distance from the centre of the galaxy, making a black hole-related event a possibility, based on the assumption that supermassive black holes (SMBHs) reside at the galactic centre [13]. For example in van Velzen et al. (2020) a cutoff distance of 0.3" was deployed [13]. Another requirement often implemented is that the host galaxy is quiescent, to remove active galactic nuclei (AGNs) from the sample [13]. However, this this will also remove real TDEs from the sample as TDEs should also exist in AGN galaxies. This selection-bias likely means that our confirmed subset of TDEs and our understanding of them doesn't fully capture their properties.

TDEs are intrinsically blue[1], so the sample of TDE candidates must reflect this. Where spectroscopy is available, candidates must have a blue, featureless continuum, and broad hydrogen or helium emission lines[13]. The temperatures must be high, e.g. in van Velzen et al. (2020), they required blackbody temperatures around peak light to be $> 1.2 \times 10^4$ K [13]. Temperatures must remain high over a long period of time, rather than cooling rapidly[13].

2.3 Kinematics of TDEs

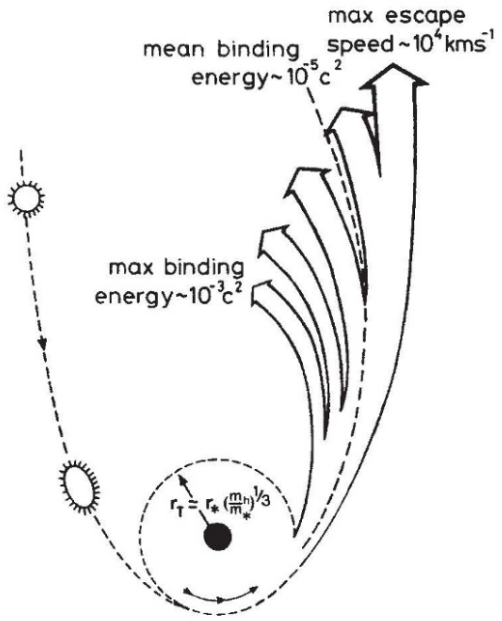

Figure 1. Diagram of a star being tidally disrupted, showing the path of the star around the black hole and different possible paths for disrupted material to follow. Figure via [14].

Tidal disruption occurs when the black hole's tidal forces outweigh the star's gravity:

$$\frac{GM_{BH}R_*}{r^3} > \frac{GM_*}{R_*^2}, \tag{1}$$

where G is the gravitational constant, M_* is the mass of the star, R_* is the radius of the star, M_{BH} is the mass of the black hole and r is the distance between them[1]. Rearranging this equation and solving for r gives us the maximum distance a star can be from a black hole to experience tidal disruption, known as the tidal disruption radius, R_T[1]. If accretion efficiency η (which is usually assumed to be ~ 1)[15] is also accounted for, this gives

$$R_T = R_*(\eta^2 \frac{M_{BH}}{M_*})^{\frac{1}{3}}[1]. \tag{2}$$

During this process approximately half of the star's matter (for a total TDE) becomes gravitationally bound to the black hole [1]. This matter circularises around the black hole, forming an accretion disk over timescales of months[1] (or contributing to it if one already exists)[14], as we can see for the inner material in Fig 1. For efficient circularisation, the bound debris must lose orbital energy e.g. by shocks, in order to form an accretion disk at a distance $\geq (2^{1/2})R_P$, where R_P is the pericentre distance [16]. When circularisation occurs promptly, it occurs on the timescale of the fallback time, t_{fb}, the time taken for the most bound debris at highly eccentric orbits to fall back to the pericentre where

$$t_{fb} = 2\pi G M_{BH}(2E)^{-3/2} = \frac{\pi}{M_*}(\frac{M_{BH}R_*^3}{2G})^{1/2}, \tag{3}$$

and E is energy distribution of the debris stream [1].

It is this process of in-falling matter which occurs during accretion which is thought to be the origin of the flare we observe during a TDE [14], though the emission mechanism may be more complicated than this which we will see in section 2.4.

Eq 4 describes the rate at which material returns to the pericenter,

$$\frac{dM}{dE}\frac{dE}{dt} = \frac{2\pi}{3}(GM_{BH})^{2/3}\frac{dM}{dE}t^{-5/3}[1]. \tag{4}$$

The theoretical basis of the $t^{-5/3}$ fallback rate is the assumption that fallback rate is the same as the rate of accretion[1]. This is to say that the accretion occurs very promptly, or the emission observed is from a process unrelated to accretion [1] e.g. debris stream collision [17](explored further in section 2.4). The fallback rate may also be impacted by the density profile of the star [18] and by relativistic effects [19]. It is also affected by the star's structure[20], the spin of both the star[21] and the black hole[19], and the impact parameter β of the star's orbit [22]. β is the strength

of the tidal encounter, and is given by

$$\beta = R_T/R_P[1]. \tag{5}$$

The spread of specific binding energy of the debris post-disruption is given by

$$\Delta\epsilon = \pm\frac{GM_*}{R_T^2}R_* = \frac{GM_*}{R_*}(\frac{M_{BH}}{M_*})^{\frac{1}{3}}, \tag{6}$$

where half of the star's mass is gravitationally bound to the black hole [1].

Of course, the flare may only be observed if the event occurs outside the black hole's Schwarzschild radius r_S where

$$r_s = \frac{2GM_{BH}}{c^2}, \tag{7}$$

and c is the speed of light in a vacuum [1]. Therefore, in order for a TDE to be visible, $R_T > r_s$ [1].

The radius of the photosphere during a TDE is typically $\sim 10^{15}$ cm, as inferred by the blackbody radius given the UV/optical luminosity[23]

2.4 X-Ray TDEs Vs. UV/optical TDEs

Since thermal emission from the accretion disk was expected to be the driving mechanism of TDEs [24], this was expected to correspond to temperature of $\sim 10^5$K [25] which would indicate that the peak emission lies in soft X-rays [14]. The first TDE searches were focused on X-rays, and this criteria indeed proved effective for discovering TDEs in soft X-rays[26].

However, TDE emission is not entirely consistent with the initial predictions. In actuality we observe multiple groups of TDEs; those which exhibit X-rays, those which exhibit UV/optical emission, those which exhibit both, and those which exhibit neither[1]. TDEs are additionally observed in other wavebands (see sections 2.8 and 2.7) and neutrinos (see section 2.10), but the main contribution of the light is usually down to X-ray and UV/optical emission. Since we have started observing

TDEs in UV/optical, nowadays these are proving a more efficient band for detecting TDEs, and now account for $\sim 2/3$ of all TDE detections[1]. This is partly due to optical telescopes being a much cheaper and more plentiful resource to employ since these can be done from ground-based observations.

TDEs which emit X-ray, optical or UV light are known as 'thermal TDEs' as they are generally well-described by blackbody distrubutions which peak at UV or soft X-ray wavelengths [27]. Out of the TDEs which are observed in both, there is significant variation as to how the ratio of X-ray to UV/optical light compares[1]. X-ray emission can be very variable, and is noted for being particularly soft[1]. Only $\sim 10\%$ of TDEs have been detected in X-rays, all of which have showed signs of having accretion disks[28][29]. This supports the assumption that X-ray emission is the result of accretion, but evidently accretion is not the only emission mechanism in TDEs. X-rays generally follow a $t^{-5/3}$ decline rate, corresponding to the fallback rate arising from accretion[30]. While the UV/optical light is often similar to the $t^{-5/3}$ mass fallback rate, there is some variation as to their luminosity decline rates, and they do not entirely align with following the mass fallback rate[31]. Even if they were to align exactly with $t^{-5/3}$, this would still be in contention with the theory since the optical light is expected to follow a $t^{-5/12}$ decline if arising from accretion and treated as a blackbody with a Rayleigh-Jeans distribution peaking in the X-ray [32].

There are two main theories as to the source of the UV/optical light; one being that optically thick material surrounding the accretion disk reprocesses X-rays as UV/optical light[33]. The other being that the source of the UV/optical light is shock emission from debris stream-stream collisions[17]. However, this stream-stream collision model is inefficient; with efficiencies of well below 50% [34]. If this were the source of the UV/optical light, we would expect the lightcurves in these bands to decline less steeply than the well-known $t^{-5/3}$ rate which we have come to expect[35]. However, since there is variation in the decline rate in UV/optical TDEs

particularly, this may be one of the causes.

In the reprocessed X-ray scenario, the reprocessing material may be in the form of debris from the TDE forming a hydrostatic envelope around the black hole[36], or outflows from the TDE[37][38]. The temperatures of UV/optical TDEs are an order of 1-2 lower than those of X-ray TDEs [39], and their temperatures remain approximately the same over a period of months [40]. It has been suggested that this lower temperature is due to a reprocessing layer at 10-100R_T [40]It is expected that at later epochs, if TDEs exhibit emission under this regime, observations will be more uniform after the reprocessing layer has become transparent, allowing for observation of the disk directly[41]. However at early times there will be more variability among TDEs. This explanation has its problems too; if the X-ray emission arises from in-falling matter during accretion, the accretion disk must form promptly[16], however simulations show that rapid circularisation is not always the case, and in some cases can be very inefficient [42]. Additionally, the UV/optical emission is not particularly variable, unlike the X-ray emission[1]. If the UV/optical emission were a result of reprocessed X-rays, we would expect the variability of the X-rays to be reflected in the reprocessed lightcurve. The UV/optical emission mechanism, as well as the variability in X-ray to UV/optical ratio remain two of the biggest questions in TDE-astrophysics to date.

2.5 Spectroscopy

TDE spectra are dominated by broad emission lines (corresponding to speeds 3 - 13 x 10^4 km s^{-1}), which may be a result of electron scattering[1]. These broad lines become narrower over time[1]. This is the opposite to AGNs[43], and may be a viewing angle effect[44].

The underlying continuum is hot and blue [45]. Some TDE spectra have boxy shaped line profiles, or blue-shifted features[1]. Some exhibit double peaks e.g. of the

H-α emission line, which suggests an elliptically-shaped accretion disk[46]. TDEs with smaller blackbody radii, higher blackbody temperatures and lower optical luminosities tend to exhibit Bowen fluorescence [47][23]. Additionally, some TDEs exhibit Balmer lines, the broadest of which have a width of $> 10^4$ km s^{-1} [40].

Sometimes, TDE spectra reflect lines which are also seen in the host galaxy, indicating that they are not only probing the bound debris from the tidal event, but also the galaxy's interstellar medium (ISM) and circumnuclear medium[40]. Because of this, TDEs may be used as tools to observe these media[40], but care should be taken not to conflate host-derived emission lines with those originating from the TDE's material.

2.6 Spectral Type

TDEs can be classed into three different spectral types under the most basic classification system[45]. The first is TDE-H which are dominated by broad Hα and Hβ emission lines[45]. The next is TDE-H+He which also features these lines, as well as other emission lines around He II λ 4686 [45]. Many of these TDE-H+He also feature N III λ4640 N III λ4100 emission lines, and some O III λ3760 emission lines[23]. The much rarer class TDE-He does not feature any hydrogen emission lines, only the He II λ4686 line[23].

Depending on classification scheme, TDEs which have Bowen fluorescence features may be categorised as TDE-Bowen[23], or one of the above spectral types if following the more basic three-category system. TDEs which exhibit Bowen fluorescence have longer rise times, smaller blackbody radii and higher rates of disruption[23].The spectral type is dependent on the chemical makeup of the disrupted star [48], and may also be influenced by ionised debris [49], the effects of radiative transfer [50] or the reprocessing of x-rays [51].

There have been a handful of TDEs which have been observed to change spec-

tral type e.g. AT2017eqx (see section 3.2.14 for more detail on this TDE) which transitioned from TDE-H+He to TDE-H over a time period of about 100 days[52]. Transitions in spectral class may be due to a contracting atmosphere resulting in hydrogen emission suppression[52]. In the case of AT2017eqx, this may have been combined with wind streams emitted from the poles, which were not visible until later times[52]. This would imply that viewing angle also plays a part in spectral type[52].

2.7 Infrared TDEs

Infrared (IR) radiation has been observed in conjunction with TDEs in the form of dust echos[53]. These occur when a layer of dust absorbs UV/optical light from the TDE flare, which heats the dust to sublimation temperature at around 1500K[54], and re-emits the light as a mid-IR (MIR) flare[55][53]. The MIR flare mirrors that of the UV/optical flare, but less luminous, with a time delay owing to the time taken for the UV/optical light to travel to the location of the dust. By inferring the radius of the dust cloud from the time delay, and measuring the temperature of the echo, the bolometric luminosity of the TDE can be measured independently[53].

These dust echos allow us to probe the environment around the TDE[53]. The fraction of energy which has been re-radiated, f_{dust} is only ~ 0.01 for TDE dust echoes, significantly smaller than those of 'changing-look' AGN (CLAGN) dust echoes[53], due to the presence of dust tori in the latter[56]. CLAGN are a class of event in which broad UV/optical emission lines appear or disappear in the spectra, resulting in a transition from either a Type I AGN to a Type II, or a Type II to a Type I[57]. This difference in f_{dust} may allow for classification of CLAGN vs TDEs in cases which exhibit dust echoes[56].

Photoionisation by TDEs may cause the fading of narrow [FeVII] and [Fe X] - [Fe XIV] emission lines, known as 'extreme coronal line emitters' (ECLEs)[58].

Fading MIR emission has been observed along with these fading lines[59]. ECLEs may provide us with another way to study the effects that TDEs have on their environment [1].

2.8 Radio TDEs

Observing TDEs in radio can reveal outflows and jets[27]. In some cases radio flares last $\sim$ a year, and peak at $\sim 10^{38}$ erg/s[27]. Radio emissions in TDEs are produced by synchrotron emission by electrons accelerated to relativistic velocities, as a result of outflows driving shockwaves through the circumstellar medium (CSM)[27].

Most TDEs are radio-quiet with radio observations often only obtaining an upper limit, and for some TDEs, jets can be ruled out[27]. However, mildly relativistic jets have now been firmly observed in a handful of TDEs[27]. A few percent of TDEs exhibit luminous radio emission and even fewer exhibit strong jets[27]. This difference is likely a result of radio-loud TDEs launching jets on-axis, while radio-quiet TDEs will either launch jets off-axis or not at all[27]. Factors such as disruption geometry, magnetic field strength and circumnuclear density may all play a part in these differences[60][27]. It also seems that TDEs at higher redshifts (z$\sim$1) are jetted, while TDEs at lower redshifts (z$\sim$ 0.1) are thermal TDEs, most of which do not have radio detections[27]. However, currently the TDE rate's dependence on redshift is unknown[61].

Since Very Long Baseline Interferometry radio observations have such a high resolution, the structures of jets and outflows of nearby TDEs can be well-resolved[62][55][27]. This allows for the studying of the formation and evolution of such jets and outflows. Additionally, radio TDEs can be used to probe the cicumnuclear medium via interactions between it and the outflow[27]. Radio-TDEs give us the unique opportunity to infer ambient density of the cicumnuclear medium[27]. Radio emission can also be produced independently by other AGN activity, or star formation in the galactic

nucleus, so this must be taken into account when observing radio-TDEs[27].

2.9 Relativistic TDEs

At early times, the Eddington accretion rate may be exceeded by the fallback rate and accretion rate for TDEs corresponding to BHs $\lesssim 10^7$ $M_\odot$[16][63]. As a result of the super-Eddington accretion, the debris matter cannot cool efficiently. This may lead to the formation of jets[60] or winds[64]. The class of 'relativistic TDEs' have such properties, where the jet is launched along our line of sight, much like the blazar class of AGNs[1]. Such relativistic jets only occur in $\sim 1\%$ of TDEs[65]. These events are radio-bright[1], and in a few cases have been observed in gamma-rays[66]. The X-ray lightcurves of relativistic TDEs are observed to follow those of the radio[1], consistent with the assumption that the X-ray emission in such cases mostly stems from the jet rather than the disk[66]. It is thought that the X-ray emission from the jet may also be reprocessed as UV/optical light, enabling relativistic TDEs to be observed in more wavebands[65].

2.10 Neutrino-TDEs

There is only one confirmed TDE with a likely neutrino detection, AT2019dsg[67]. The neutrino was found to have a 99.8% likelihood of originating fromAT2019dsg[67]. There are also an additional two TDE candidates which are also the likely source of a neutrino detection each (AT2019fdr [68], discussed more in section 3.2.20 and AT2019aalc[53]). AT2019aalc and AT2019fdr both reside in AGN galaxies [69] [68], which are considered prime candidates for producing high-energy neutrinos [70]. TDEs themselves have also been suggested as sources of neutrinos e.g. by internal shocks in relativistic jets [71] (analogous to blazar neutrino production [7]), from a super-Eddington magnetically arrested accretion disk, or radiatively inefficient flow of accretion [70].

All three of these events feature strong dust echos [69], indicating a large volume of matter in their surroundings, and therefore a high star formation rate (SFR)[68]. This high SFR is likely linked to the production of high-energy neutrinos[68].

2.11 Gamma Ray TDEs

There have been a few TDEs observed to emit gamma rays from jets, such as Swift J1112.2-8238 which was a variable gamma ray source, much longer-lived than typical gamma ray bursts[66]. The production of neutrinos is expected to accompany gamma-ray production, since they are both produced by pions[70]. So gamma-ray observations may be useful in confirming a TDE-origin for neutrinos in the future[69]. However, gamma-rays were not observed in any of these three events. This is likely due to the large optical depth of the super-Eddington magnetically arrested accretion disk or highly efficient pair production of the radiatively inefficient accretion flows[70].

2.12 TDEs in AGNs

AGNs are galaxies where the central black hole is strongly accreting. As mentioned in section 2.2 AGN galaxies are often ruled out when searching for TDEs. This is because it is difficult to detect when flares occur against the bright backdrop of the active galaxy[72]. An additional issue is that AGN exhibit variability in brightness (usually over years), so distinguishing between a transient and AGN variability can be problematic[72]. However, this does not mean that TDEs don't occur in AGNs. In fact, TDE may be more common in active galaxies since TDEs may favour black holes with steady accretion [3]. Additionally, new stars will form around the black hole at a faster rate due to the molecular clouds, offering up more TDE victims to the black hole[72][55]. Blanchard et al. (2017) found that AGN-TDEs are able to reach the Eddington luminosity associated with the accompanying

black hole[72]. This more efficient luminosity level is likely due to the additional interactions with the accretion disk[72]. This work's sample includes an AGN-TDE AT2016ezh, more detail on which can be found in section 3.2.13, as well as several AGN-TDE candidates.

2.13 Partial TDEs

A star may be partially disrupted, as opposed to totally disrupted if the star orbits close to the black hole, but at a pericentre distance of greater than the tidal disruption radius[73]. This causes a smaller impact parameter β, of $\lesssim 1$ [31]. In these cases, a portion of the star survives the encounter, while some material becomes gravitationally bound to the black hole, though this is a lower bound fraction than in total tidal disruption events [73] (TTDEs, also sometimes referred to in the literature as full TDEs, FTDEs [74]). The surviving stellar core post-disruption is left hotter than other stars of the same mass [75]. Partial TDEs (PTDEs) are expected to exhibit lower peak luminosities than TTDEs, due to less material circularising [76]. Since β is lower, which impacts the energy distribution of the debris, and therefore the fallback rate [22], PTDEs have steeper decline rates of $\sim t^{-9/4}$[75] In some cases, in the first few months after peak, the decline rate may be as steep as t^{-4} [31]. Interestingly, in the case of the most probable observed PTDE, ASASSN-14ko, its slope followed a meagre $t^{-1.33}$ decline rate[77]. The key here was that this was significantly steeper than other TDEs of similar luminosities[77], since less luminous TDEs tend to decay less steeply than their brighter counterparts[78]

PTDEs do not exhibit outflows during circularization, unlike many TTDEs [76]. This is a result of the lower mass of the debris stream allowing for more efficient radiative diffusuion[76]. This makes them ideal candidates for studying circularisation, and the formation of an accretion disk around a black hole, since it is a cleaner process than with TTDES[76].

The lightcurves of PTDEs are expected to show double peaks or plateaus as two different processes dominate at different times[76]. According to Chen et al. (2021)'s modelling, the first dominant process is circularisation (on timescales of $\sim 10^2$ - 10^3 days), and the second is accretion (on timescales of $\sim 10^3$ - 10^4 days), corresponding to the formation of the accretion disk[76].

In PTDEs, the temperature rises as the lightcurve rises, and then falls as luminosity begins to fall[76]. Temperature is expected to increases again, as the accretion disk forms, and then continues to gradually fall[76]. The effective temperatures lie in the rage of 10^4 - 10^6 K, and are mildly dependant of the masses of the black hole and star, and on the UV peak luminosity[76].

Since the star escapes being completely destroyed, they may become partially disrupted again at a later time, a concept dubbed a 'repeated PTDE'[75]. This is possible only if conditions such as the star's orbit, mass and radius remain similar post-disruption [73]. There are a number of TDE candidates which have undergone rebrightening, the cause for which is not well understood, though could be consistent with repeated PTDEs[73], or the two-phase emission of a singular partial tidal disruption event. PTDE candidates among the known TDE population are rare; there is only one probable repeating PTDE, ASASSN-14ko [77], though there are also a handful of low-luminosity, rapid decline events which fit the profile of PTDEs[73]. Despite this, PTDEs are predicted to be more common than TTDEs[73]. This is in part due to a larger cross-sectional area in which partial disruption is able to occur [79], and in part as they may be partially disrupted multiple times [74]. The lack of PTDE candidates is somewhat due to their lower luminosities, making detection less likely[75][73]. It is also likely due to some PTDEs being conflated with TTDEs, as distinguishing between the two based on their luminosity decline rate is not always definitive[73].

2.14 Intermediate Mass Black Holes

The existence of a TDE comes hand in hand with the presence of a black hole. Therefore, TDEs can be indicators of nearby dormant black holes. This may be particularly pertinent in the case of intermediate mass black holes (IMBHs), which have only recently been observed [8]. Smaller mass stars can only be tidally disrupted by smaller mass black holes[1]. An intermediate mass black hole (10^2-10^5 $M_\odot$) [8] would only be able to tidally disrupt a white dwarf star, and so white dwarf TDEs are paramount to look out for as they could be the key to discovering the corresponding IMBH[1]. However, there is some overlap between the lower mass SMBH which can also tidally disrupt white dwarfs[1], so a white dwarf TDE doesn't automatically correspond to an IMBH. An IMBH-TDE poses detection challenges since lower mass black holes are expected to correspond to lower luminosity flares[80].

2.15 Disruption Rate

The rate of tidal disruption is dependent on black hole mass, nuclear density of the star [81] and the orbital distribution citation[82]. Numerical calculations put the rate between 10^{-5} - 10^{-4} year^{-1} galaxy^{-1} [4] [83] [81]for TTDEs. Meanwhile for PTDEs, the theoretical rate is an order of $\sim$ 1 - 10 greater [73]. In fact, since it's entirely possible that some of the PTDE populations have been misclassified as TTDEs, this would put the PTDE rate as even greater[73].

The predicted rate is inversely proportional to black hole mass[81]. TDEs are thought to be more common in smaller galaxies[73] and the rate greatest in nucleated dwarf galaxies which have black holes [81]. Meanwhile observed rates are greater in hosts with larger nuclear stellar density [84], and hosts which reside in the 'green valley' [23] (galaxies which have colours between red and blue).

Optical TDEs have a preference for E + A type galaxies, a subtype of post-starbust galaxies with spectra which seem to be a composite of an old elliptical

galaxy and a galaxy with young A-type stars [45]. More broadly speaking, they prefer quiescent galaxies with strong Balmer lines, and in 2016 75% of the canonical TDE population resided in one of these galaxies, despite only making up $\sim 2\%$ of the galactic population [85]. While this connection does impact TDE searches, and therefore lead to new TDE discoveries, this is not purely an observational bias [84]. The preference for these galaxy types may in part be due to galaxy mergers, possibly resulting in a binary SMBH, and therefore increasing the chances of a disruption, or changing existing stars' orbits, causing them to be diverted toward the black hole[85]. However, based on galactic symmetry, TDE hosts do not show signs of mergers [84]. The A-type stars themselves may be contributing to the increased rates; if they are highly concentrated towards the core, this will increase the number of tidal disruptions[85]. Or the increased probability for a TDE may occur once the stars evolve into giants, which are more likely to be disrupted by a SMBH[85].

3 Sample

3.1 Sample Selection

The sample used in this thesis originates from the sample detailed in Hinkle et al. (2021), which published corrected photometry for 37 nuclear transients and one non-nuclear transient[6]. However, not all of these 38 transients have been incorporated into the sample used in this work. One of the key components of this thesis is comparing different objects using their peak epoch as the zero point, and therefore finding this date was important. Of the 38 objects provided in the Hinkle et al. (2021) publication[6], 16 of them had their peak epochs published in the literature. Of the 22 remaining, all but two of them had last non detection dates reported in the Transient Name Server. The midpoint between the last non detection date and the discovery date was used as an estimate of peak time for those objects without

a known peak date. A liberal cutoff of 14 days between discovery date and last non detection date removed a further eight objects from the sample. AT2018lni was also removed from the sample despite having a well constrained peak time, due to the fact that there were only two magnitude measurements in the Hinkle et al. (2021) data tables (both in UVM2)[6], meaning no science could be done with it. This left a total of 27 objects in the sample, as detailed in Table I. The decision to include events without firm TDE classifications in the sample was made, so as to analyse the possibility of TDE-origin for ambiguous events, and have non-TDEs for comparison purposes.

3.2 Background Information on Transients in the Sample

3.2.1 AT2017bgt

AT2017bgt was discovered on the 21st of February 2017 in an early type galaxy [100]. The galaxy brightened by $\sim 50\%$ over a period of two months, with most of this increase being in the UV[101].

The object has several features which would mark it as AGN activity; its X-ray spectral energy distribution is consistent with an unobscured AGN [101] and its spectra contains strong single peaked Balmer emission lines, and weak, narrow forbidden [O III] $\lambda\lambda$4959, 5007 and [N II] $\lambda\lambda$6548, 6584 lines[101]. However there are some properties which are not consistent with an unobsured AGN; its UV to optical and monochromatic UV to X-ray luminosity ratios are much larger than expected[101][102][103], and the presence of a strong O III λ3133 emission line and a double peaked feature at 4680Å are not observed in AGNs[101]. The double peaked feature may be a 'Wolf-Rayet' emission line from N III λ4640 which has been observed in some TDE spectra [101][104] [105] [106], hence the inclusion of this event as a possible TDE. However, its X-ray evolution is quite flat[101], meanwhile TDEs exhibit high X-ray variability. Additionally, the high UV flux, and spectral features

Table I. Table of transients included in sample. The symbol * indicates that the peak time has been inferred based on the last non-detection date and the discovery date. Detection name is provided in the first column for clarity, but going forwards, only the TNS names will be used to refer to the transients where applicable.

Detection Name	TNS Name	Classification	Peak Time (MJD)
ASASSN-17cv	AT2017bgt	AGN	57802*
ASASSN-18el	AT2018zf	Ambiguous	58210 [86]
ASASSN-18pg	AT2018dyb	TDE	58341 [87]
ASASSN-18ul	AT2018fyk	TDE	58364*
ASASSN-18zj	AT2018hyz	TDE	58429[88]
ASASSN-19bt	AT2019ahk	TDE	58547 [89]
ASASSN-19dj	AT2019azh	TDE	58562[90]
ATLAS18qqn	AT2018cow	FBOT	58287[91]
ATLAS18way	AT2018hco	TDE	58395*
ATLAS18yzs	AT2018iih	TDE	58427*
ATLAS19qqu	AT2019mha	TDE	58693*
iPTF16fnl	AT2016fnl	TDE	57632[26]
PS16dtm	AT2016ezh	TDE	57657[92]
PS17dhz	AT2017eqx	TDE	57922[52]
PS18kh	AT2018zr	TDE	58193[93]
ZTF18aajupnt	AT2018dyk	LINER	58268*
ZTF19aabbnzo	AT2018lna	TDE	58476*
ZTF19aaiqmgl	AT2019avd	Ambiguous	58517*
ZTF19aakswrb	AT2019bhf	TDE	58527*
ZTF19aatubsj	AT2019fdr	Ambiguous	58704[94]
ZTF19abhhjcc	AT2019meg	TDE	58688*
ZTF19abidbya	AT2019lwu	TDE	58685*
ZTF19abvgxrq	AT2019pev	AGN	58755[95]
ZTF19abzrhgq	AT2019qiz	TDE	58764[96]
iPTF15af	-	TDE	57077[97]
OGLE16aaa	-	TDE	57403[98]
OGLE17aaj	-	AGN	57757[99]

undergo few changes over a 14 month period[101], a period greater than the lifespan of most TDEs. This indicates that AT2017bgt is a more long-term high-accretion event, and Trakhtenbrot et al. (2019) classify it as a new class of flare from an accreting supermassive black hole[101].

3.2.2 AT2018zf

The event AT2018zf was discovered on the 23rd of December 2017 [107] and initially classified as a Type II narrow-line active galactic nucleus, one of only a few 'true Type II' AGNs which did not exhibit broad emission lines or line of sight obscuration[108]. Follow-up spectroscopy showed that the object had had a large increase in UV/optical emission, resulting in a very blue continuum with no features, resembling that of an AGN[108]. However, further follow-up monitoring revealed the presence of strong Balmer lines which onset 1-3 months after the rise in optical light[108]. This would mark the event as one of a small number of 'changing-look' AGNs. The lag between the UV/optical brightening and the Balmer lines suggest that the event was not caused by a change in the line of sight obscuration[108]. Rather, the UV/optical component was a result of accretion of material into the supermassive black hole and the delayed onset of Balmer lines a result of the UV/optical light later being reprocessed by the broad line region (BLR) gas[108].

This event's accretion-driven nature is what gives it its place as a TDE candidate. There have been a handful of cases previously where TDEs have been considered a possibility in driving a 'changing-look' AGN [109] AT2018zf does indeed have some features which are consistent with a TDE; the lightcurve follows a $t^{-5/3}$ power law, which is the smoking gun of tidal disruption events[108]. The mass of the SMBH associated with the event is $\sim$ 2 x 10^7 $M_\odot$, which is consistent with other SMBH masses observed in relation to TDEs, though fairly high[108]. Additionally, the X-rays are very soft which is a sign of a TDE [110].

However, the X-ray rebrightening is not indicative of a TDE [110]. Nor is the absence of the strong, broad He II λ4686 emission line which has previously been observed in TDEs within a few months of discovery[108]. Hinkle et al. (2022) note the stochastic variability of the event, which is more pronounced at late-times[86]. They point out that while this is consistant with an AGN explanation, a TDE explanation is unlikely as they do not tend to exhibit this kind of variability [86].

Ricci et al. (2020) believe that a TDE could be the driving mechanism of this event[110], meanwhile Trakhtenbrot et al. (2019) and Hinkle et al. (2022) are not convinced[108] [86].

3.2.3 AT2018dyb

On the 11th of July 2018 the All-Sky Automated Survey for Supernovae (ASAS-SN)[12] discovered AT2018dyb [111] and it was classified as a TDE on the 18th of July based on its spectrum [112]. Its peak luminosity was $\sim$ 2.4 x 10^{44} erg/s, making it one of the brightest known TDEs[113]. It occurred at a distance of 78.6 Mpc, also making it one of the closest TDEs[113]. Its spectra shows strong Bowen fluorescence of N and O, which would be a hallmark of extreme ultra violet (EUV) emission and reprocessed X-rays, and thereby supports the X-ray reprocessing school of thought for the origin of the UV/optical light[87]. The spectra additionally shows the presence of Balmer lines[113]. AT2018dyb did not have any X-ray emission, nor radio jets[113]. The UV/optical lightcurve has a luminosity decline power-law index α of close to the expected value for a TDE of 5/3, however in later epochs this index is a little steeper than the luminosities observed[113]. Though it should be noted that theory predicts that the emission mechanisms in TDEs may change over time, transitioning from fallback dominated to disk-dominated emission[32] [114], causing the power-law luminosity index to reduce.

3.2.4 AT2018fyk

The ASAS-SN survey discovered AT2018fyk on the 8th of September 2018, with the last non-detection being 10 days prior[51]. Its host galaxy is LCRS B224721.6-450748 and it resided at approximately 0.85 arcsec from the galactic nucleus[51]. Its spectrum was typical of a TDE; it had a blue continuum with no features besides broad H and He lines, though it may also have featured O III λ3444 or Fe II ($\lambda\lambda$3449,3499) lines[51]. However, at $\sim$ 40 days post-peak the UV/optical lightcurve plateaued, and did not follow the typical TDE decline rate of $t^{-5/3}$ [51]. At the same time, the X-ray lightcurve plateaued and narrow emission lines appeared, such as high-ionization O III, low-ionization Fe II and low excitation He I[51]. After $\sim$ 50 days, the UV/opical lightcurve continued declining and the X-ray lightcurve continued brightnening[51]. These three occurrences coinciding would strongly imply that they are produced by the same mechanism, and that in this case the UV/optical light is reprocessed X-rays[51]. The presence of Fe II emission lines has also been observed in the TDE ASASSN–15oi which indicated that there is a class of Fe rich TDEs[51]. Fe II emission lines may be an indication of a forming compact accretion disk, further supporting the X-ray reprocessing theory[51].

Roughly two years after this event's peak, it experienced a rebrightening[115]. This has been suggested to be a repeating PTDE, or as a result of inner disk instabilities, or a SMBH binary [115]. These possibilities are explored more in section 5.7.4

3.2.5 AT2018hyz

AT2018hyz was first discovered on the 6th of November 2018 by ASAS-SN[29]. Its host galaxy 2MASS J10065085+0141342 lies at a redshift $z = 0.0457$. It had bright optical emission, and dim X-ray emission [29] The transient was classified as a TDE on the basis of its spectrum which had a blue continuum and featured

broad emission lines of H-α, and possibly H-β and He I λ5876 [116] . Follow-up spectroscopy revealed that the H-α emission line evolved into a double-peaked line profile[29].

At 50 days after the initial peak, there was a bump in the UV which is consistent with the lightcurve profile of a PTDE[88]. Indeed, modelling of the lightcurve implied a PTDE origin since the impact parameter β was found to be 0.6[88].

3.2.6 AT2019ahk

ASAS-SN discovered the TDE AT2019ahk on the 29th of January 2019[89]. It was the first TDE to be observed by TESS[89]. Due to its location in TESS' continuous viewing zone, observations of the event were made at 30 minute intervals, meaning the pre-peak observations are the most complete of all known TDEs[89]. It is also one of the closest observed TDEs[89]. Its host galaxy 2MASX J07001137-6602251 may be a shocked post-starburst galaxy, similar to an E + A galaxy, but younger and with more dust obscuration[89]. Its rise to peak lasted 41 days, and at 32 days pre-peak there was a luminosity and temperature bump which lasted 12-14 days[89]. Similar occurrences have not been observed in other TDEs, but no other TDE has such thorough pre-peak data[89]. The TDE has weak X-ray emission which is not as soft as in other TDEs, which could be caused by a jet, but which softens post-peak[89]. It has a blue continuum, a key feature of a TDE, with narrow emission lines and apparently no broad features[89]. Most TDEs exhibit broad H and He emission lines, but TDE spectra without these features are not unheard of at pre-peak epochs[117].

3.2.7 AT2019azh

The TDE AT2019azh was discovered on the 22nd of February 2019 by ASAS-SN in the E + A galaxy KUG 0810+227[90]. It possessed a featureless, blue continuum, marking it as a possible TDE[90]. Both UV/optical and X-ray light were observed

from this event[90]. Like AT2019ahk, the X-rays are harder at earlier epochs but later soften[90]. The X-ray lightcurve experiences a rebrightening at $\sim$ 200 days post-peak by 30-100 times[90]. Meanwhile the UV/optical continues dimming as expected[90]. This indicated that the X-rays and UV/optical emission are not produced by the same mechanism[90]. The X-ray rebrightening is an indication of an increase in accretion rate, making this the second case of a TDE showing the onset of late-time accretion[90].

3.2.8 AT2018cow

A very luminous transient AT2018cow was first detected by ATLAS on the 16th of June 2018 in a spiral arm of the dwarf galaxy CGCG 137-068[91][118]. The last non-detection date has been constrained to 1.3 days prior, meaning that the transient increased brightness by a magnitude of 4.2 in this time[91][118]. It peaked at $M_r \sim$ -19.9 with a rise time of only $\sim$ 2.5 days, making the rise time faster and the peak luminosity brighter than almost any other supernova[118]. The exceptions to this are some Type IIn and superluminous supernovae[118]. However, these supernovae exhibit long rise and decay times, meanwhile this transient experienced exceptionally fast timings; it faded to half its peak luminosity in around 4 days[118]. When supernovae exhibit early, luminous peaks, powered by shock-heating, the lightcurves then plateau or a second peak occurs, however AT2018cow's luminosity continued to rapidly decay[118]. The transient was hot (with a characteristic temperature of 17,000K) and blue[91], which is seen in the early phases of supernovae, however it was remarkably blue even for an early stage supernova[118]. It retained these properties for a much longer period than supernovae do, though it did slowly lose its blueness[118].

The spectrum of the event was initially featureless, with only a hot, blue continuum[118]. Then the spectra went on to show several interesting features. Four days post-discovery, a bright radio afterglow was seen [119][120] [121], in conjunction with a

very broad absorption line resembling an Fe II line, which can be seen in Ic-BL supernovae[118][122][123]. However this feature disappeared within four days[124], which is not how Type Ic-BL supernovae develop[118]. Then, weak and somewhat broad emission lines appeared, most likely H and He lines, including Balmer lines[118]. The spectrum continued to get bluer, causing wedge-shaped line profiles[118]. At later times He I λ7065, Ca II $\lambda\lambda$7291,7324 and what may have been O I $\lambda\lambda$6300, 6363 lines appeared[118]. The spectral evolution of AT2018cow is not like any seen in other transients[118].

The spectrum more closely resembles that of a TDE; it's populated by H and He emission lines[118]. It has several other features which are in line with those observed in TDEs; the persistent high temperatures and blue colour are typical of TDEs[118]. The bolometric lightcurve follows a powerlaw decline, albeit steeper than the expected $t^{-5/3}$[118]. However the rise time and decay timescales are much faster than even the shortest observed in TDEs[118]. Its location in a spiral arm would seem to disfavour the tidal disruption explanation for the transient as all TDEs discovered thus far have been nuclear transients[118]. However, this doesn't rule out the possibility of a TDE entirely. If the black hole mass were to correspond to that of an IMBH, it could reside outside the galactic centre, with the IMBH originating perhaps from a globular cluster[118]. Additionally, this would explain the short timescales, as there is both observational and theoretical evidence that lower mass black holes cause shorter TDE decay times, though there doesn't seem to be a correlation between black hole mass and rise time, despite theoretical predictions[1][118]. However, the TDE explanation does not solve all the problems with AT2018cow. The peak bolometric luminosity was $\sim 4 \times 10^{44}$ erg, an order of 2 greater than the Eddington luminosity corresponding to an IMBH of 10^{42} $M_{\odot}$[118]. TDEs are generally not expected to supersede the Eddington luminosity[125], however there are two ways in which this might be possible[118]. The first is via anisotropic radiation, which could be a result of jets, though the optical radiation is strongly thermal and

does not support this[118]. The second is heating by other methods than accretion, such as via circularisation[118].

AT2018cow is now considered as part of the class of fast blue optical transients (FBOTs)[126][127]. These are transients which, like AT2018cow, have blue colours of g-r$\leq$0.2, and decay rapidly, reaching half the peak luminosity within 12 days[128]. There have now been $\sim$ 100 FBOTs identified[126], however only a handful of them have similar properties to AT2018cow, and its thought that such transients only make up $\leq$ 0.1% of the core collapse SN rate[129].

3.2.9 AT2018hco

AT2018hco was an ATLAS discovery made on the 4th October 2018 [130]. Its constant, blue colour (g-r $\sim$ -0.1) indicated it as a TDE candidate[130]. It was a UV-bright event, and was located within 0.2 arcsec of the galactic centre[130]. The TDE classification was confirmed by spectroscopic observations which showed featureless blue continuum[130]. Followup revealed spectroscopic evolution; a strong, broad H α emission line had emerged, as had a strong, broad He I λ5876 emission line [130] and a weak HeII λ4685 emission line[131]. Based on its much stronger H component, it was classified as a TDE-H [23].

3.2.10 AT2018iih

The transient AT2018iih was discovered by ATLAS on 9th November 2018 [132] and classified as a TDE-He [23], making it one of only a handful of TDEs to fit into this spectral class.

3.2.11 AT2019mha

AT2019mha was discovered on 30th July 2019 by ATLAS [133] and was subsequently classified as a TDE-H [23].

3.2.12 AT2016fnl

The TDE AT2016fnl was discovered by the intermediate Palomar Transient Factory (iPTF) survey [26] at the centre of a post-starburst E+A spindle galaxy[26]. The position and galaxy type are typical of TDEs, and its blue colour (g-R =-0.28)[26] and spectrum containing broad He II and H α emission lines[26] confirmed its nature as a TDE. Spectroscopy also revealed a He I emission line at λ6678 and an Hβ emission line [26]. It is one of the closest UV/optical TDEs at only 66.6 Mpc away[26].

With a peak bolometric luminosity of (1.0 $\pm$ 0.15) x 10^{43} erg/s[26], it was, at the time, the faintest known TDE[26]. Its decay timescale was also the shortest at the time[26], and it decayed according to an exponential decay rate[26]. These may be explained by the Blagorodnova at al. (2017)'s low black hole mass of $\sim$ 2 x 10^6 $M_\odot$ (obtained via the M-σ relation)[26] and low disrupted star mass of $\sim$ 0.03 $M_\odot$ (obtained by fitting the black hole mass to Guillochon & Ramirez-Ruiz (2013)'s lightcurves [31])[26]. It is expected that fallback timescale scales to black hole mass [1].

3.2.13 AT2016ezh

The Pan-STARRS Survey for Transients (PSST) first discovered AT2016ezh on the 12th of August 2016 [134]. It lay in the nucleus of a narrow-line Seyfert 1 (NLSy1) galaxy [72] The interesting feature of AT2016ezh is its multi-peaked nature; there are two clear peaks, accompanied by a $\sim$ 100 day plateau, and a third, smaller rebrightening[72].

The event was initially classified as a Type II supernova based on Hydrogen Balmer lines in its spectra [135]. This classification proved contentious; it was later classified as a Type IIn superluminous supernova (SLSN) based on its bright absolute magnitude[136], which peaked at -21.7 [72]. However, Blanchard et al.

(2017) disagree with this classification for a number of reasons[72]. First, there is little spectral evolution which is not expected from supernovae as they continue to cool[72]. The spectra consists of strong broad Fe II emission lines, which can be seen in supernovae but are more similar to the spectrum of the narrow-line Seyfert 1 galaxy itself[72]. In fact, the event seems to be connected to the galactic nucleus; AT2016ezh's peak luminosity was on the order of the Eddington luminosity of the galaxy's black hole (with a mass of $\sim 10^6$ $M_\odot$)[72]. Additionally, during the transient's lifetime, the host galaxy's X-ray emission decreased by an order of 1, indicating a link between the two objects[72].

AGN variability was also considered as a potential cause of the brightening[72]. In 'changing-look' AGNs the properties of the AGNs change dramatically over a period of years [57] or more rarely, months [108]. Emission lines appear or disappear and the continuum level may increase or decrease by an order of magnitude [12] [57]. CLAGNs may be explained by obscuration by dust clouds or changes in accretion rate [137]. However, given that the rise time of AT2016ezh is only ~ 50 days, this is much too fast for even the most rapid known 'changing-look' AGNs[72]. Nor does this scenario account for the decrease in the host's X-ray emission[72].

This, combined with the blue underlying continuum of the spectra, high constant temperature, and little colour evolution (except reddening of the UVW2-U colour), caused Blanchard et al. (2017) to classify the event as a TDE[72]. This could explain the observed decrease in galactic X-ray emission as it would be obscured be the debris stream[72]. The TDE's debris stream interacting with the AGN's accretion disk could excite the AGN's broad line region, causing the similarity between the transient's observed spectrum and that of the narrow-line Seyfert 1 galaxy that it resides in[72]. A TDE-scenario would also account for the rapid rise time compared to CLAGNs[72]. Blanchard et al. (2017) fitted AT2016ezh's lightcurve using the programme `TDEFit`[49], and found that the rise and plateau of AT2016ezh was able to be reproduced[72]. They also found that the plateau was likely a result of viscous

time delay, though may also be contributed to by the maximum luminosity being the Eddington luminosity[72].

3.2.14 AT2017eqx

PanSTARRS Survey for Transients [138] discovered the TDE AT2017eqx on 7th June 2017 [52]. It was located 0.06 ± 0.08 arcsec from the galactic centre[52]. The host galaxy was of the Balmer-strong absorption type[52], which is a typical environment for a TDE to reside [45]. Its blackbody temperature of $\sim$ 25,000K was indicative of a TDE, as was its peak blackbody luminosity of $\sim 10^{44}$ ergs/s[52]. Modelling showed that the event was consistent with total tidal disruption of a near-solar-mass star[52].

Initial spectroscopy showed a blue continuum with broad He II and H I emission lines, which had velocities of $\sim$ 0 km s^{-1}[52]. However, within 100 days, the He I lines had vanished from the spectra, and the He II lines had become blueshifted by $\geq$ 5000 km s^{-1}[52]. This is the first TDE in which both a stark HeII/Hα evolution, and blueshifting are observed[52]. No radio or X-ray emissions were detected, which ruled out a jetted-TDE explanation[52]. The evolution may be a result of slow atmospheric contraction and polar wind streams only becoming visible at later times. This would indicate that line of sight is a key factor in the spectral types of TDEs[52].

3.2.15 AT2018zr

The TDE AT2018zr was discovered by the Pan-STARRS Survey for Transients [138] on the 2nd of March 2018 in the nucleus of the galaxy SDSS J075654.53 +341543.6[139]. It was a UV-bright event, marking it as a likely TDE, and showed weak soft X-ray emission, though the X-ray emission was not detected at later times[139]. There was a re-brightening which occurred in the UV bands at $\sim$ 50 days post-peak[139]. This corresponded to a temperature increase of $\sim$ 11,000K over three weeks[139]. The UV luminosity and temperature increase is not typical

of TDEs[139], though there are some TDEs, particularly those in AGN galaxies, which do experience re-brightening[140]

The spectra showed a blue underlying continuum which was initially featureless[139]. However, the spectra showed considerable evolution; strong Balmer emission lines soon appeared, and continually got stronger[139]. The Hα line, and possibly the Hβ line became more 'boxy' over time, and the Hα line may even have become double-peaked[139]. This is consistent with the TDE forming an elliptical disk, making it the third TDE with spectral features which may be described by this[139]. Meanwhile there may also be weak He I 5875 Å present, though due to its weak and uncertain nature, this TDE is classified as spectral type TDE-H[139].

3.2.16 AT2018dyk

The dim event AT2018dyk was initially classified as a TDE; it was located $0.''19^{+0.''28}_{-0.''19}$ from the galactic centre [56] and spectra showed potential broad Hα , Hβ and He II emission lines[141]. However, the continuum was not blue, and there were also narrow Hβ and He II emission lines which are not features of TDEs[141]. There were several other features which were not consistent with a TDE classification; it was several orders of magnitudes dimmer than the majority of TDEs, its decay was very slow for its rise time, and the decay was not well described by a power-law decline [56]. Additionally, the Mg II line became stronger at late times, which is not a phenomenon which has been observed in TDEs, while it did not exhibit any broad absorption features which would be expected in a TDE [56]. After consideration of these properties, the event was classified as a transformation from a low-ionisation nuclear emission line region galaxy (LINER) to a narrow-line Seyfert 1 galaxy, i.e. a "changing-look" LINER [56].

3.2.17 AT2018lna

ZTF discovered AT2018lna on 12th December 2018[142]. It was a UV-bright event with a and constant blue colour of UVW2-g $\sim$ -1 [142]. This, paired with its central location within the host galaxy, and broad emission lines observed, gave it its TDE classification[142]. Its spectral classification was given as TDE-Bowen [23].

3.2.18 AT2019avd

The transient AT2019avd was discovered on 9th February 2019 by ZTF coincident with the host's nucleus[140]. The host had shown no historic variability but Frederick et. al (2021) classify it as a NLSy 1 galaxy on the basis of its spectra [140]. AT2019avd was a blue event with UVW1-g = -0.2 [140]. The UV/optical lightcurves showed two peaks, the second of which, 350 days after initial detection, was also observed in soft X-rays, while previously there had been no X-ray detection[140]. These two peaks mirrored each other in shape, though the second peak was half the luminosity of the first[140]. Additionally, there was an infrared flare 100 days after initial detection[140]. Spectroscopy initially showed strong Balmer emission and a weak FeII complex[140]. Follow-up spectroscopy $\sim$ 440 days after the initial peak revealed the onset on HII lines, features associated with Bowen fluorescence and a blue horned profile of the Hβ line[143]. At this epoch, the FeII complex could no longer be seen[143].

Due to its complex nature, there has been some debate on the provenance of AT2019avd. A TDE scenario is supported by the lack of previous AGN activity, as well as the presence of very soft X-rays[144]. However, the Balmer emission lines are narrower than typical of a TDE, and the spectra's underlying continuum less blue[144]. The second peak is much brighter than those of other TDE candidates which rebrighten[144], with the possible exceptions of AT2019pev[140], which we will see in section 3.2.23, and SDSS J015957.64+003310.5[109]. AT2019avd is not

consistent with a typical TDE, though it was suggested to result from a double TDE (DTDE), in which both stars in a binary system become disrupted[144]. This would explain the two lightcurves seen, with only one corresponding to X-ray emission[144]. However, Malyali et. al (2021) found in their modelling that no combination of black hole mass and stars' mass could result in the timescales corresponding to the peaks in the lightcurve[144]. A more complex DTDE scenario has also been suggested, in which, post disruption, the two debris streams collide, causing an additional flare[145][144]. This scenario would also explain the emergence of the X-rays at the second peak only, which would correspond to accretion once the disk has been formed[144]. It may also explain the onset of Bowen lines, though this would require dense gas and a strong ionising flux[144]. Alternatively, it may be a TDE corresponding to a SMBH binary, in which accretion flow can be perturbed between the two BHs, resulting in lightcurves with two peaks[146][144].

Another theory is that it arose due to non-TDE AGN activity[144]. NLSy1 galaxies do exhibit large X-ray variability[147], however the X-rays observed are softer than one would expect[144], even in a NLSy1 galaxy which produce soft X-ray emission[140]. NLSy1 galaxies generally exhibit strong Fe II emission[148], and while a weak Fe II complex was observed, this is not indicative of activity from the host's nucleus[144]. Additionally, such a double-peaked optical lightcurve has not been observed from AGN activity in NLSy1 galaxies[144], once again with the possible exception of AT2019pev[140] (see section 3.2.23).

A SN interpretation has also been considered, though the X-rays are too soft to correspond to a Type IIn SN[149], and the event was brighter than would be expected[144]. However, it is possible that the first peak was a Type IIn SN and the second, an AGN 'turn-on' event, in which the BH accretion rate suddenly increases[144]. These 'turn-on' events are rare[150], and it is unlikely, but not impossible, that one would be observed so soon after a SN in the same region[144].

3.2.19 AT2019bhf

AT2019bhf was discovered by ZTF on 28th Februray 2019[151] and classified as a TDE the following year[152]. It was spectroscopically classified as TDE-H[23].

3.2.20 AT2019fdr

ZTF initially discovered AT2019fdr on 27th April 2019[140]. It was located at 0.13" from the nucleus of a NLSy1 galaxy[140]. The AGN host had previously exhibited variability in observations from 2009-2013, however prior to the event, none was detected[140]. The event was exceedingly bright; the peak UV/optical bolometric luminosity was 1.4 ± 0.1 x 10^{45} erg/s, making it one of the brightest transients ever observed. As discussed in section 2.12, being located in an AGN host might enable a TDE to be more luminous due to the additional energy of the AGN disk.

The UVW2-g colour reported by Fredrick et al. (2021) was red at 0.8 mag[140]. There was some colour evolution towards the red which is not common in TDEs, though can occur[140].

During its rise, there were two plateau phases which lasted $\sim$ a month each [153][140]. This shape is similar to the one seen in AT2016ezh [140], likely a TDE in an AGN galaxy (see sections 3.2.13 for more about AT2016ezh and 2.12 for a refresher on AGN-based TDEs). In TDEs, this signature is understood as rebrightening due to later disk formation [93] Microlensing was ruled out as the cause of the plateaus as there was g-r colour evolution towards the red, while microlensing would cause the colour to be identical at the different epochs [154].

As well as UV/optical light, X-rays were detected 11 months after it was discovered, though not at any other epochs where the event was monitored in X-rays[68]. The X-rays were very soft; in the 0.3-2.0 keV band[68]. Soft X-rays are indicative of TDEs, but very rare in AGNs[68]. In NLSy 1 galaxies, X-rays are generally softer compared to other AGNs, but even so, the X-rays observed corresponded

to a blackbody temperature of 56^{+32}_{-26} eV, which is lower than expected for these AGN galaxies[68]. X-rays are rarely observed in SLSNe[155], also making a SLSN classification unlikely[68].

AT2019fdr's spectrum reveals blueshifted narrow Balmer emission lines, which may be a sign of an unknown separate component[140]. There was an additional Fe II complex, only after 368 days[140]. This was dependent on the brightness of the continuum[140]. This Fe II complex only being present at certain times was also seen in the TDE AT2018fyk (see section 3.2.4)[140]. The spectrum taken 8 days post-peak showed Hβ with a 'blue horn' component, an offset blue component of the emission line[140]. This may be a result of wind ejecta with a velocity different to that of the AGN[140]. It also showed weak H II emission, while a spectrum taken 368 days post-peak showed no H II emission[140].

Though it was initially earmarked as a Type II superluminous supernova (SLSN-II)[156], there are several features of the event which are not consistent with this classification; there were X-rays detected at late epochs, a strong infrared echo and the location was very close to the nucleus[140][68]. Additionally, the flare was very long-lived, the UV and U band emission persisted even at late times, (a hallmark of TDEs), while with supernovae they fade quickly [140]. The HII emission also appears much too late for a SN [140]where flash ionisation only occurs at early phases [157].

It shared several features with the Type IIn SN in an AGN CSS100217; soft X-rays, g-r colour evolution, the very luminous peak magnitude of -23$\lesssim M_V \lesssim$ -22 and the Fe II complex[140][158]. However, AT2019fdr faded on a much longer timescale than CSS100217, its Fe II complex is not present throughout the event (unlike CSS100217[158]), and there were Balmer emission lines which are not expected in SNe[140].

Frederick et al. (2021) postulate that this event is a TDE, though given the complex nature of the event, warn the reader that this is not a definitive classification

as an AGN flare was still a possible explanation[140]. Due to the presence of the Hβ line but no He lines, the object would be classified as TDE-H under van Velzen et al. (2021)'s classification system[23][140]. If this were the case, the FeII signature must be a result of the NLSy1 host galaxy [140].

An interesting development arose a year after discovery; this TDE candidate was the likely origin of a high-energy neutrino IC200530A, detected by IceCube [68][159]. At the time of neutrino detection, the transient was still active, despite being nearly a year old, with a flux of $\sim$ 30% of its peak flux[68].

3.2.21 AT2019meg

ZTF discovered AT2019meg on 31st July 2019 [160]. It was classified as a TDE based on its spectra which showed a blue continuum marked by broad Hα and Hβ emission lines, as well as strong, narrow emission lines resulting in star-formation in the host galaxy [161]. This makes it a TDE-H type [23]. Additionally, its high blackbody temperature was consistent with a TDE[161]. There was no X-ray detection[161].

3.2.22 AT2019lwu

First discovered by ZTF, AT2019lwu was classified as a TDE based on its blue spectral continuum featuring broad Hα, Hβ and He II emission lines[162]. The spectrum also featured NIII emission lines and Ca II absorption lines[162]. Its spectral type is TDE-H [23].

3.2.23 AT2019pev

AT2019pev was discovered by ZTF on the 4th of September 2019 0.15" of the nucleus of a NLSy1 galaxy[140]. The event had a long lifetime of over 500 days[140]. During that time, it experienced a rebrightening at $\sim$ 100 days post-peak, in both UV/optical and X-ray light[140]. The second peak was nearly half the luminosity of the first[140]. Rebrightening is rare, though is occasionally seen in both TDEs

and SNe[140]. The double peak may also be explained by microlensing, causing a symmetric peak to appear later[154][140].

The spectra of AT2019pev comprised of strong, broad He II lines, and less broad Balmer lines[140]. It was classified spectroscopically by Frederick et al. (2021) as being in a He II + NIII spectral class[140]. Strong He II lines are only observed at early times in SNe [157] [163] and are rare among AGNs [164], but common among TDEs [97], which is why this event is being considered as a TDE-candidate, along with its prime position. However, the subclass of Trakhtenbrot AGNs and rapid 'changing-look' AGNs do see He II line profiles [108] [56]. Strong Bowen fluorescence features were also present at early epochs, before disappearing[140].

Another piece of evidence supporting the TDE-scenario is the X-ray lightcurve which initially declined following a power-law of $t^{-1.67}$, consistent with a TDE[95][51]. However, both the X-ray lightcurve later plateaus, and then rebrightens which is only occasionally observed in TDEs[95]. A SN explanation is not well supported; the event had strong X-ray and UV emission, and the long-lived He II line profiles which are only observed in supernovae spectra during the early phases[140]. Nor is the TDE scenario seen as feasible by Fredrick at al. (2021) due to the double peaked lightcurve, with the second peak being nearly as luminous as the first [140]. However, Yu et al. (2022) do not rule out a TDE scenario based on this alone, since there are other TDEs such as AT2018fyk which experience such rebrightenings[51][95].

Ultimately Fredrick et al. classified the event as a Trakhtenbrot et al. [108] class of AGN flare and a result of enhanced accretion[140]. However, Yu et al. (2022) do not agree with this classification, as its weak UV excess and steep decline are not consistent with other objects of that class[95]. Instead they put it down to AGN-activity more generally[95].

3.2.24 AT2019qiz

The TDE AT2019qiz was discovered on the 18th of September 2019 by ATLAS [107] in a weak AGN galaxy[40]. The last non detection date was 2 days prior[40]. Its spectrum won it its TDE classification[40] with the class TDE-H+He [23]. It also featured Balmer lines and it was the first TDE seen to exhibit Fe and low ionization broad absorption lines (FeLoBALs) in its spectra[40]. The Hα line has two components; one very broad (FWHM $\gtrsim 10^4$ km s^{-1}) and one narrow (FWHM ≈ 3000 km s^{-1})[40].

The TDE was observed in both UV/optical and X-ray light, with the X-ray component being 2-3 orders of magnitude less than the UV/optical[40]. Not only that, but AT2019qiz is one of the few TDEs to have been detected in radio waves [165]. The peak bolometric luminosity was 4.9 x 10^{43} erg/s[40]. This, accompanied by its medium rise time puts it in the middle of the pack of observed TDE properties[40].

Until the peak luminosity, the photosphere was expanding at a constant velocity of 2700 km s^{-1}[40]. Along with broad absorption lines, this indicated the presence of an outflow[40]. This would explain the broad Hα component as the full width half maximum (FWHM) was $\sim$ the broad absorption line velocity[40]. Meanwhile, the narrow absorption lines are likely a product of host galaxy dust rather than from the TDE itself[40].

3.2.25 iPTF15af

The TDE iPTF15af was discovered by iPTF on 15th January 2015[97]. The host had a high nuclear stellar density and showed signs of recent starburst[97]. Within the host, iPTF15af was coincident with the nucleus[97]. The TDE rose to a peak at $\sim$ 1.5 x 10^{44} erg/s over a period of $\sim$ 60 days, and declined over 5 months[97]. Its spectra showed a blue featureless continuum overlayed by HeII lines[97]. A Hα line later revealed itself, and narrowed over time[97]. Additionally, the Bowen

Fluorescence features of [OIII] and [NIII] were observed[97]. The impact parameter β was very low at $0.10^{+0.36}_{-0.1}$, consistent with a PTDE[97]. However it was a bright event, so its high luminosity has been ascribed to its efficient dM/dt[97].

3.2.26 OGLE16aaa

OGLE16aaa was discovered by the Optical Gravitational Lensing Experiment (OGLE-IV)[166] survey on 2nd January 2016 within the nucleus of a weak-line AGN galaxy which had experienced recent star formation[166]. It reached an NUV peak apparent magnitude of 20.83 $\pm$ 0.12 within 34 days[98] and decayed slowly[166]. Its spectra show blue continua with narrow Hα, Hβ, NII and OIII emission lines[166]. Its luminosity, rise and decay times, consistent high temperatures, spectra and location are all consistent with a TDE scenario[166].

Interestingly, an X-ray brightening occured $\sim$ 180 days after the commencement of the optical emission when previously, the X-ray levels had been undetectable[98]. Despite a sudden X-ray increase by more than a factor of 10, no corresponding changes were observed in the UV/optical[98]. This is the third such TDE to have exhibited such delayed X-ray emission[98]. There are several theories as to the cause. One such model which may explain this behaviour is the 'thinning disk' model[167][98], in which X-rays are initially obscured due to a thick disk, which then thins as a result of the accretion rate no longer being greater than the Eddington limit, allowing X-rays to be visible from our viewing angle. Similarly, the phenomenon may be a result of variable local absorption e.g. by the debris themselves, or the host's ISM[98]. Alternatively, the UV/optical emission mechanism could be shocks during circularisation, and the X-ray component a result of delayed accretion[98].

3.2.27 OGLE17aaj

The OGLE-IV Transient Detection System discovered OGLE17aaj on 2nd January 2017, within 0.10 ± 0."13 from the centre of its host, a weak AGN galaxy[99]. Due to its position, lack of colour evolution, and high temperatures of up to 40,000K, a TDE explanation was considered[99]. Its spectra showed hydrogen and helium emission lines, as well as forbidden oxygen and silicon emission lines, however the HeII lines were considerably narrower than is typical of TDEs[99]. Additionally, at a peak absolute I-band magnitude of only -18.8, OGLE17aaj was fainter than most TDEs, though some fainter TDEs have been observed such as AT2016fnl[99]. The lightcurve is also not consistent with a TDE; while it rose to peak over 50 days, it declined very slowly and plateaued after $\sim$ 200 days [99]. Gromadzki et al. (2019) believe it to be a result of a new class of AGN phenomena[99], in the same class as that of AT2017bgt[168] (see section 3.2.1 for more on this object).

4 Reductions

Swift's Ultraviolet and Optical Telescope (UVOT) photometry has 6 filters; V, B, U, UVW1, UVWM2, and UVW2. This work uses the central wavelengths calculated by the SVO Filter Profile Service [169](5425.3 Å, 4349.6, 3467.1 Å,2580.8 Å, 2246.4 Å, and 2054.6 Å respectively). These were the same wavelengths used by Hinkle et al. (2021)[6], so our photometric results can be compared for a consistency check. Throughout this thesis, all magnitudes presented are in the AB magnitude system.

4.1 Obtaining Flux Densities

Since all known tidal disruption events have been extragalactic, TDEs cannot be directly observed; the entire host galaxy's nucleus (including the TDE) must be observed. In order to measure the TDE's flux, the host galactic nucleus' flux must

be removed from the measurement to avoid contamination. Without such a host subtraction we would not truly be measuring the TDE, and when comparing data in different bands it would become problematic since the host will have a different contribution in different wavelengths.

The host's flux may be obtained from observations before the transient occurred, or from follow-up observations when the transient is no longer active (when the galaxy is quiescent). However, this archival data doesn't always exist, so other methods must be used to estimate the host galaxy's flux. The host's flux in different filters must be subtracted from each of the corresponding bands' flux measurements from when the TDE was still active. This is particularly important in the redder bands, as TDEs tend to be found in redder hosts, so more host contamination would occur compared to the bluer bands. TDEs are also blue by nature (in early epochs at least), and dim in the red bands, compounding the importance of the hots-subtraction in the redder bands.

The Table 3 of Hinkle et al. (2021) provided AB magnitudes and errors of the host galaxies in a range of filters[6]. These host magnitudes were acquired in a number of ways; AT2019ahk and AT2018cow 's host magnitudes were acquired from Swift observations when the galaxy was quiescent [89] [118], with the host magnitude of AT2018cow measured at the position that the transient was observed[6]. The rest of the sample did not have archival quiescent Swift photometry[6]. However, some galaxies did have published host galaxy magnitudes in the literature. Meanwhile, for those without, the host magnitudes were measured in Pan-STARRS data [138] with the exception of OGLE16aaa and AT2019ahk which were not observed by Pan-STARRS[6]. For these two events, catalogue host magnitudes were obtained from the Dark Energy Survey [170] and AAVSO Photometric All-Sky Survey [171][6], respectively. These magnitudes were then converted into fluxes and fitted to spectral energy distributions (SEDs) with Kriek et al. (2009)'s Fitting and Assessment of Synthetic Templates code (`FAST`)[172] to obtain synthetic host fluxes in all 6 of the

UVOT filters, and assuming an exponentially declining star formation rate[6]. UV magnitudes from the Galaxy Evolution Explorer [173] All-sky Imaging Survey (AIS) catalogue and W1 and W2 magnitudes from the Wide-field Infrared Survey Explorer [174] AllWISE catalogue were also deployed to help constrain the host flux[6].

The errors for these fluxes were estimated by perturbing the literature host fluxes with Gaussian errors in a Monte Carlo simulation[6]. The differences between the median and the 16th and 84th percentile were taken, and the larger of the two was adopted as the uncertainty in host flux[6]. However, some host errors are particularly large, e.g. for AT2019lwu the UVW2 magnitude error is 3.262[6]. These large UV errors arise from lack of GALEX magnitudes which results in poorly constrained star formation rates and therefore poorly constrained UV uncertainties[6].

Hinkle et al. (2021) [6] Table 5 provided AB magnitudes and equivalent flux densities of the transients (non-host-subtracted) in different filters and in different epochs. The host and non-host-subtracted magnitudes m were converted to flux densities f_λ (with units of erg cm^{-2} s^{-1} Å^{-1}) using the AB magnitude to flux density equation [175], adapted for f_λ

$$f_\lambda = (c/\lambda^2) \cdot 10^8 \cdot 10^{-0.4(m+48.6)}, \tag{8}$$

where c is the speed of light (3 x 10^{10} cm/s) and λ is the central wavelength of the filter (Å). The errors were propagated using

$$\Delta f_\lambda = \log(10^{0.4}) \exp(-\log(10^{0.4})(\Delta m + 48.6)) \frac{\Delta mc \cdot 10^8}{\lambda^2}. \tag{9}$$

Two objects (AT2018cow and AT2019ahk) used different host galaxy magnitudes than the ones provided in Hinkle et al. (2021) Table 3, instead they used archival photometry given in Hinkle et al. (2021) Table 2[6]. The same process of converting to flux densities was also applied to these host magnitudes.

4.2 Extinction Correction

Given the extragalactic origins of TDEs, all light from them must first travel through both their own galaxies, and the Milky Way in order to reach us. This invariably means that this light becomes red-shifted by dust particles it encounters. Fortunately, the extinction caused by the Milky Way is well-studied, and can be correction for along different lines of sight[176].

The `python` package `extinction` [177], following a Cardelli extinction law [176], was employed to remove the effects of interstellar extinction via the Milky Way from the host and non-host subtracted fluxes. This used the extinction coefficients A_v as provided by Hinkle et al. (2021) [6] Table 4. However, this does not account for extinction from the TDE's own host, nor intergalactic extinction. Applying an extinction correction for the host galaxies is not feasible in the same way that it is for the Milky Way, since they are not well-studied like our own galaxy is. For this reason, no additional extinction correction was applied, despite the fact that the reality of the situation demands it. Since I compare the results of my host-subtraction with Hinkle et al's (2021)[6] (see section 4.3 for this), it was necessary to follow the same reduction steps as them, and leave out additional corrections. Fortunately TDEs are intrinsically blue, and the results reflect this, meaning that the impact of the reddening that was not corrected for is not so large as to significantly change the perceived properties of TDEs.

4.3 Performing the Host-Subtraction

The host subtraction was then implemented by subtracting the host fluxes from the transient's fluxes for each object in each of the V, B, U, UVW1, UVW2 and UVM2 UVOT filters. These host-subtracted fluxes were then compared to the extinction and host-corrected fluxes given by Hinkle et al. (2021) Table 6 [6].

During the data processing, it was discovered that the flux densities of four

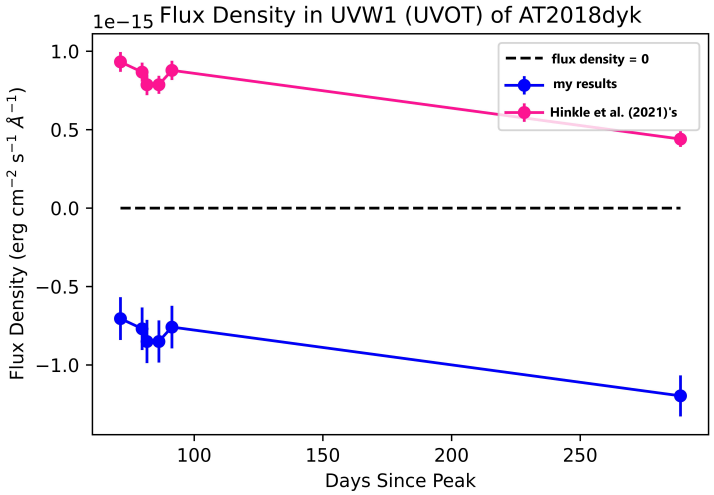

Figure 2. Initial lightcurve of AT2018dyk in UVW1 UVOT filter. Calculated flux densities are in blue and reference flux densities from Hinkle et al. (2021) [6] are in pink.

objects (AT2017bgt, AT2018dyk, AT2019avd, AT2019qiz) did not agree with the host-subtracted fluxes as published by Hinkle et al. (2021)[6], as in Fig 2. The values that I obtained were clearly non-physical as they produced negative flux densities, and it was evident that there had been an error in the data obtained. After private correspondence with Jason Hinkle, coauthor of the Hinkle et al. (2021) publication, to locate the source of the discrepancy, it emerged that Hinkle et al. (2021)[6] had used different host galaxy magnitudes than the ones provided in their tables. He provided an updated version of the table for the four objects (see Appendix A for full table). Once these new host galaxy magnitudes were adopted in the host subtraction, the lightcurves matched up with the Hinkle et al. (2021) reference values[6], as in Fig 3.

After the fluxes were corrected for extinction and host subtracted they could be converted back into magnitudes using the following equation:

$$m = -2.5log_{10}(\frac{f_\lambda \lambda^2}{c \cdot 10^8}) - 48.6. \tag{10}$$

The errors for the host-subtracted magnitude were propagated as

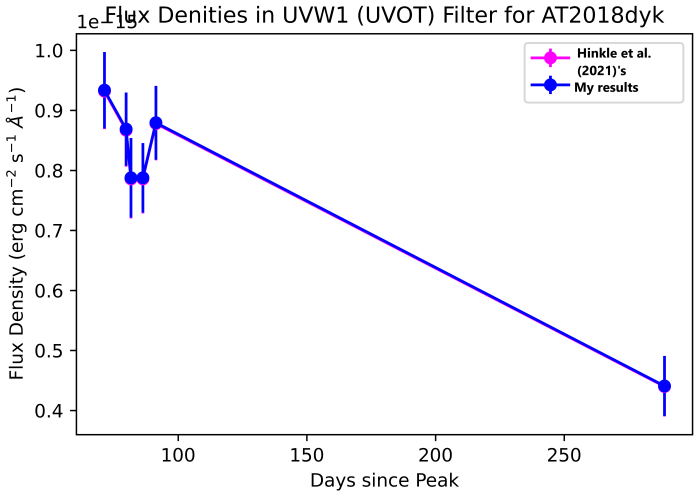

Figure 3. Lightcurve of AT2018dyk in UVW1 UVOT filter, using the host magnitudes provided by Jason Hinkle through private correspondence. Calculated values are in blue, and underneath are Hinkle et al. (2021)'s reference values in pink [6].

$$\Delta m = \sqrt{(\Delta m_{host})^2 + (\Delta m_{measured})^2} \tag{11}$$

where m_{host} is the magnitude of the host galaxy, and $m_{measured}$ is the non-host-subtracted magnitude.

For some epochs in the Hinkle et al. (2021) non-host-subtracted data only upper limits for AB magnitude were available[6]. The Hinkle et al. (2021) reference data (in Table 6 of that publication) showed yet more upper limits[6]. All the epochs for which only upper limits were available have also been removed from my sample, so as to only use well-constrained data.

5 Findings

5.1 Lightcurves

Lightcurves show the evolution of an object's brightness, and can often be key in identifying TDEs. Optical and UV lightcurves may be powered by reprocessed X-rays or by stream-stream collisions. In the UV/optical bands particularly, there is

some variation as to the luminosity decline rate, and not all events follow the $t^{-5/3}$ fallback rate[18]. The reason for this is not well-understood since it relies on the emission mechanism which is unclear and contentious for the UV/optical bands.

Lightcurves using both flux density (Fig 4) and magnitudes (Fig 5) for the 27 events in the sample were plotted in each of the 6 filters. A 20% percentage error cutoff (in the flux density, and then applied to the magnitudes) was introduced to remove epochs with large errors. Between the percentage error cutoff, and removing epochs which only had upper limits of detection, not all events had data to plot. As such, for the different filters (V,B,U,UVW1,UVW2 and UVM2), only some events are present in the plots.

We see in Figs 4 and 5 that peak flux density varies a lot between events; with by far the brightest event in the sample (not taking distance into account) being AT2018cow which was more than twice as bright as AT2018dyb, the next brightest event. This is entirely expected, as section 3.2.8 mentioned that AT2018cow was more luminous than any TDE observed at the time. Of the events in the figure, AT2018cow also has by far the steepest decline. The brightest events appear to have the steeper declines such as AT2018dyb, AT2019ahk, and AT2018cow (this is explored more thoroughly in section 5.4). Meanwhile, the dimmer events such as AT2016fnl do not appear to exhibit as steep decay rates. This is an observational phenomenon seen in TDEs, and predicted theoretically, by which brighter TDEs decay faster [6], though there doesn't seem to be a correlation between peak luminosity and rise time[1].

Besides AT2018cow's extremely high flux density and decay rate, the feature that stands out the most in Figs 4 and 5 are the double-peaks of AT2016ezh's lightcurve. This is a well-known feature of the event and is likely a product of viscous time delay or perhaps a result of reaching the Eddington luminosity [72] (see sections 3.2.13 and 5.7.1 for more discussion on its double-peaked nature).

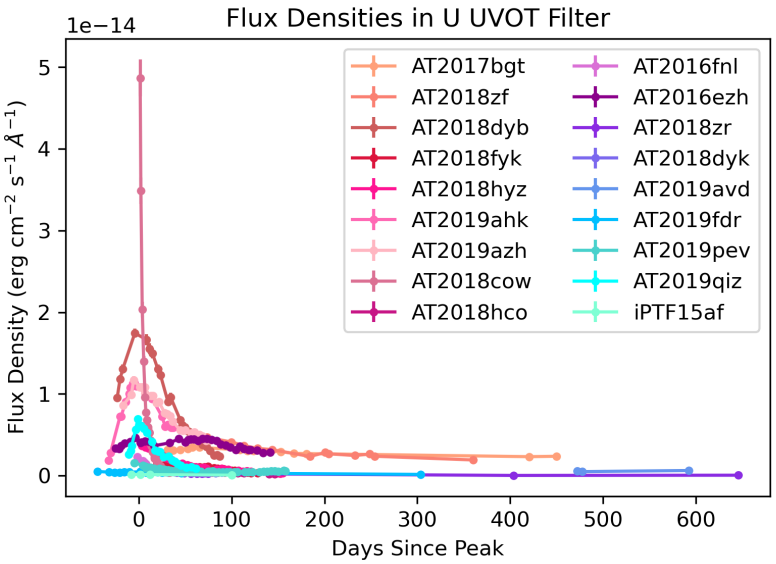

Figure 4. U band flux density lightcurves for events in the sample

5.2 Spectral Energy Distribution Fits

For each object with 3 or more filters with data (which were not upper limits) at each epoch, plots of flux density against wavelength were made. Epochs were rounded to the nearest day. No percentage error cutoffs were made so as to not disregard precious and finite data. Blackbody distributions were fitted to the data from each epoch to create spectral energy distribution (SED) fits. SEDs are a method of observing how energetic a system is and at what wavelengths the peak radiation is expected to populate. From this, blackbody temperature and radius can be obtained. Blackbody radius is the expected photosphere radius assuming perfect spherical dimensions, and isotropic blackbody emission. Meanwhile blackbody temperature is the temperature that such a system would operate at. However, as these are fits, and TDEs operating as blackbodies is an assumption, results should be taken as more of an indication than a certainty.

The blackbosy equation[178], modified for distance, was fitted to the plots at each epoch to create the SED fits, with the free parameters R_{BB} (blackbody radius)

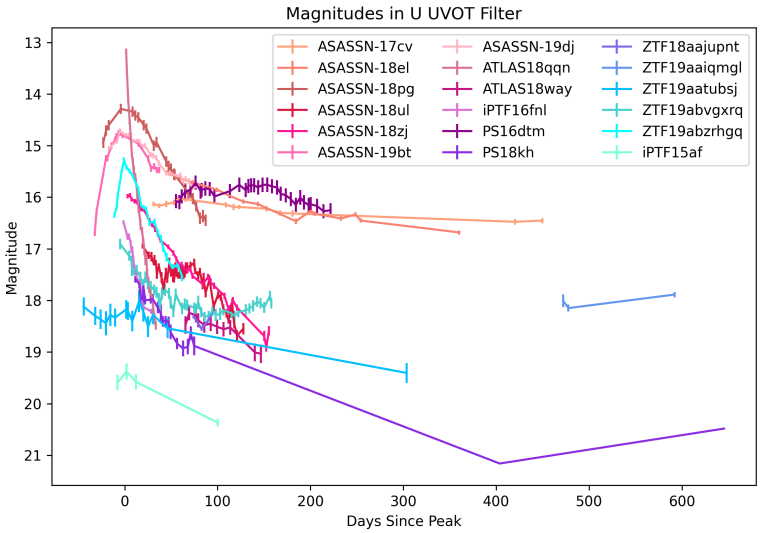

Figure 5. U band apparent magnitude lightcurves for events in the sample

and T_{BB} (blackbody temperature):

$$f_\lambda = \frac{\pi(\frac{R_{BB}}{D_L})^2(z+1)^4}{\lambda_{obs}^5} \frac{2hc^2}{exp\frac{b(z+1)}{\lambda_{obs}T_{BB}} - 1}, \tag{12}$$

where

$$b = \frac{hc}{k_B}, \tag{13}$$

D_L is the luminosity distance, z is the redshift, λ_{obs} is the wavelength of the band, h is the Planck constant, c is the speed of light, and k_B is the Boltzmann constant. Redshift z, was provided in Hinkle et al. (2021) Table 4 [6], and the luminosity distance D_L was calculated from z using CosmoCalc provided by UCLA [179].

The fits were performed using the `scipy python` package `curve_fit`[180]. The package uses a non-linear least squares method to fit a given function to data. It has proved difficult fitting spectral energy distributions to the data. The uncertainties of many of the objects are large; particularly in the UV bands due to the large uncertainty in the host measurement. This in turn provides a wide window of values that the radius and temperature may take. When there are only three or four wavelengths with data (either due to lack of measurement of all bands during

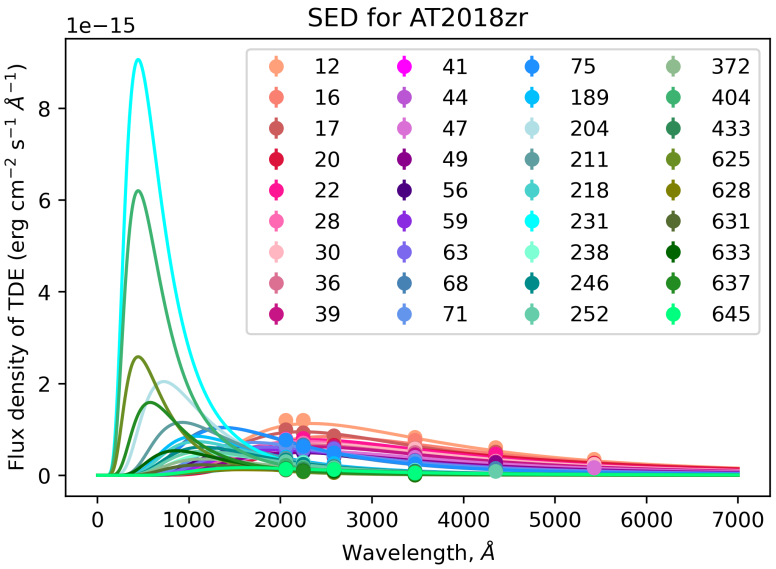

Figure 6. SED fits for AT2018zr at many different epochs, overlayed on one graph. Each epoch is represented in a different colour, with the epoch (in days since peak) shown in the legend

the epoch or the data available being an upper limit), this provides very little data for the function to fit, thereby increasing the uncertainty of the fit. Another issue encountered was that for most of the epochs and events, it was ambiguous as to whether the data was at the peak or on the tail of the equation. This ambiguity lead to the two distinct distributions in Fig 6 ; the earlier epochs which the fit considers to be at the peak of the distribution and at less energetic wavelengths, and the later epochs which have more energetic fits. Taken at face value, this figure would imply that the TDE experiences a rebrightening at later times, but since the temperatures of the energetic fits are considerably higher, and the epochs of the energetic fits are non-consecutive, this is non-physical. A more likely explanation is that the energetic fits are a result of having few data points to fit; which tends to be the case for most of the late time observations which are often without V and B band data. Another explanation is that the late-time epoch fits are accurately representing the system, and the earlier epochs are even more energetic than these, but are too far along the tail for the fit to be able to pick up on this.

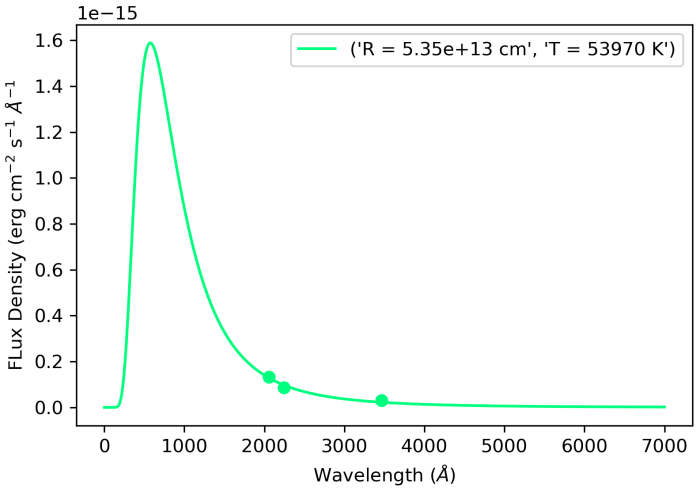

Figure 7. AT2018zr SED fit for 637 days post-peak. The best-fit blackbody radius at this epoch is 5.35 x 10^{13} cm and the best-fit blackbody temperature is 53,970 K.

In order to test whether the energetic fits were caused by lack of data or because they are a better reflection of the true energetic nature of the event, I tested a variety of fixed temperatures to see how well they could describe these data for the three AT2018zr datapoints at 637 days post-peak. I compare the initial energetic fit in Fig 7 with new fits with specified temperatures in Fig 8. The 10,000K and 30,000K fits are clearly not describing the data. However the higher temperature fits appear to be good, despite large χ^2 values[1]. This doesn't offer much insight as to whether the high energy fits with only 3 data points are in fact that energetic, or if they are in fact less energetic and are being described by bad fits due to lack of data.

Let us assume momentarily that the original fit in Fig 7 is able to accurately reflect the energy of the system, and take the temperature at 637 days post-peak to be 53,970K. Since TDE temperature slowly declines, we would expect the temperatures before this epoch to be even greater. To test whether this would be feasible, I changed the bounds of the SED fits before 637 days to have a minimum temperature of 54,000K, as in Fig 9. Unsurprisingly, this caused most of the fits to output a

[1]Throughout this publication, the χ^2 values referred to are non-reduced, as the degrees of freedom needed to truly calculate reduced χ^2 are impossible to determine for non-linear fits[181].

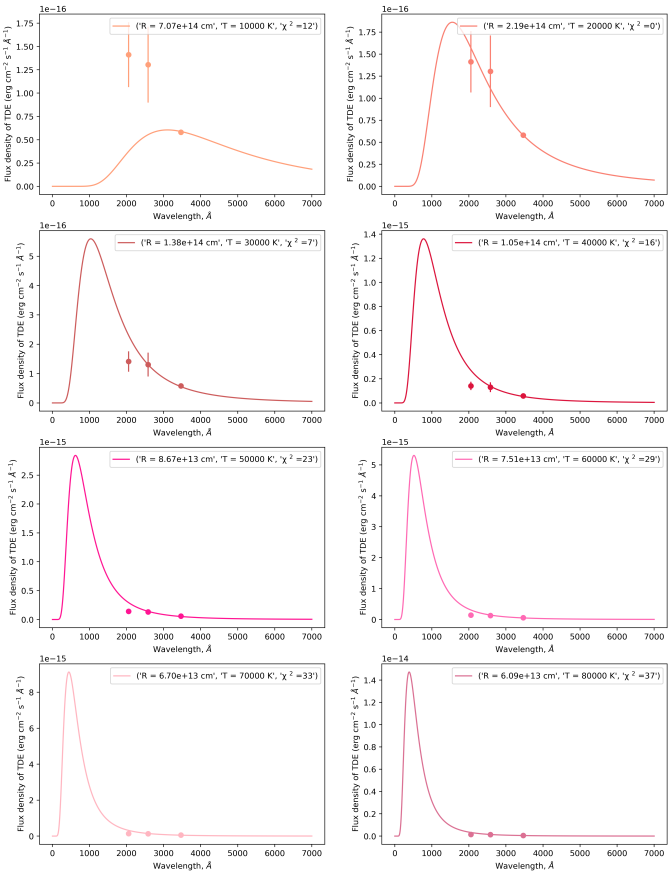

Figure 8. SED fits of AT2018zr at 637 days post-peak with fixed temperatures and free parameter radii. The values used in the fits, as well as the χ^2 of these fits are shown in the legends.

blackbody temperature of exactly 54,000K. Some were higher, although these were all fits which had been energetic in the first place. Most of the 54,000K fits appeared good, for example the 218 days post-peak epoch in Fig 9, is fitting the data to the tail of the blackbody distribution well. However some epochs, particularly earlier times such as 16 days post-peak, did not fit the tail so well, since they appear to be genuinely on a peak. However when we look at the initial fit in Fig 9, we see that there is a dip in the UVW1 (2580.8 Å) flux, and so it is not described perfectly by a blackbody distribution.

After these exercises, the validity of the SED fits and the positions of the data on the tail or peak of a blackbody distribution continues to remain elusive. This highlights the need for more observations at higher energies in order to detangle

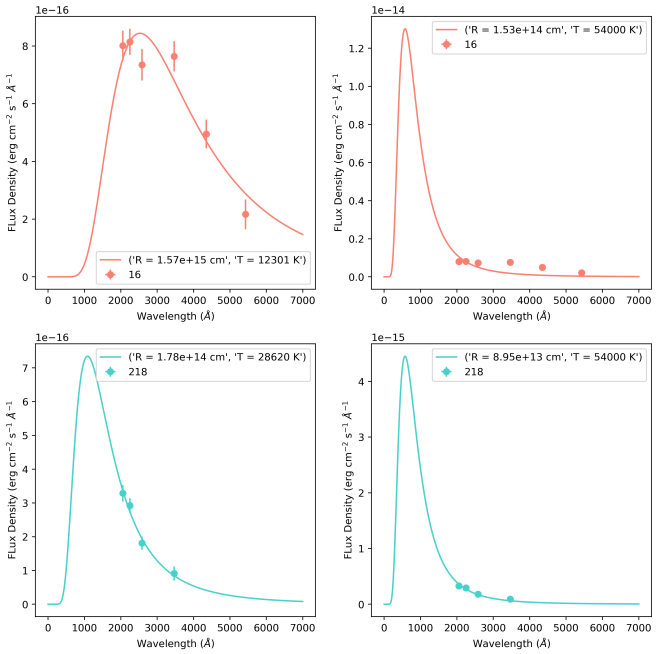

Figure 9. SED fits for AT2018zr at 16 and 218 days post-peak, shown in orange and blue respectively. The left hand side shows the initial SED fits with minimum temperature bounds of 5,000K, and the right shows the fits with minimum temperature bounds of 54,000K.

this dichotomy. Due to the uncertainty in the accuracy of the fits when only three datapoints are used, data using a three-point SED fit is indicated with an open symbol henceforth, to show that these data may not be accurate.

5.3 Blackbody Radius, Blackbody Temperature and Bolometric Luminosity

The outputted free parameters from the SED fits, blackbody radius R_{BB}, and blackbody temperature T_{BB}, were plotted over time for different events in the sample. A liberal 40% percentage error cutoff was introduced for both radius and temperature. Between some events not having enough data to be able to perform SED fits in the first place, and the high errors outputted for both temperature and radius, only 21

of the events had any data to plot.

The bolometric luminosity L was then calculated using the Stefan-Boltzmann equation:

$$L = 4\pi R_{BB}^2 \sigma T_{BB}^4, \tag{14}$$

where σ is the Stefan-Boltzmann constant[182], and plotted on the same graph. As the luminosities came from the radii and temperatures, which already had large errors, a percentage error cutoff was not introduced for the luminosity, as long as both the corresponding radius and temperature fulfilled the 40% percentage error criterion.

The general trend, as in Fig 10 is of decreasing radius and luminosity post-peak. Temperature is generally quite flat, with a slow decrease which is the typical temperature evolution of a TDE. For some plots, such as the temperature evolution in Fig 10, large errorbars (often a result of the ambiguity of the SED fits) cause the evolution to be less clear-cut. However, there are some objects with more exotic evolutions which are explored further in section 5.5.

5.4 Luminosity Power-Law Fits and Decay Rate

Since TDEs have been found to decline according to a power-law, often at a rate close to $t^{-5/3}$, this feature was tested for each of the 18 events which had more than two post-peak luminosity datapoints. Post-peak bolometric luminosity fits were performed using:

$$L = L_0(t - t_0)^{-\alpha}, \tag{15}$$

with L_0 (luminosity scale), t_0 (time of disruption), and α (luminosity decline power-law index) as free parameters, and the residuals for the fit calculated, as in Fig 11 and tabulated in Table III. An additional fit where α was not a free parameter, and was instead 5/3 was also completed for each of the events with sufficient post-peak data. These are tabulated in Table IV The residuals for these fits were also

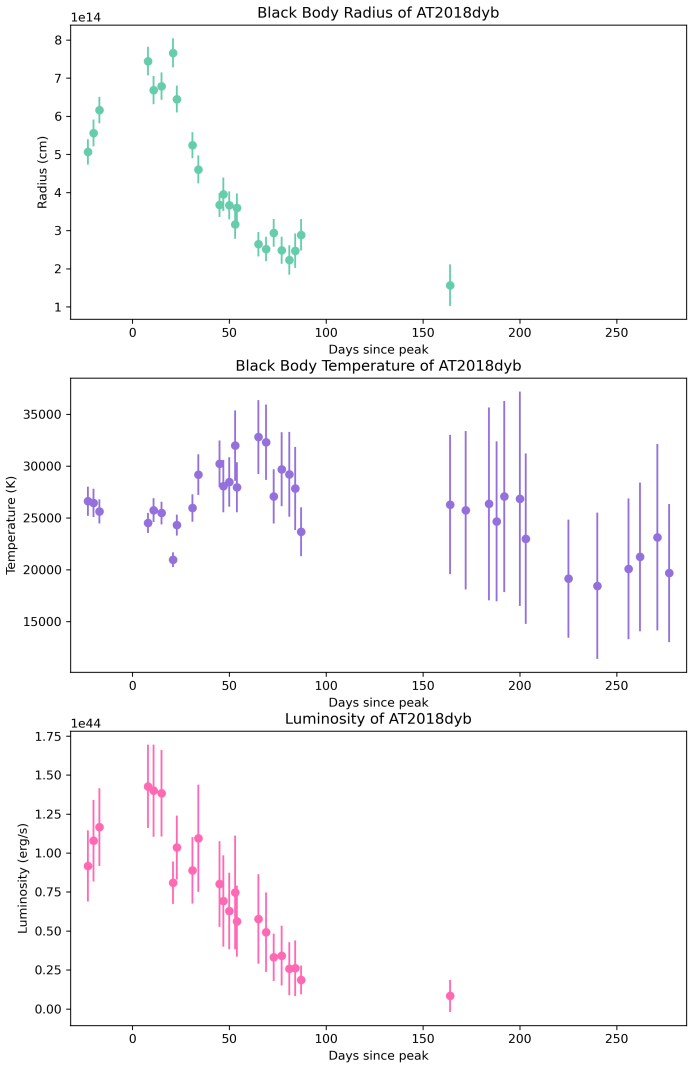

Figure 10. blackbody radius (teal) and temperature (purple) evolution as outputted by the SED fits for AT2018dyb. Bolometric luminosity evolution (pink) as calculated from the blackbody temperatures and radii.

Table II. Table detailing the interpolated values of blackbody radius, blackbody temperature and bolometric luminosity at peak. AT2018hyz and AT2018cow, marked with * symbols, were not measured at peak, but at 3 and 2 days post-peak respectively.

Object Name	Peak R_{BB}(cm)	Peak T_{BB} (K)	Peak L_{peak} (erg/s)
AT2018dyb	(7.03 ± 0.49) x 10^{14}	24875 ± 1549	(1.34 ± 0.35) x 10^{44}
AT2018hyz*	(11.39 ± 0.44) x 10^{14}	19653 ± 495	(1.38 ± 0.18) x10^{44}
AT2019ahk	(13.27 ± 0.50) x 10^{14}	16886 ± 373	(1.02 ± 0.12) x 10^{44}
AT2019azh	(6.80 ± 0.72) x 10^{14}	27748 ± 2975	(1.95 ± 1.05) x 10^{44}
AT2018cow*	(7.50 ± 0.42) x 10^{14}	32352 ± 1905	(4.39 ± 1.14) x 10^{44}
AT2016fnl	(1.73 ± 0.19) x 10^{14}	34029 ± 3393	(2.84 ± 1.31) x 10^{43}
AT2019fdr	(44.21 ± 5.74) x 10^{14}	13979 ± 841	(5.29 ± 1.85) x 10^{44}
AT2019pev	(14.66 ± 1.58) x 10^{14}	19421 ± 1250	(2.20 ± 0.81) x 10^{44}
AT2019qiz	(4.49 ± 0.35) x 10^{14}	21972 ± 1239	(3.34 ± 0.94) x 10^{43}
AT2016ezh	(62.22 ± 4.37) x 10^{14}	9940 ± 280	(2.69 ± 0.49) x 10^{43}

calculated, as seen in Fig 11. For both sets of residuals, the mean and median of the residuals was also computed, and tabulated in Tables III and IV.

There were several power-law fits performed on AT2016ezh due to its two peaks. The first was performed on all data post-peak, which was evidently not a good fit given its unconventional lightcurve. For this fit, the α value obtained was 0.49 ± 2.10. The second fit performed was on the second half of the first peak, but with only 6 datapoints gave an unhelpful result of $\alpha = 1.70 \pm 32.63$. The third and final fit was performed from the second peak onwards, which gave a rather low α value of 0.44 ± 0.71.

Unfortunately, most of the fitted alpha values have large errors, so it's difficult to say truly how close they are to the expected TDE fallback rate of $t^{-5/3}$. However for most of the 18 events, the α=5/3 fit, is a good one despite the fitted α value not always being close to 5/3. For some events, the median of the residuals is actually

Table III. Table of fitted luminosity decline power-law index α values for the post-peak bolometric luminosity fits

Object Name	α	α error	χ^2	Residuals Mean	Residuals Median
AT2017bgt	0.8214	0.7353	2.07	1.49 x 10^{43}	9.09 x 10^{42}
AT2018zf	0.5588	0.2325	8.56	4.29 x 10^{41}	7.55 x 10^{41}
AT2018dyb	2.166	1.559	7.73	7.11 x 10^{42}	7.63 x 10^{42}
AT2018fyk	0.756	0.2763	6.30	1.78 x 10^{43}	2.12 x 10^{43}
AT2018hyz	1.135	0.1209	6.49	1.32 x 10^{42}	1.09 x 10^{42}
AT2019ahk	2.158	2.330	0.07	-2.31 x 10^{40}	-3.51 x 10^{41}
AT2019azh	1.878	2.938	3.07	6.16 x 10^{42}	5.44 x 10^{42}
AT2018cow	3.263	0.242	4.22	4.48 x 10^{42}	-2.25 x 10^{40}
AT2018hco	1.668	13.33	6.17	2.10 x 10^{42}	2.95 x 10^{42}
AT2016fnl	2.809	2.801	1.28	8.65 x 10^{42}	8.10 x 10^{41}
OGLE16aaa	0.3226	0.16	0.08	-3.78 x 10^{41}	5.85 x 10^{41}
AT2018zr	0.5166	0.06132	1.50	1.56 x 10^{42}	1.07 x 10^{42}
AT2018dyk	2.003	35.81	0.09	4.04 x 10^{41}	-5.94 x 10^{40}
AT2019avd	0.001	1.116	0.19	-1.85 x 10^{41}	-1.96 x 10^{40}
AT2019fdr	1.653	2.356	0.82	5.61 x 10^{41}	-6.77 x 10^{41}
AT2019pev	0.2432	0.04585	2.57	2.24 x 10^{42}	1.45 x 10^{42}
AT2019qiz	1.904	0.2018	1.84	9.06 x 10^{40}	6.92 x 10^{40}
AT2016ezh (all post-peak data)	0.49	2.10	18.19	3.43 x 10^{42}	1.57 x 10^{42}
AT2016ezh (first peak)	1.70	32.63	0.62	1.87 x 10^{43}	1.12 x 10^{43}
AT2016ezh (second peak)	0.44	0.71	3.15	2.08 x 10^{44}	2.22 x 10^{44}

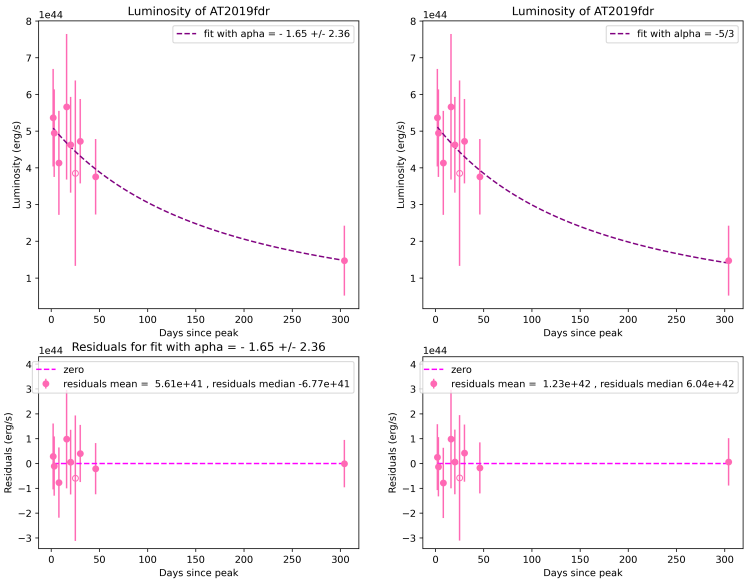

Figure 11. Post-peak bolometric luminosity for AT2019fdr, fitted with a power-law, with the power-law index α as a free parameter (top left) and with $\alpha = 5/3$ (top right). Respective residuals for these fits are given in the bottom panels. The open marker indicates that the SED fit from which the bolometric luminosity was derived only used 3 datapoints, and therefore may not be the most accurate reflection of the system at that time.

lower in the α=5/3 fits than the free α fits. Most of these events do seem to be able to be described by a $t^{-5/3}$ fallback rate, even if the α value fitted is not always close, which indicates that fallback emission could well be powering the lightcurve.

There were 8 events with both pre and post-peak R_{BB}, T_{BB}, and L data. To estimate the values of these at peak, linear interpolation was performed between the final pre-peak and first post-peak datapoints. The uncertainty in inferred peak luminosity L_{peak} is given by

$$\Delta L_{peak} = \sqrt{\frac{-t_1}{t_2 - t_1}^2 \Delta L_2^2 + (\frac{t_1}{t_2 - t_1})^2 \Delta L_1^2 + \Delta L_1^2}, \tag{16}$$

where t_1 and L_1 are the final epoch and luminosity pre-peak respectively, and t_2 and L_2 are the first epoch and luminosity post-peak. There were an additional 2 events, (AT2018hyz and AT2018cow) which had their first datapoints a few days after the

Table IV. Table detailing goodness of fit for the post-peak bolometric luminosity fits with fixed $\alpha = 5/3$

Object Name	χ^2	Residuals Mean	Residuals Median
AT2017bgt	17.38	3.66x 10^{43}	3.74 x 10^{43}
AT2018zf	11.49	7.15x 10^{41}	1.14 x 10^{42}
AT2018dyb	8.25	7.14x 10^{42}	8.62 x 10^{42}
AT2018fyk	6.63	1.89x 10^{43}	2.63 x 10^{43}
AT2018hyz	8.50	2.15x 10^{42}	2.10 x 10^{42}
AT2019ahk	0.08	-1.24x 10^{40}	-3.37 x 10^{41}
AT2019azh	3.14	6.18x 10^{42}	5.42 x 10^{42}
AT2018cow	54.16	1.76 x 10^{43}	-5.68 x 10^{40}
AT2018hco	0.60	2.10 x 10^{42}	2.95 x 10^{42}
AT2016fnl	1.66	9.20 x 10^{42}	2.04 x 10^{42}
OGLE16aaa	0.09	-7.47 x 10^{41}	4.05 x 10^{41}
AT2018zr	4.96	2.83x 10^{42}	9.43 x 10^{41}
AT2018dyk	0.09	4.07 x 10^{41}	-7.06 x 10^{40}
AT2019avd	22.72	4.27 x 10^{42}	4.53 x 10^{42}
AT2019fdr	0.82	1.23 x 10^{42}	6.04 x 10^{42}
AT2019pev	5.44	2.46 x 10^{42}	-1.74 x 10^{42}
AT2019qiz	2.02	4.89 x 10^{40}	6.70 x 10^{40}
AT2016ezh	161	1.64 x 10^{43}	2.91 x 10^{43}

peak (3 days and 2 days respectively). These datapoints are being considered as if they were peak values, but they are indicated with open markers from now on to show that these are not accurate peak data. However, it is a good estimate; the calculated bolometric luminosity for AT2018cow at 2 days post-peak was 4.39 x 10^{44} $\pm$ 1.14 x 10^{44} erg/s, which is consistent with the literature peak value of $\sim$ 4 x 10^{44} [118], as detailed in section 3.2.8. These peak R_{BB}, T_{BB} and L data (L_{peak}) are all

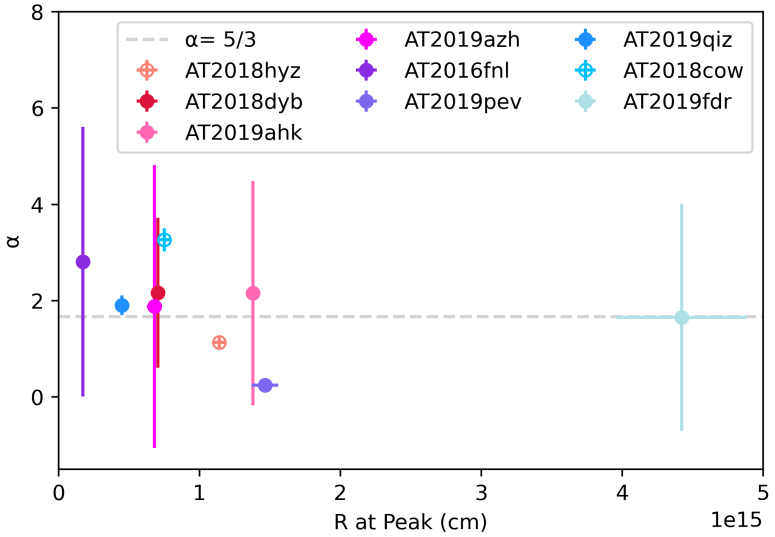

Figure 12. Fitted luminosity decline power-law index α against interpolated values of R at peak. The dashed line is at $\alpha = 5/3$, corresponding to mass fallback in TDEs, and the expected luminosity decline power-law index of a TDE. The open markers of AT2018hyz and AT2018cow indicate that these radii were measured post-peak, at 3 and 2 days respectively.

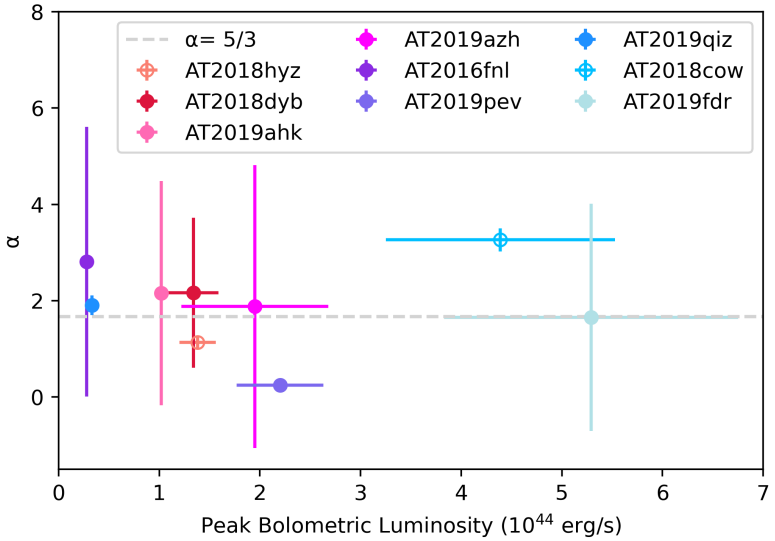

Figure 13. Fitted values of α against the interpolated bolometric luminosity at peak. The open markers of AT2018hyz and AT2018cow indicate the measurements were done post-peak (3 and 2 days respectively). The grey dashed-line represents the expected luminosity decline power-law index for a TDE, $\alpha = 5/3$.

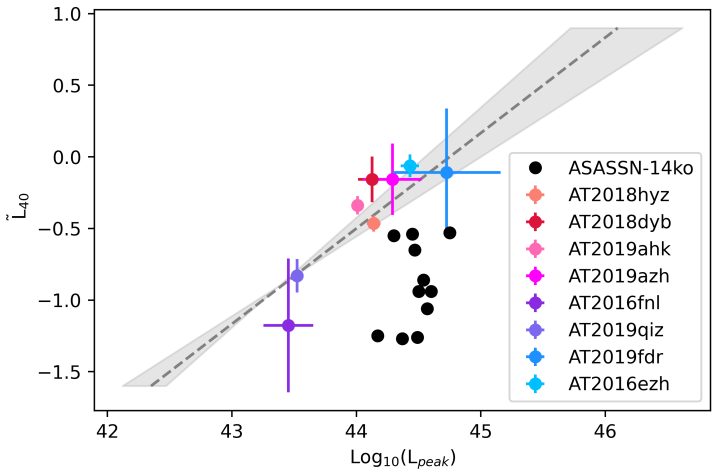

Figure 14. $\tilde{L}_{40}$ (given by eq 17) against $\log_{10}(L_{peak})$ for 8 TDEs in the sample. In black is the likely repeating PTDE ASASSN-14ko at the peaks of its outbursts (some in V filters, g filters and the TESS filter), obtained via Payne et al. (2021) [77]. The grey dashed line indicates the best-fit luminosity decline rate obtained via Hinkle et al. (2021) [6] and given in Eq 20, with the lighter grey bands indicating the uncertainty in this fit.

tabulated in Table II.

Table V. Table of calculated $\tilde{L}_{40}$ values for events with both peak bolometric luminosities, and luminosities past 40 days post-peak.

Object Name	$\tilde{L}_{40}$	$\Delta\tilde{L}_{40}$
AT2018hyz	-0.466	0.056
AT2018dyb	-0.157	0.160
AT2019ahk	-0.338	0.064
AT2019azh	-0.156	0.250
AT2016fnl	-1.177	0.468
AT2019fdr	-0.109	0.446
AT2019qiz	-0.830	0.117
AT2016ezh	-0.062	0.080

Of these 9 events (excluding AT2016ezh since the α obtained was not a good fit due to its double peaks) with calculated or estimated peak values, there doesn't

appear to be a relation between α and radius at peak in Fig 12. However the errorbars associated with α are very large in some cases, so this must be taken with some scepticism. In this figure, AT2019fdr stands out as having a blackbody radius of more than double the next largest event. TDEs do exhibit variation in their properties such as luminosity, blackbody radius, and blackbody temperature and decline rate, so this is somewhat expected. This is a result of different types, sizes, and masses of stars being disrupted by different mass black holes. TDEs generally have blackbody radii of $\sim 10^{15}$ cm [23]. AT2019fdr also has a larger uncertainty in R compared to the others which was due to the somewhat poor quality of the SED fits for this event.

There are 2 events in Fig 12 which were classified as phenomena other than TDEs, and they appear distinct from the classified TDEs. The first is AT2019pev which was classified as an AGN flare, and has a luminosity decline power-law index α much closer to 0 than the other objects, meaning its luminosity was slow to decay. Since AGNs outbursts do not dim in accordance with a power-law, they are not expected to be well described by the traditional $t^{-5/3}$ decline rate for TDEs. In both Fig 12 and Fig 13 we see that AT2019pev occupies both a similar blackbody radius, and bolometric luminosity as most of the remaining TDEs in the sample. Based on this, as well as by definition being located in the nucleus, it would be impossible to distinguish it from a TDE. Fortunately AGN flares may be distinguishable from TDEs in several ways; they tend to exhibit harder X-rays than TDEs, are generally more variable in their luminosity and more prone to rebrightening [86].

The second likely non-TDE event in Figs 12 and 13 is AT2018cow, classified as a FBOT, a rare and little-understood class of transient. It has the luminosity decline power-law index α value furthest from 0 which is expected since section 3.2.8 discussed how AT2018cow's speedy luminosity decay was almost unheard of. In Fig 12 we see that AT2018cow has a blackbody radius at peak very similar to the TDEs in the sample. However, in Fig 13 we are able to see AT2018cow occupies a

more distinct α-bolometric luminosity space. Its peak bolometric luminosity is not the greatest in the sample; that is won by AT2019fdr, though there is considerable cross-over in their L errors. At the time of AT2018cow's discovery its unprecedented brightness was considered evidence against a potential TDE classification. AT2019fdr's subsequent discovery and likely TDE classification lends credence to the proposal that AT2018cow could be a TDE. However it is also worth remembering that AT2018cow had a peak blackbody temperature 3 times greater than that of AT2019fdr (see Table II), and a blackbody radius of less than 1/6 of AT2019fdr's, meaning that these systems must be very physically distinct and not comparable.

Figure 13 doesn't appear to show a relation between luminosity decline power-law index α and peak bolometric luminosity. This is not entirely surprising given the large error bars associated with the α values, but one would generally expect to see brighter TDEs decaying more rapidly, since this is a noted trend [6]. A better comparison of decay rate in this case is of $\tilde{L}_{40}$, given by

$$\tilde{L}_{40} = log_{10}(L_{40}/L_{peak}), \tag{17}$$

where L_{40} is the bolometric luminosity at 40 days post-peak and L_{peak} is the peak bolometric luminosity[6]. The bolometric luminosity at 40 days was obtained via linear interpolation for all events, with the exceptions of AT2016fnl which had a bolometric luminosity reading at 40 days, and AT2019ahk which did not have bololmetric luminosity data after 37 days, so the luminosity at 37 days was taken instead. The uncertainty in L_{40} is given by

$$\Delta L_{40} = \sqrt{(\frac{40 - t_1}{t_2 - t_1})^2 \Delta L_2^2 + (\frac{t_1 - 40}{t_2 - t_1})^2 \Delta L_1^2 + \Delta L_1^2}, \tag{18}$$

where t_1 and L_1 are the final epoch and bolometric luminosity respectively before 40 days, and t_2 and L_2 are first the epoch and luminosity after 40 days. Meanwhile uncertainty in $\tilde{L}_{40}$ is given by

$$\Delta\tilde{L}_{40} = \sqrt{\frac{1}{(L_{40}log(10)\Delta L_{40})^2} + \frac{1}{(L_{peak}log(10)\Delta L_{peak})^2}}. \quad (19)$$

This $\tilde{L}_{40}$ quantity was used in Hinkle at al. (2021) to compare decay rates, and they obtained the following best-fit TDE relation for peak bolometric luminosity against $\tilde{L}_{40}$,

$$log_{10}(L_{peak}/(ergs^{-1})) = (44^{+0.1}_{-0.1}) + (1.5^{+0.3}_{-0.2})(\tilde{L}_{40} + 0.5)[6]. \quad (20)$$

In Figure 14 I compare TDEs with both peak luminosities and luminosities at epochs of 40 days post-peak with the relation given in Eq 20. The $\tilde{L}_{40}$ values obtained are given in Table V. We now see in Figure 14 that the TDEs in the sample do indeed have a faster decline rate when the peak bolometric luminosity is greater. The TDEs generally follow the relation given by Eq 20, shown in grey in the figure, which is to be expected since all the TDEs in Fig 14 with the exceptions of AT2019fdr and AT2016ezh were included in the 21 TDEs used by them to obtain this relation [6]. However, it is worth noting, as I explore in section 5.7, that some of the events used in obtaining the relation in Eq 20 may in fact be PTDEs, which decline more rapidly. If this were the case, a relation for solely TTDEs, would be shifted towards the upper left in Fig 14.

AT2016fnl may decay more rapidly for its luminosity in Fig 14, which is consistent with discussions in the literature in which it is noted for its fast but dim properties[26]. Though since this event has large $\Delta\tilde{L}_{40}$, I cannot make a definitive statement. This seemingly rapid decline is of note, as it shows that not all dim TDEs decay slowly, and there may be a population of fast-decaying dim TDEs that are being missed due to their lower luminosities[26].

Meanwhile, the rest of the TDEs in Fig 14 have a decline rate as expected given Eq 20, with the exceptions of AT2019azh and AT2018dyb which have slightly slower decays.

Interestingly, there are several events with low fitted luminosity decline power-law index α values. Of these, AT2018dyk, AT2019avd and AT2019pev, can be explained by their status as AGN- derived activity detailed in sections 3.2.16, 3.2.18 and 3.2.23. There are five other events which also have α values considerably lower than the expected $t^{-5/3}$ decline rate; three confirmed TDEs (OGLE16aaa, AT2018fyk and AT2018zr) and a further two TDE candidates (AT2018zf and AT2017bgt). Of these, OGLE16aaa, AT2018zf, and AT2017bgt have values which are consistent with a $t^{-5/12}$ decline rate ($\alpha = 0.3226 \pm 0.16$, $\alpha = 0.5588 \pm 0.2325$ and $\alpha = 0.8214 \pm 0.7353$ respectively), which is expected for disk-dominated emission[32]. Meanwhile AT2018fyk and AT2018zr have slightly higher decline rates, but still less than the expected rate for mass fallback ($\alpha = 0.756 \pm 0.2763$ and $\alpha = 0.5166 \pm 0.06132$ respectively), indicating that both mass fallback and disk emission may be contributing to their decline rates.

5.5 Colour Indices

The extinction-corrected and host-subtracted magnitudes were used to calculate the colour indices B-V, U-B and UVW2-UVW1, as in Fig 15. TDEs typically have blue colours in early phases[1], so colour indices can be evaluated to discover if a candidate is consistent with what is known of TDE colour. Indeed, Fig 15 does show blue events for the most part. Colour evolution can indicate changes in the temperature, with bluer light corresponding to hotter systems, so it is useful to compare colour and temperature evolution.

There was some variation in which epochs different filters had data for, for each of the various events. In order to calculate the colour indices, linear interpolation had to be used between 2 existing nearby epochs to calculate synthetic flux values at the same epoch as the other filter. This once again uses a 20% percentage error cutoff in the flux densities. These fluxes were then converted into magnitudes, and

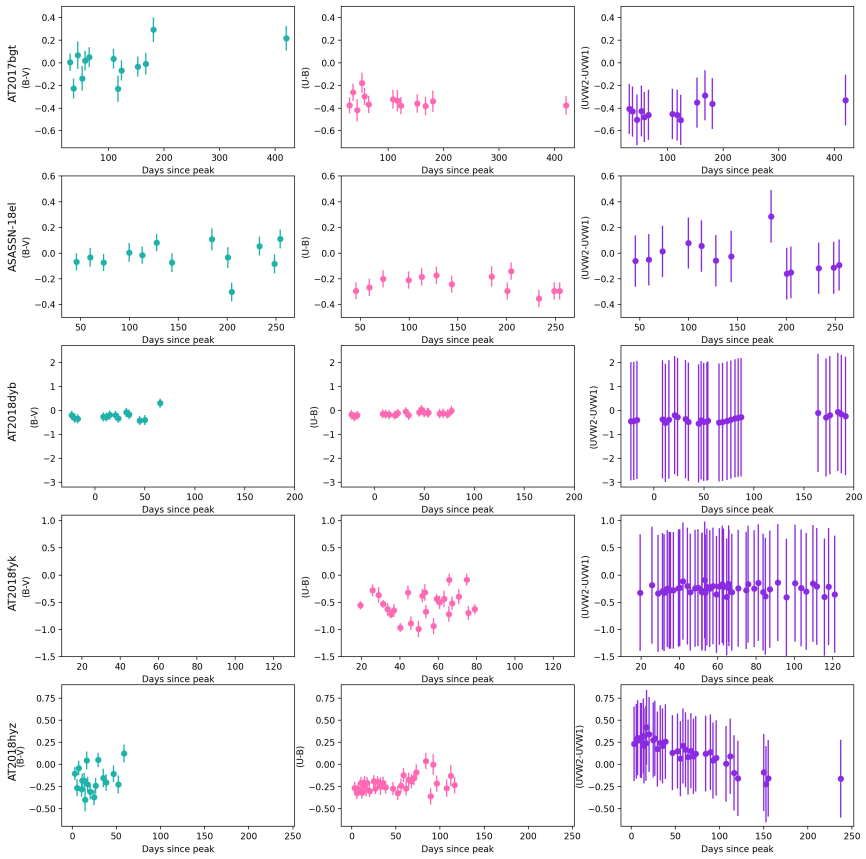

Figure 15. B-V (teal), U-B (pink) and UVW2-UVW1 (purple) colour indices for the events AT2017bgt, AT2018zf, AT2018dyb, AT2018fyk and AT2018hyz. The TDE AT2018fyk does not have any $B-V$ colour indices shown due to no data remaining after the 20% percentage error cut introduced in the flux density.

the magnitudes of the different bands were subtracted from each other at each epoch in order to obtain B-V, U-B and UVW2-UVW1 colour indices. Colour evolution plots for five events are shown in Fig 15.

Many of the objects have have good data in the UVW2 and UVW1 filters, but very large host magnitude errors due Hinkle et al. (2021)'s [6] synthetic host galaxy error calculations. For example, for AT2019lwu the host magnitude in the UVW2 band was 24.460 $\pm$ 3.262. These errors have been propagated into the UVW2-

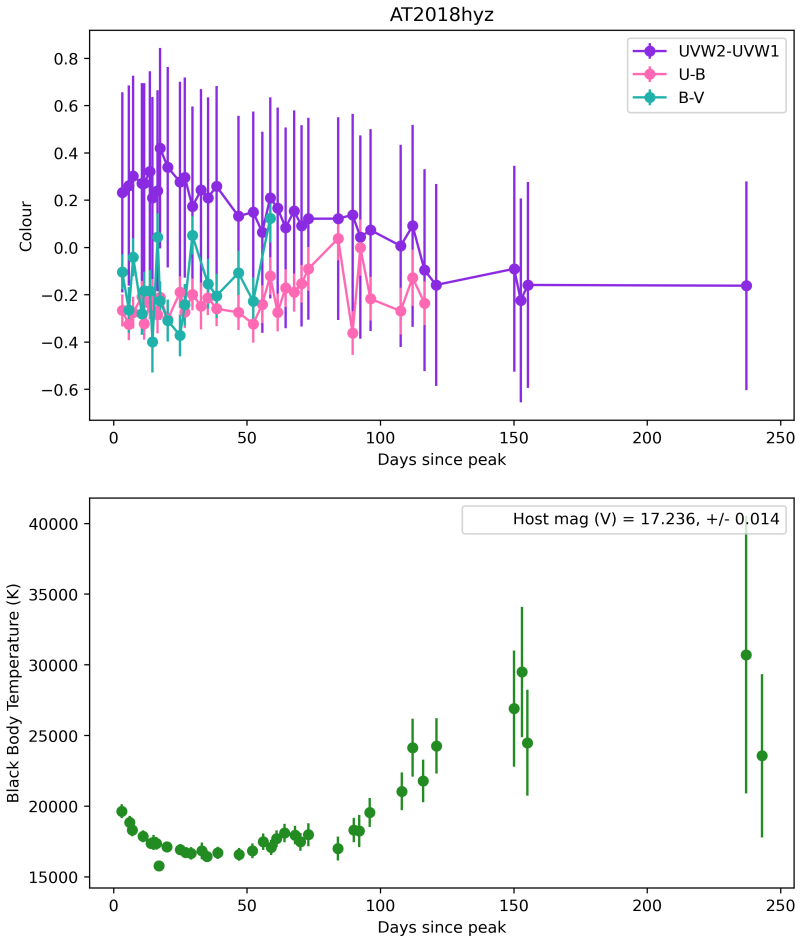

Figure 16. B-V, U-B and UVW2-UVW1 colour indices for AT2018hyz, compared to blackbody temperature evolution

UVW1 colour indices causing very large uncertainties, even despite the 20% flux density error cut.

Many of the events in the sample have relatively flat colour evolution, another hallmark of TDEs. There are a few exceptions to this; we see in Figs 15 that AT2018hyz is steadily getting bluer in the UVW2-UVW1. It is hard to say whether this is also reflected in the B-V and U-B indices as these don't have as many epochs with good data as the UVW2-UVW1 colour index. Meanwhile, the temperature in

Fig 16 initially decreases, evolving from $\sim$ 20,000K at peak, to $\sim$ 16,000K at 17 days post-peak, and then increasing again. This temperature evolution has been noted by Gomez et al. (2020) as a likely result of a contracting photosphere as the accretion rate decreases, due to opaque radiatively driven winds releasing photons at large radii [88][32]. The evolution is also consistent with a PTDE; in which we would expect temperature to fall post-peak as the emission from circularisation drops, and have a second rise corresponding to the the accretion emission becoming dominant. This scenario is further explored in section 5.7.3.

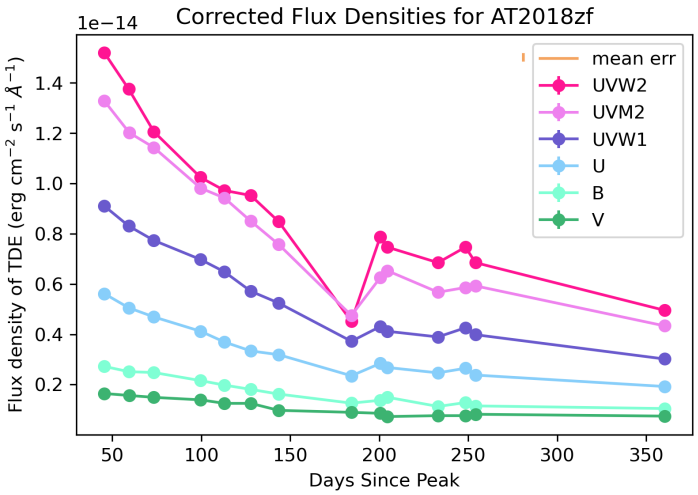

Figure 17. Flux density lightcurves of AT2018zf in UVW2, UVM2, UVW1, U, B and V filters. Mean error is shown in orange in the top right hand corner.

We see that for AT2018zf in Figs 15 and 18 there is a sudden reddening in UVW2-UVW1 at 184 days post-peak. This corresponds to a dip in the lightcurves (as in Fig 17), which is most pronounced in the UVW2 and UVM2 bands, while it is smaller in the UVW1, U and B filters and unnoticeable in the V band. While this increase is not evident in the B-V or U-B indices, there is an additional dip at 205 days post-peak in the B-V colour. This corresponds to a small decrease in flux density seen in certain bands (V, U, UVW1, UVW2) while it is a small increase in other bands (UVM2 and B). This dimming and reddening is also consistent with the blackbody temperature decrease measured as this time, noticeable in Fig 18. This

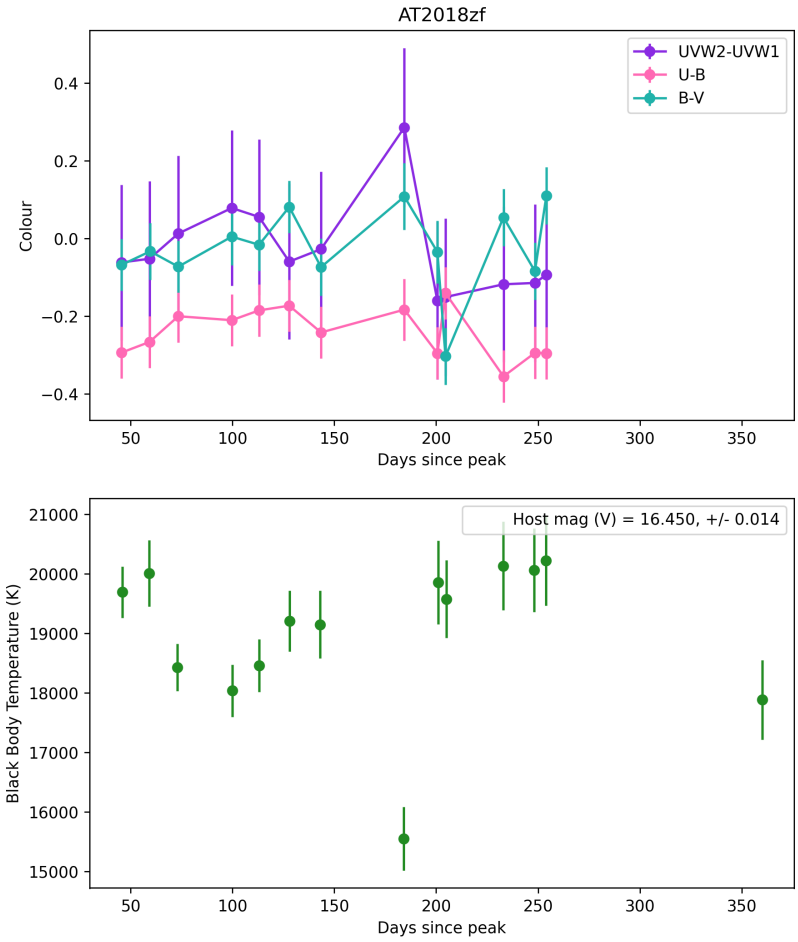

Figure 18. B-V, U-B and UVW2-UVW1 colour indices for AT2018zf, compared to blackbody temperature evolution

event was noted by Hinkle et al. (2022) for its variability, a feature of AGN activity [86], which would explain the colour and blackbody temperature evolution.

AT2019ahk also has interesting colour evolution; There are three distinct colour evolution gradients seen in Fig 19, corresponding to 32 days pre-peak up to 19 days pre-peak, 19 days pre-peak to 15 days post-peak, and finally from 15 days onwards. This is consistent with the luminosity and temperature bump at 32 days pre-peak discussed in section 3.2.6. The three phases of colour evolution are also

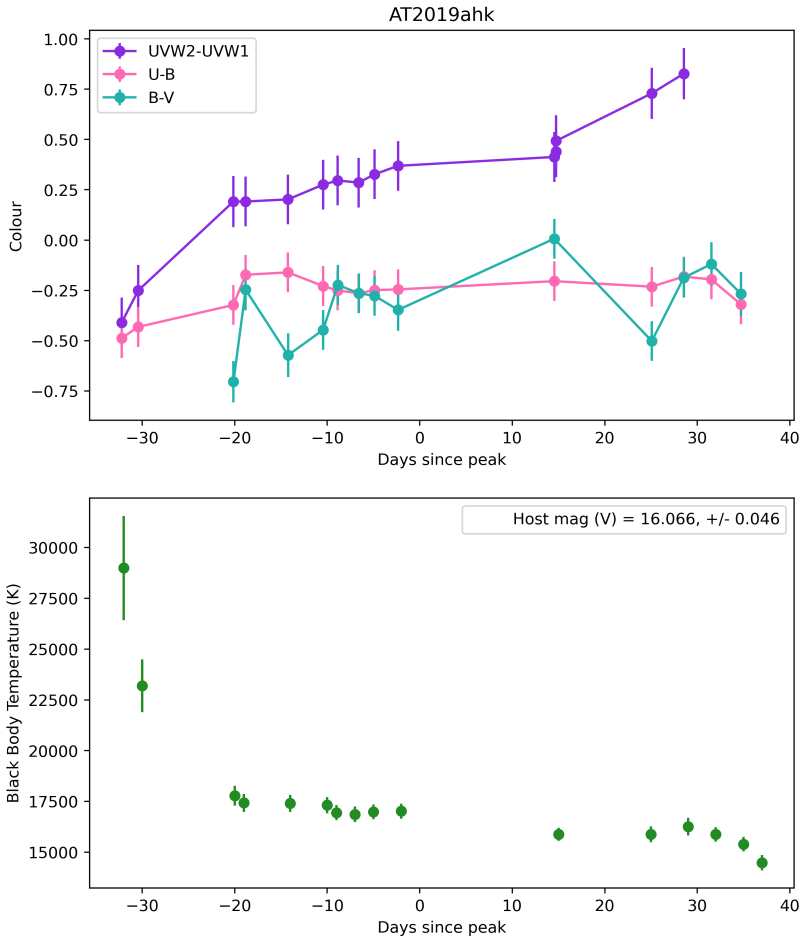

Figure 19. B-V, U-B and UVW2-UVW1 colour indices for AT2019ahk, compared to blackbody temperature evolution

consistent with the temperature evolution seen in Fig 19, of initial rapid cooling, followed by a fairly flat temperature, and then further cooling. Since AT2019ahk is one of the best-studied TDEs pre-peak, it is difficult to say whether its early rapid cooling is typical of TDEs or not, though early-time cooling has also been observed in ASASSN-14ae and AT2019qiz (further explored below)[40]. Hung et al. (2021) postulate that the initial cooling in these events could be a result of photon trapping[40], in which most of the matter from the disrupted star forms an

optically thick, expanding outflow which encompasses the black hole, and suppresses emission [35]. The gas cannot cool radiatively, causing high temperatures[35]. It is only when the trapped photons reach a radius at which the time for photon diffusion is less than the outflow expansion time, that the photons can radiatively diffuse and the ejecta can cool.[35] After a period of rapid cooling, such as the one observed for AT2019ahk, the temperature then flattens, causing the relatively steady temperatures generally associated with TDEs. Photon trapping would cause the lightcurve to track a more shallow decline at early times than $t^{-5/3}$ which is associated with mass fallback. With only 6 post-peak bolometric luminosity data points to fit, the luminosity decline power-law index obtained for AT2019ahk was not well constrained, with a value of $\alpha = 2.158 \pm 2.330$. With such large errorbars, and a lack of Swift data in the days following the peak, this is an inconclusive piece of evidence as to whether freshly un-trapped photons are in fact driving AT2019ahk's initial cooling. However, more early-time TDE observations are needed in order to understand whether the behaviour of AT2019ahk is common.

In Fig 20 AT2018cow's colour evolution is initially flat, but at ~ 5 days post-peak the UVW2-UVW1 colour index starts to increase, meanwhile at 10 days post-peak the U-B colour starts decreasing. The decrease in U-B and temperature is expected since AT2018cow becoming bluer over time was discussed in section 3.2.8. However, the UVW2-UVW1 index is becoming redder. This would imply that there are two distinct mechanisms occurring simultaneously. One, the driving mechanism of the U and B band light, is heating up. Meanwhile the driving mechanism of the UVW1 and UVW2 bands of light is cooling, which is the dominant process since the blackbody temperature continues to cool until around 30 days post-peak. This is corroborated by the lightcurves of AT2018cow in which the UVW1 and UVW2 fluxes are an order of one greater than the U and B. (See Appendix B for this lightcurve, as well as black body radius, black body temperature and colour evolutions of the rest of the events, and luminosity power-law fits.) After 30 days, there looks to be

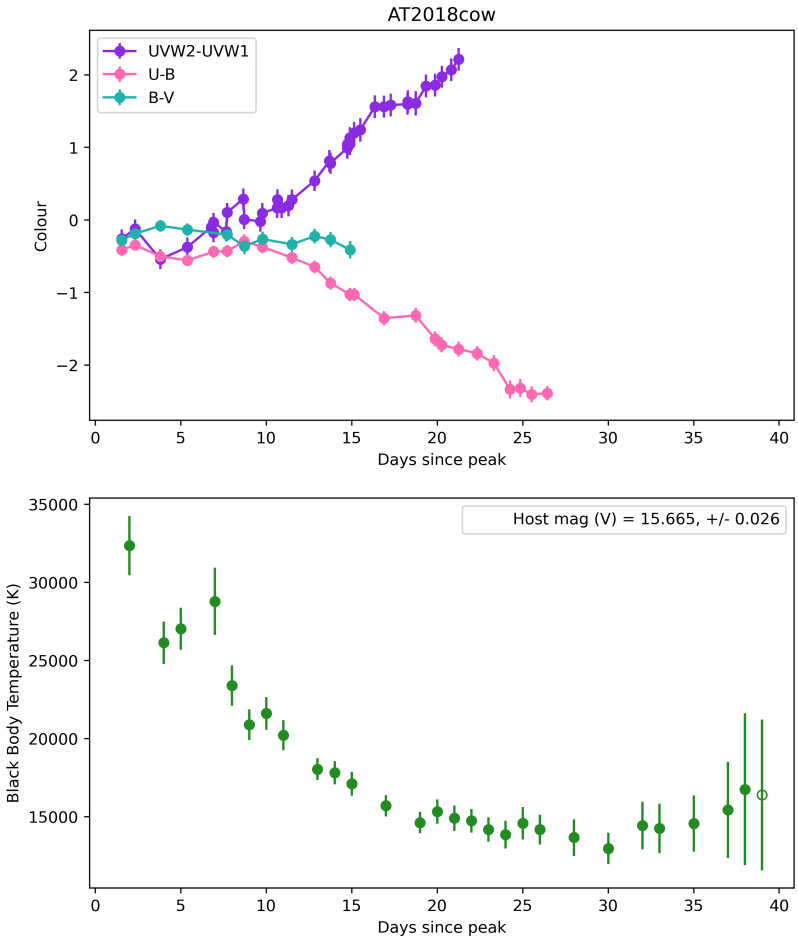

Figure 20. B-V, U-B and UVW2-UVW1 colour indices for AT2018cow, compared to blackbody temperature evolution.

a slight increase in blackbody temperature, though it may be a plateau since the uncertainties in temperature at these epochs are higher. These distinct components may be a reflection of the two main theories on the source of UV/optical light in TDEs; one component may derive primarily from X-ray reprocessing, while the other may be predominantly a result of stream-stream collisions. Though, for the reasons detailed in section 3.2.8 , the reader is reminded that AT2018cow's status as a TDE candidate is tenuous.

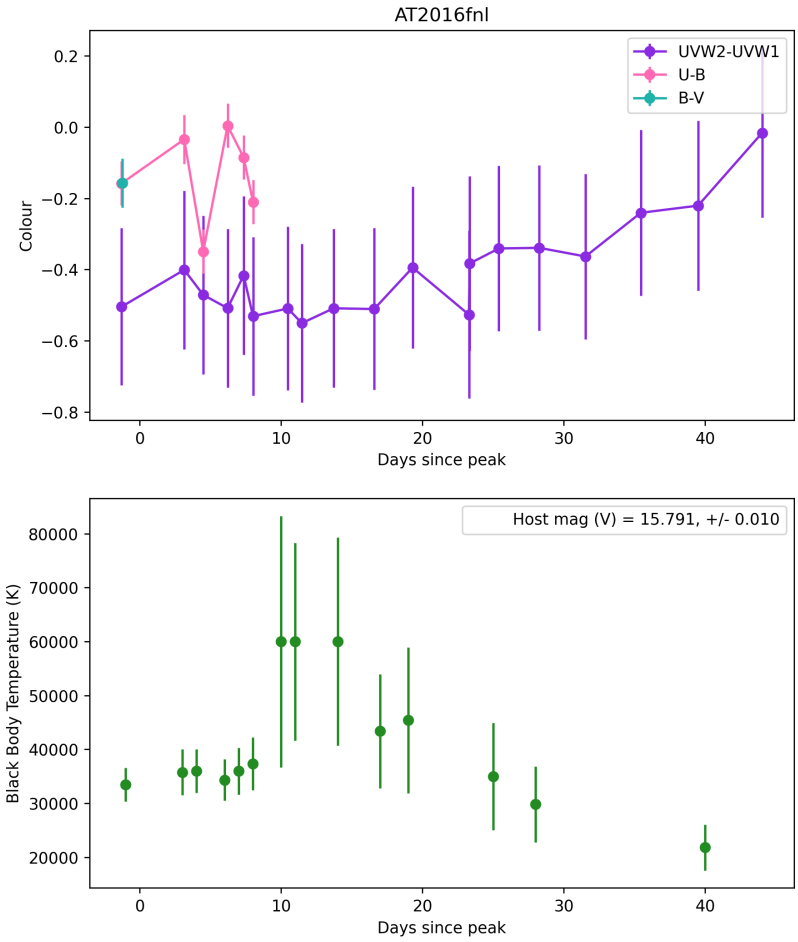

Figure 21. B-V, U-B and UVW2-UVW1 colour indices for AT2016fnl (top) and blackbody temperature evolution of the event (bottom).

Both the colour, and temperature evolution of iPTF16fnl in Fig 21 are initially flat. There appears to be a temperature increase at 10 days, and at 14 days post-peak the temperature starts to decrease, meanwhile at $\sim$ 22 days post-peak the colour starts to redden. There is a small dip in the UVW2-UVW1 colour at 22 days post-peak, which corresponds to a small bump in the UVW2 lightcurve at this time. In the literature for this event, there is tension as to its blackbody temperature and its evolution; Blagorodnova et al. (2017) put it as a non-evolving temperature of

19,000 ± 2,000K [26], while Brown et al. (2018) put it as $\gtrsim$ 30,000 K and note a little a small change in temperature within the first 30 days [105]. This discord is driven by the different UV host galaxy fluxes taken by the respective authors during the host subtraction data reductions. My results favour Brown et al (2018)'s version [105]; the temperatures are high and there appears to be an increase in temperature at around 10 days (though this is not reflected in the colour evolution, and the uncertainty in the temperature is particularly large at this time), followed by a decrease which is accompanied by a reddening of the UVW2-UVW1 colour at the same time. The temperature and colour evolution of AT2016fnl may be consistent with a PTDE scenario as postulated by Blagorodnova et al. (2017) [26]. PTDEs are expected to have two-phase emission mechanisms and when the second mechanism (accretion) starts to dominate, temperature rises correspondingly, and then cools again once the strength of the emission lessens. A PTDE explanation is further explored in section 21.

AT2018zr exhibited a UV re-brightening at $\sim$ 50 days post-peak. This was coincident with the UVW2-UVW1 colour becoming bluer and the temperature rising. At early times AT2018zr may not have been blue, the opposite of what is expected in a TDE, however this may just be due to large errorbars. van Velzen et al. (2019) speculate that AT2018zr had both a low and high temperature component, the hotter of which became more prominent over time as the cooler one faded, giving rise to the observed increases in blackbody temperature and luminosity[93]. This is supported by evidence of blue excess at early times [93]. The evolution of AT2018zr is reminiscent of a PTDE in that a second emission mechanism becomes dominant at a later time, corresponding to a rebrightening and temperature increase. This possibility is further explored in section 5.7.6.

We see in Fig 23 that AT2019qiz started to rapidly cool after peak, by $\sim$ 10,000K over a period of 32 days. After this initial cooling, the temperature starts picks up again, though there is an additional dip from 51 days - 84 days. While the UVW2-

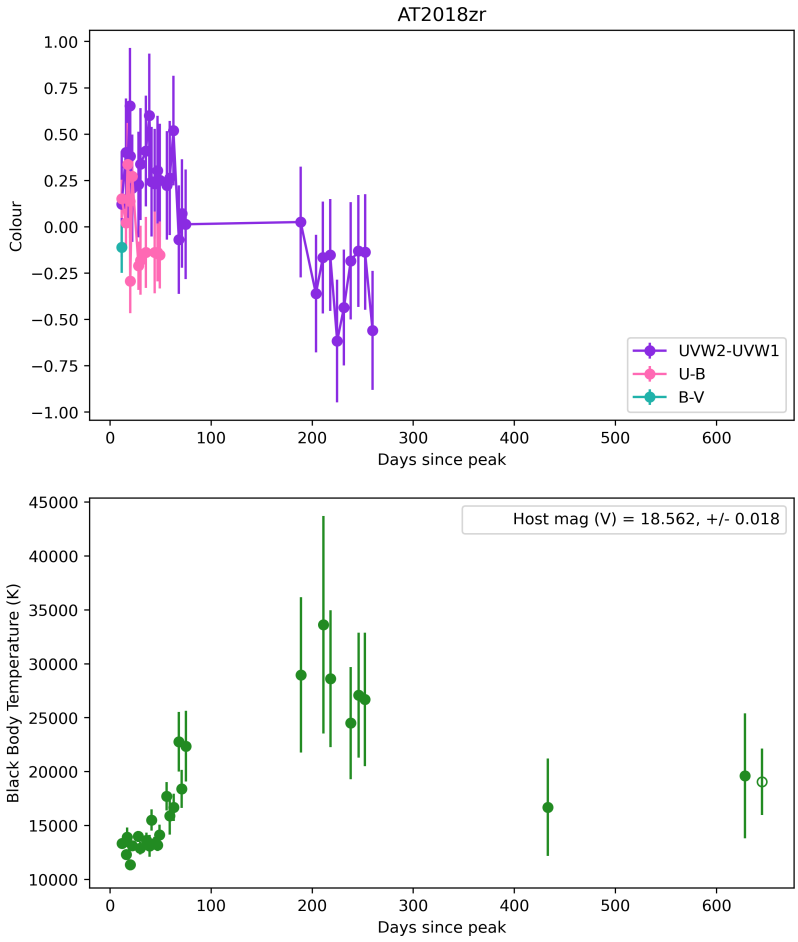

Figure 22. B-V, U-B and UVW2-UVW1 colour indices for AT2018zr

UVW1 colour evolution does initially track that of the temperature evolution, becoming bluer in the fist few days as the temperature initially increases, and redder as the temperature decreases, it continues to steadily redden, even as the temperature decrease ceases. Hung et al. (2021) note that the initial temperature decline is consistent with the effects of photon trapping [40][35]. However, they do not observe a second temperature dip[40]. Notably, this different temperature evolution I observe does not appear to be a result of difficulty in fitting late-time data with SEDs, since this event did not have any much higher energy SED fits. Photon trapping would

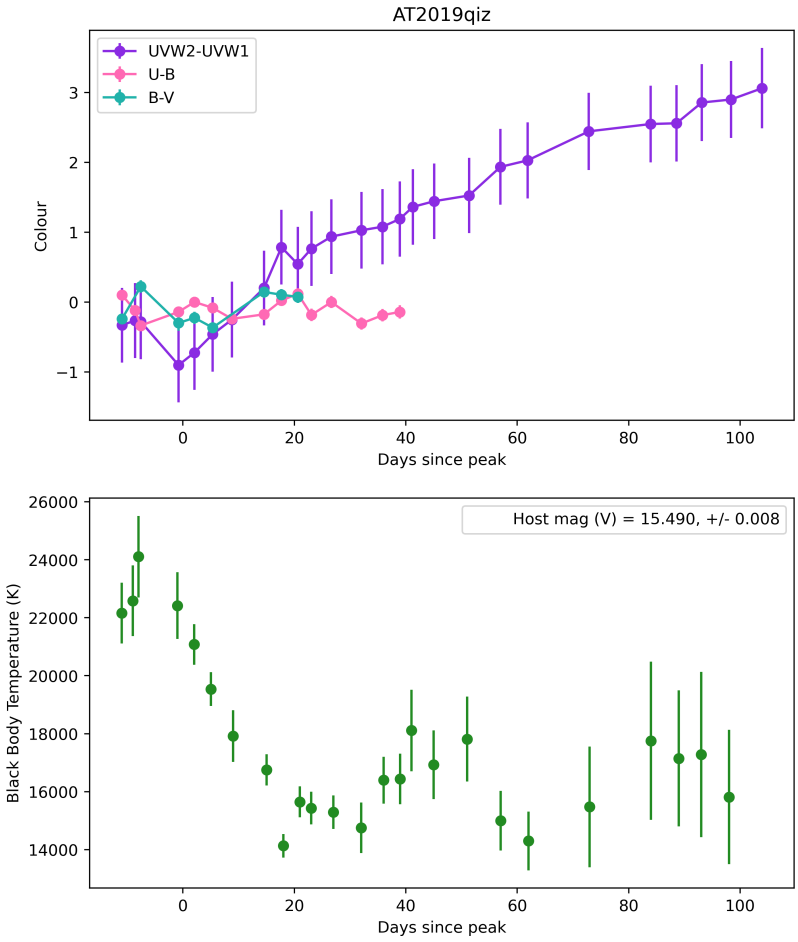

Figure 23. B-V, U-B and UVW2-UVW1 colour indices AT2019qiz

cause a flatter luminosity evolution at early times than the $t^{-5/3}$ expected which corresponds to mass fallback [35].[40] This is not observed in AT2019qiz, which has a luminosity decline power-law index α value of 1.904 ± 0.2018, and is well described by the $\alpha = 5/3$ fit, even at early times.

5.6 Black Hole and Disrupted Star's Mass

Ryu et al's (2020) `TDE mass inference software` [183] was implemented to infer the disrupted star and black hole masses of 10 events. After inputting the observed

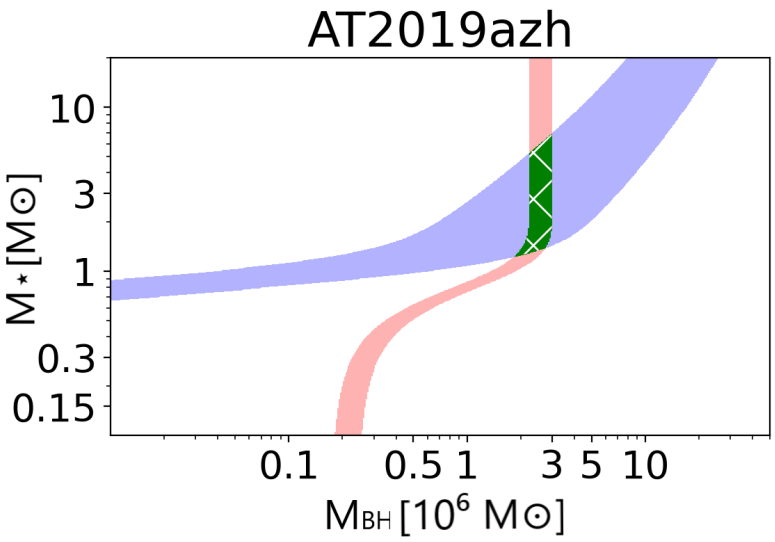

Figure 24. Graph of possible black hole and star masses for AT2019azh. Pink denotes the range that the black hole mass can occupy, given the input parameters and purple indicates the same for the star's mass. The green intersection is the range of masses which would correspond to a tidal disruption event, given the input values.

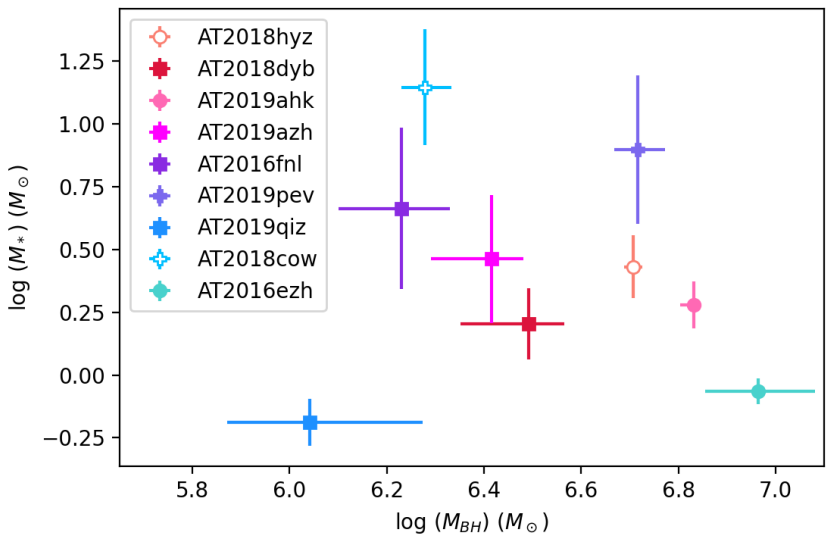

Figure 25. Inferred black hole and disrupted star masses for 9 events. The open markers denote that the inputted luminosities and temperatures were from post-peak data, so there is additional uncertainty in these data. A square marker indicates that the event has been spectrally classified as TDE-H+He, a circle indicates a TDE-H classification, and a cross indicates that the event has not been classified as a TDE.

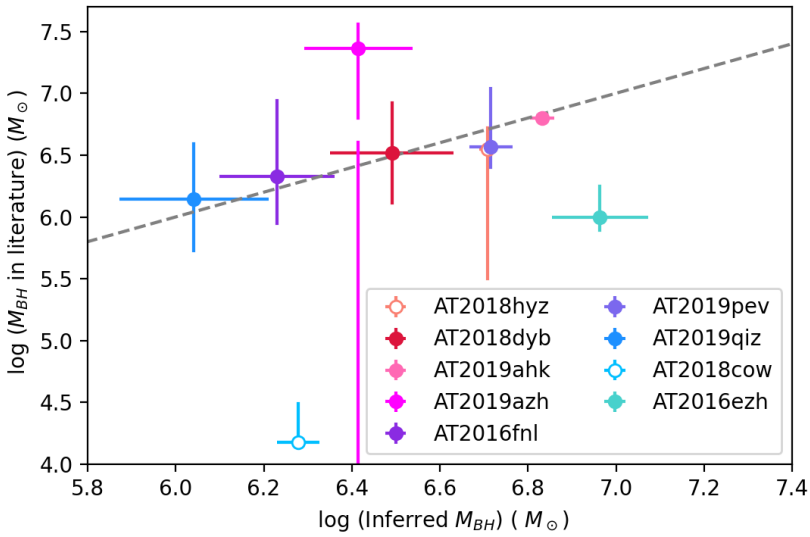

Figure 26. Black hole masses inferred by other means in the literature against those inferred via Ryu et al (2020)'s TDE mass inference software[183]. The grey dashed line indicates where they would be equal. AT2018hyz and AT2018cow are shown as open markers as the software used post-peak values, rather than peak values. Literature black hole masses were obtained via [90], [87] , [184], [29], [118], [140], [185] [26], [40], [142] and [185].

values of blackbody temperature at peak and L_{peak} (given in Table II, the programme solves the following equations for black hole mass $M_{BH,6}$ (in units of 10^6 $M_\odot$) and disrupted star's mass M_* (with units $M_\odot$),

$$T_{BB} = (\frac{L_{peak}}{\sigma \Delta\Omega c_1^2 a_0^2})^{1/4} = 2.3 \cdot 10^4 (\Delta\Omega/2\pi)^{-1/4} c_1^{-3/4} \cdot M_{BH,6}^{-3/8} \Xi^{9/8}(K)[183] \quad (21)$$

and

$$\Delta v = (2\Delta E/c_1)^{1/2} = 6400 M_{BH,6}^{1/6} M_*^{-1/9} c_1^{-1/2} \Xi^{1/2}(kms^{-1})[183] \quad (22)$$

where σ is the Stefan–Boltzmann constant, Δv is the characteristic orbital speed of accretion flow, ΔE is the width of the debris' specific energy distribution and a_0 and Ξ are given by:

$$a_0 = GM_{BH}/\Delta E[183] \quad (23)$$

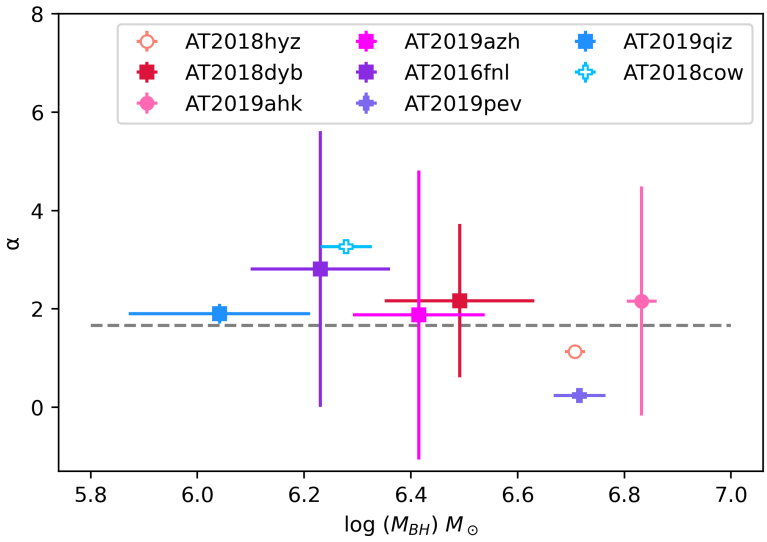

Figure 27. Luminosity index α against black hole mass for 8 different events, with a straight line (grey) indicating the fallback rate for a TDE at α=5/3. Spectral type is indicated by square (TDE-H+He) or circle (TDE-H), while the events without TDE classification are indicated with a cross. AT2016ezh has been ommitted since it didn't follow the typical TDE decline on account of its two peaks.

$$\Xi = \Delta E/\Delta\epsilon [183]. \tag{24}$$

$c_1 \cdot a_0$ is the distance from the black hole where a significant amount of energy has been dissipated by shocks, and $\Delta\Omega$ is the solid angle, corresponding to an emitting region with an effective surface area of $\Delta\Omega(c_1 a_0)^2$. The parameters c_1 and $\Delta\Omega$ are not well understood and have been set to 1 and 2 respectively, as advised by Ryu et al. (2020)'s [183] guide to the software. This will cause an unknowable uncertainty in the outputted parameters, since we cannot know how large the effect of this assumption will be.

M_{BH} is obtained by the software from:

$$M_{BH} = 0.5(T_{BB}/10^4)^{-8/3}(\Delta\Omega/2)^{-2/3}c_1^{-2}\Xi(M_{BH}, M_*)^3 m_* =$$
$$5(L_{peak}/10^{44})^{9/4}(T_{BB}/10^{4.5})^{-1}(\Delta\Omega/2)^{-1/4}c_1^{3/2}\Xi(M_{BH}, M_*)^{-9/2}\ [183] \tag{25}$$

The software is based on the assumptions that UV/optical light follows a blackbody distribution and that this light arises from shocks close to the apocentre of the orbital debris, rather than subscribing to the X-ray reprocessing model [183]. It assumes that there is indeed a strong relation between black hole mass and peak luminosity, which is the case theoretically, but the observational evidence for this is uncertain[1]. It also assumes total disruption.

Once T_{BB} and L_{peak} have been inputted, the software considered the range of BH and star masses would be possible, and the output given was the range of masses where they could coexist in a physically possible way (see Fig 24 for an illustration of this process). The default model bounds were 0.1-20 $M_{\odot}$ for M_{*} and (0.1 - 50.0) x 10^{6} $M_{\odot}$ for M_{BH}. However, this only corresponded to SMBHs, while AT2018cow has been postulated to accompany an IMBH. So the lower M_{BH} bound was decreased by an order of 1 to account for this possibility.

Inferred black hole mass and star mass were successfully found for nine of the events, as tabulated in Table VI and plotted in Fig 25. All of these black hole masses correspond to supermassive black holes, meanwhile there are a range of stellar masses. However, no result could be found for AT2019fdr, as the range of possible black hole masses did not correspond in a physically realistic way to the range of possible star masses.

I compare the mass estimates obtained with those in the literature in Fig 26. Where multiple literature values exist, I indicate the range between these values. There is generally good agreement between the black hole masses inferred via Ryu et al. (2020)'s methods [183] and the literature values for black hole mass. This is perhaps a little surprising given the assumptions made, and the fact that the inference required only temperature and bolometric luminosity at peak. The fact that this method is able to capture black hole mass well in most cases shows that the model of shocks powering the UV/optical lightcurves is describing the energies of TDEs well, and is evidence supporting the shock origin of the UV/optical

component.

For AT2019ahk, there were 3 literature estimates, which are not all in agreement with each other. The inferred mass I obtain for AT2019ahk is in agreement with van Velzen et al. (2019) who estimated a black hole mass of $< 4 \times 10^6$ $M_\odot$ based on velocity dispersion [142], but not in agreement with Liu et al. (2021) or Hinkle et al. (2021) who between them estimated a black hole mass range of (1.1 - 3.6) x 10^7 $M_\odot$ based on the stellar mass-black hole relation for the galaxy[90], and the bulge mass-bulge mass relation respectively[184]. It is not surprising that Liu et al. (2021)'s and Hinkle et al. (2021)'s estimates are consistent with each other since they both rely on stellar mass of the galaxy. However, it is intriguing that the four methods of mass inference used produce two distinct results.

The inferred mass value for AT2016ezh was not consistent with the literature value. This is likely because the host was an AGN galaxy, and it is thought that TDEs in these galaxies have more efficient luminosities as a result of the extra material available to interact with. Since the luminosity is greater than TDEs corresponding to similar mass black holes, the model assumes a larger mass black hole than actuality.

Interestingly, the black hole supposedly corresponding to AT2018cow was inferred to be a SMBH. This is not at all in accordance with the literature values. As discussed, this event could only be a TDE if it corresponds to an intermediate mass black hole, and Perley et al (2018)'s simulations put the black hole mass as 1.5 x $10^4 M_\odot$ (following Guillochon & Ramirez-Ruiz (2013)'s simulations[31]) or 1.9 x $10^4 M_\odot$ (with the MOSFiT model[186]), and a star mass of 0.6 $M_\odot$ using the MOSFiT model[118]. Meanwhile the values I have obtained using Ryu et al. (2020)'s method [183] puts both the black hole mass and star's mass as an order of 2 greater than Perley at al. (2018)'s. These values should not be physical for reasons already discussed in section 3.2.8 which, given the good general agreement in Fig 26, is more likely an indication that AT2018cow is not a TDE, than that the model used

is lacking. However, it could be that the emission mechanism is different in different events, and that Ryu et al. (2020)'s model [183] is only successful in reflecting events which were powered by shocks.

Since Ryu et al. (2020)'s [183] method of mass inference is generally in good agreement with the literature, the fact that no black hole mass was able to be obtained for AT2019fdr, indicates that the event is not a TDE. It could be that since AT2019fdr resides in a NLSy1 galaxy, it was able to obtain a higher luminosity due to the increased efficiency in AGN galaxies, which may explain the unprecedented brightness of the event, and why the `TDE mass inference software`[183] was unable to pick up on its TDE-origin. However, AT2019fdr is not a confirmed TDE, and could also be a result of AGN activity. The best fit luminosity decline power-law index α I obtain has a large uncertainty, so it is ambiguous as to whether the best fit α value indicates TDE-origin or not. However, the post-peak bolometric luminosity fit where α was a fixed value of 5/3 was a good fit, with a χ^2 value of 0.82, showing its decline was consistent with a TDE. Additionally, the $\tilde{L}_{40}$ value obtained for AT2019fdr, is consistent with the expected decline of a TDE by 40 days given by Eq 20. While it remains ambiguous as to whether AT2019fdr is a TDE or a result of AGN activity, given the decline and the similarities between AT2019fdr and two other TDEs which were the likely source of neutrino detection, I tentatively agree with the TDE-classification by Frederick et al. (2021) [140] of a TDE, and put the lack of inferred black hole mass down to its AGN host origin.

Surprisingly, the inferred black hole for AT2019pev, which was not a TDE but AGN activity, was consistent with the literature value. This indicates that this method should not be used as a form of TDE classification, and traditional methods such as spectra and luminosity decline power-law indices should be adhered to in order to classify TDEs.

The success of this method in inferring black hole masses shows that luminosity is dependent on black hole mass, where previously, observation evidence has been

Table VI. Table of outputted black hole and stars' masses using Ryu et al's (2020) TDE mass inference software [183]

Object Name	M_{BH} ($M_\odot$)	ΔM_{BH} ($M_\odot$)	M_* ($M_\odot$)	ΔM_* ($M_\odot$)
AT2018hyz	5.1 $\cdot 10^6$	0.22	2.7	- 0.78/+ 1.00
AT2018dyb	3.1 $\cdot 10^6$	- 1.0/+ 0.53	1.6	- 0.52/+ 1.4
AT2019ahk	6.8 $\cdot 10^6$	- 0.44/+ 0.24	1.9	- 0.41/+ 0.59
AT2019azh	2.6 $\cdot 10^6$	- 0.74/+ 0.40	2.9	- 1.7/+ 3.9
AT2018cow	1.9 $\cdot 10^6$	- 0.21/+ 0.24	14	- 7.4/+ 6.4
AT2016fnl	1.7 $\cdot 10^6$	- 0.51/+ 0.39	4.6	- 3.4/+ 8.4
AT2019pev	5.2 $\cdot 10^6$	- 0.58/+ 0.67	7.9	- 5.4/+ 10.0
AT2019qiz	1.1 $\cdot 10^6$	- 0.43/+0.59	0.65	-0.14/+0.11
AT2016ezh	9.2	-2.3/+2.5	0.86	-0.1/+0.11

unclear on this matter[187]. This is particularly encouraging, since one of the main goals of TDE-astronomy is to use TDEs to probe properties of black holes, and their surrounding environments.

Figures 25 and 27 split the 8 remaining events into spectral class, with a seemingly clear divide between TDE-H+He and TDE-H classes with TDE-H+He favouring smaller black hole masses. However, of course, with only 9 and 8 datapoints respectively, this cannot be taken for granted. There doesn't appear to be a relation between luminosity decline power-law index α and inferred black hole mass in Fig 5.6, however once again with only a handful of datapoints and large α errorbars, this isn't a particularly meaningful observation.

5.7 PTDE Candidates

There are several events with a decline rate consistent with that of a partially disrupted star which is expected to decline with a rate of $\sim t^{-9/4}$[75], though in the first few months post-peak, may be as steep as t^{-4}[31]. The events with best fit luminosity

Table VII. Table of post-peak power law luminosity fits for $\alpha = 9/4$, the expected decline rate for a PTDE

Object Name	χ^2	Residuals Mean	Residuals Median
AT2018dyb	9.63	$1.05 \cdot 10^{43}$	$1.19 \cdot 10^{43}$
AT2019ahk	1.12	$3.71 \cdot 10^{41}$	$1.57 \cdot 10^{42}$
AT2019azh	33.54	$3.50 \cdot 10^{43}$	$4.87 \cdot 10^{43}$
AT2018cow	10.82	$-5.60 \cdot 10^{41}$	$-1.85 \cdot 10^{41}$
AT2016fnl	1.41	$8.84 \cdot 10^{42}$	$1.22 \cdot 10^{42}$
AT2019fdr	13.41	$8.24 \cdot 10^{43}$	$1.33 \cdot 10^{43}$
AT2019qiz	2.05	$1.50 \cdot 10^{41}$	$1.14 \cdot 10^{41}$
AT2018hyz	18.53	$3.59 \cdot 10^{42}$	$3.45 \cdot 10^{42}$
AT2018hco	14.91	$3.73 \cdot 10^{43}$	$4.02 \cdot 10^{43}$
AT2018dyk	1.97	$6.77 \cdot 10^{42}$	$6.77 \cdot 10^{42}$
AT2018fyk	13.93	$3.03 \cdot 10^{43}$	$3.70 \cdot 10^{43}$
AT2018zr	11.84	$6.08 \cdot 10^{42}$	$5.43 \cdot 10^{42}$

decline power-law index α values consistent with 9/4 are AT2018dyb, AT2019ahk, AT2019azh, AT2018hco, AT2016fnl, AT2018dyk, AT2019fdr and AT2018cow. Of these, AT2018dyk can be ruled out as a PTDE since it has been attributed to a 'changing-look' AGN, rather than a TDE. However, most of these events have large α uncertainties which does not make this observation particularly meaningful. In order to further test their consistencies with a PTDE scenario, additional post-peak bolometric luminosity power-law fits were made for these events, in which α was equal to 9/4, the expected value for a PTDE, such as the one in Fig 28. The goodness of these fits are detailed in Table VII. However, since dimmer events fade more slowly [6], dimmer PTDEs may decline at slower rates than $t^{-9/4}$. The key is that PTDEs are rapid events for their peak luminosities, which can be tested with the $\tilde{L}_{40}$ values detailed in Table V. As previously warned, comparing potential PTDEs to the relation given in Eq 20 and obtained by Hinkle at al. (2021) may not be the best check for rapid decline, since the relation obtained used most of the events plotted in Fig 14[6]. If any of the events used were in fact PTDEs, this will have created a bias in the relation towards more rapid events.

While AT2018cow's α value is consistent with a PTDE, and the event was well-described by the $\alpha = 9/4$ power-law fit, its brightness (the B band apparent magnitude 3 days post-peak was 13.70) surely rules it out as a PTDE candidate. It could not be plotted in Fig 14 for comparison, as the final bolometric luminosity value I had obtained was at 35 days post-peak.

The remainder of the events with luminosity decline power-law indices α consistent with a PTDE, as well as some which have previously been noted in the literature as PTDE candidates, and some events with evolutions which I find to be consistent with a PTDE scenario, are explored further.

5.7.1 AT2016fnl

With a luminosity decline power-law index α value of 2.809 $\pm$ 2.801, AT2016fnl has indeed been earmarked by Blagorodnova et al. (2017) as a potential PTDE as they find an impact parameter β of $\sim$ 0.6, consistent with a PTDE [26]. The event was well described by the $\alpha = 9/4$ power-law fit, with a χ^2 value of 1.41. It experiences a small hump in luminosity at $\sim$ 23 days post-peak which is mainly evident in the UVW2 filter. Though this is very small, so it is difficult to tell whether it is of significance in potential PTDE classification. Fig 21 also seems to show a temperature increase at $\sim$ 10 days, though with the larger errorbars, it is hard to be entirely sure. These increases are signs of a PTDE, since circularising and accretion-related processes are expected to dominate at different times, though the timescales they occur on are shorter than predicted by Chen et al. (2021) [76]. However, it should be noted that theirs is a theoretical model, and does not accurately describe the probable repeating PTDE ASASSN-14ko, so their predicted timescales shouldn't be taken as fact. Comparing with ASASSN-14ko in Fig 14, we see that AT2016fnl could well have declined more rapidly than other TDEs which peaked at the same luminosity, which, more so than the α value, is an indication of a PTDE. However, this is not a concrete statement, given the large $\Delta\tilde{L}_{40}$, it may also lie within, or close to, the observed relation for TDEs given in Eq 20. However, it is at this peak luminosity that the errors on the best-fit relation are narrowest, making it less likely than at other luminosities to lie close to the expected region for TDEs.

While a PTDE scenario seems a good fit, its low luminosity and rapid decline may also be explained by the low mass of the associated black hole or the low mass of the star itself [26]. However, it still remains unclear as to how related peak luminosity and black hole mass are[187].

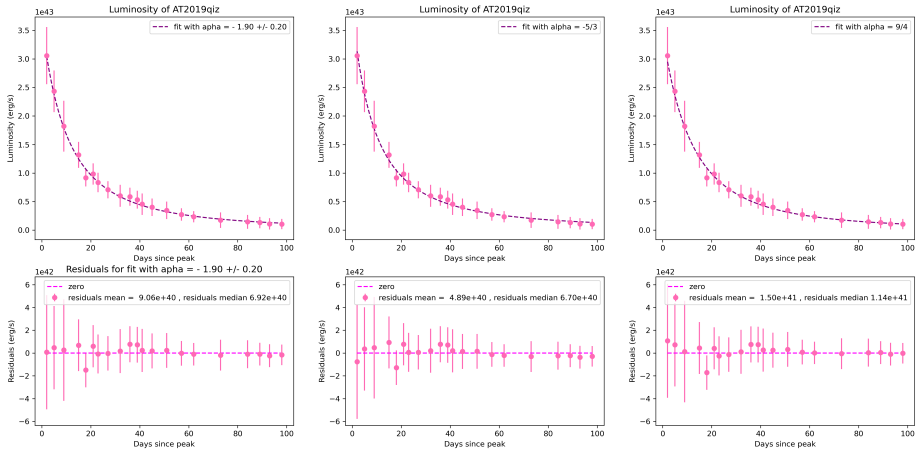

Figure 28. Power-law bolometric luminosity fits for AT2019qiz with power-law index α as a free parameter (left), as 5/3 (centre), and as 9/4 (right). Residuals for each fit are shown in the lower panels.

5.7.2 AT2019qiz

Another potential PTDE in the sample was AT2019qiz [73]. It does indeed have a small luminosity bump at $\sim$ 23 days post-peak. While two-phase emission is expected in PTDEs, this occurs considerably earlier than expected. However, I find the best-fit power-law index α to be 1.904 $\pm$ 0.202 which is more consistent with that of a TTDE. This is in conflict with the value of α obtained for AT2019qiz by Nicholl et al. (2020) of 2.54[96]. That being said, the fit for which α took the fixed value of 9/4, shown in Fig 28, was a successful fit, with a χ^2 value of 2.05.

AT2019qiz is neither a bright, nor a dim TDE (with a peak B band flux of $\sim$ 4 x 10^{-15} erg cm^{-2} s^{-1} $^{-1}$), while we would generally expect a PTDE to be dimmer. In Fig 14, AT2019qiz's decay rate is well-constrained and consistent with the expected rate given by Eq 20. Between the medium-brightness event, typical decay rate, and best fit α value, it seems unlikely that AT2019qiz's origin was a partial event.

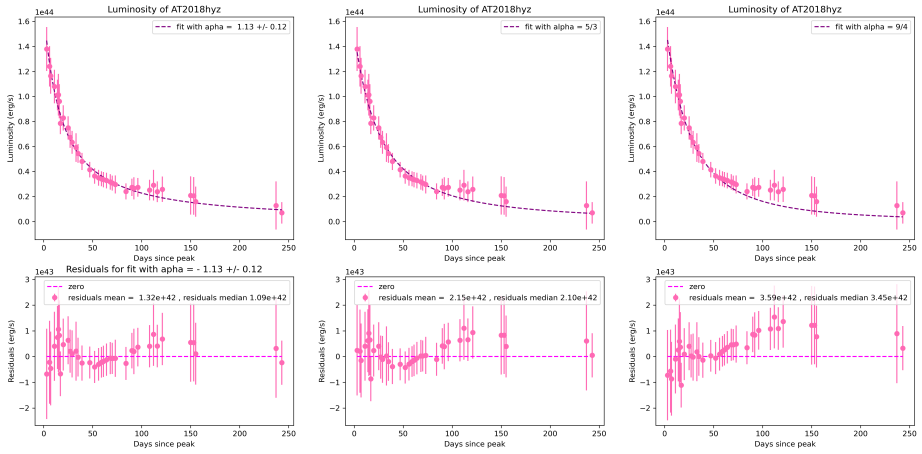

Figure 29. Power-law bolometric luminosity fits for AT2018hyz with power-law index α as a free parameter (left), as 5/3 (centre), and as 9/4 (right). Residuals for each fit are shown in the lower panels.

5.7.3 AT2018hyz

AT2018hyz is another event which has been considered a PTDE candidate in the literature, based on its double-peaked nature and modelled impact parameter β = 0.6 [88]. The second peak occurs at $\sim$ 100 days after the first[88]. This is also coincident with a rise is blackbody temperature, seen in Fig 16 which is an expected feature of PTDEs. However, the peak blackbody radius I obtain is $\sim$ 1.3 x 10^{15} cm, which is larger than would be expected for a PTDE, though Chen et al. (2021) warn that PTDEs may not be well approximated as blackbodies during circularisation [76], making this obtained blackbody radius dubious if it were indeed a PTDE. The best-fit α value I obtain, of 1.135 $\pm$ 0.1209, is not consistent with the expected PTDE fallback rate. This also remains an ambiguous piece of evidence since PTDEs' lightcurves are not entirely tracking mass-fallback, given their more disjointed dependence of circularisation and accretion [76], and since dimmer events decay less rapidly [6]. At early times the power-law fit with α = 9/4, shown in Fig 29 is describing the data well, but after $\sim$ 50 days, this is no longer a good fit. In Fig 14, AT2018hyz is consistent with the expected luminosity decline rate. Given

the average decline rate, low α, and poor $\alpha = 9/4$ fit, AT2018hyz is not consistent with a PTDE-scenario.

5.7.4 AT2018fyk

In this sample, AT2018fyk is the considered the best PTDE candidate in the literature, since a rebrightening occurred $\sim$ 2 years after the first peak, indicating a possible repeating TDE. The lightcurve shape does support a PTDE explanation; there is a hump from $\sim$ 32 days post-peak - $\sim$ 70 days which is an indication of an accretion disk forming. The timings of this aren't consistent with the model proposed by Chen et al. (2021) [76] and discussed in section 2.13. The best fit luminosity decline power-law index α value obtained of 0.756 $\pm$ 0.2763 is also not consistent with the expected fall back rate for PTDEs; though the given the χ^2 value of 6.30, this is not particularly meaningful. Additionally, the $t^{-9/4}$ fit was not particularly successful with a χ^2 value of 13.93.

Unfortunately, the first Swift epoch for this event was at 19 days post-peak, and with no peak data it was impossible to compare with the expected decline relation and ASASSN-14ko in Fig 14. However, even at 19 days post-peak, the bolometric luminosity is 3.54 x 10^{44}, making this a bright event, with a shallow decline rate, the opposite of what is expected in a PTDE (though the α value obtained is questionable, given the high χ^2 value). If AT2018fyk is not a PTDE, the rebrightening at 2 years after peak may be a result of disk instability or a SMBH binary [115]. However, this question might soon be answered since according to the PTDE scenario, it is predicted to undergo further dimming in August 2023, and another rebrightening in March 2025 [188].

5.7.5 AT2016ezh

To the best of my knowledge, a PTDE scenario has not been considered in the literature for the AGN-based TDE AT2016ezh. However, it is worth considering

as its double-peaked lightcurve could be consistent with the two-phase emission expected in PTDEs. A $t^{-9/4}$ fit was not performed for this event due to its double-peaked nature, however, free-α fits were performed on data after both the first and second peak, which are given in Table III. The first peak's fit was not well constrained, and though better constrained, the α value of the second peak (of 0.44 $\pm$ 0.71) is lower than would be expected of a TTDE, and certainly lower than would be expected of a PTDE. Though in this case, the second peak would not be tracking mass fallback since the accretion disk has already formed by this point. Once again, a better indication of decline rate is the event's luminosity at 40 days post-peak. We see in Fig 14 that AT2016ezh is not a rapidly declining event, and is consistent with the relation given in Eq 20. Therefore, a potential PTDE classification has no basis. However, as Chen et al. (2021) warn, that the effects of an AGN-environment on a PTDE are not understood[76].

5.7.6 AT2018zr

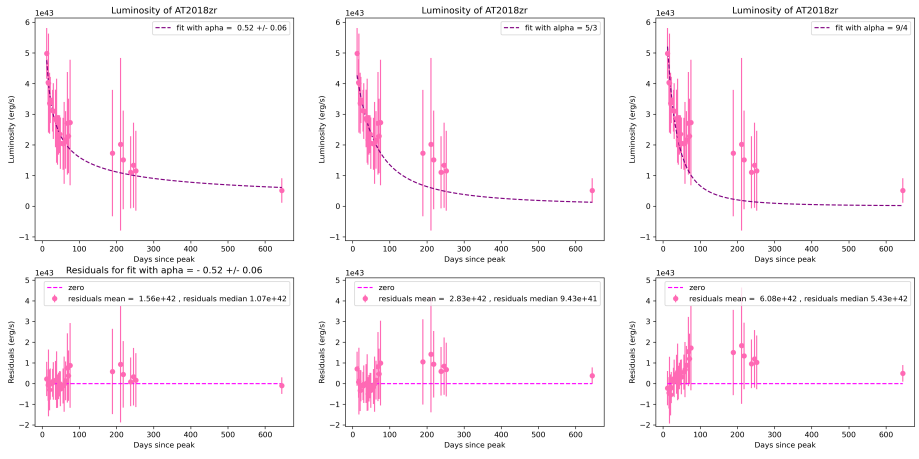

Figure 30. Power-law bolometric luminosity fits for AT2018zr with power-law index α as a free parameter (left), as 5/3 (centre), and as 9/4 (right). Residuals for each fit are shown in the lower panels.

AT2018zr presents an intriguing possibility for a PTDE candidate. It was a fairly

dim event with the bolometric luminosity at 12 days post-peak (the first epoch for which there was Swift data), of $\sim$ 5 x 10^{43} erg/s. Additionally, it experienced a rebrightening corresponding to an increase in temperature at $\sim$ 50 days post-peak, seen in Fig 22. Holoien et al. (2019) put this down to the late-time formation of an elliptical disk[139]. This is consistent with the expectation that PTDEs exhibit more distinct two-phase emission, with the formation of an accretion disk leading to a secondary increase in luminosity and temperature. The best fit luminosity decline power-law index obtained was not consistent with the PTDE scenario, at $\alpha = 0.5166 \pm 0.06132$. Furthermore, for the fit where α lay at a fixed value of 9/4, shown in Fig 30, the fit was not in good agreement of the data, with a χ^2 value of 11.84. Unfortunately, no $\tilde{L}_{40}$ value could be obtained due to lack of peak data.

5.7.7 iPTF15af

The TDE iPTF15af was found to have an impact parameter β of $0.10^{+0.36}_{-0.1}$ by Blagorodnova et al. (2019)[97], indicative of a PTDE. In the UVW1 and UVW2 filters there does seem to be a slight hump after peak which may be a result of the two-phase emission expected in PTDEs. Unfortunately, beyond this, not many comments can be made, as the SED fits mostly only used three filters, resulting in high uncertainties for the blackbody temperatures, radii and luminosities. After the 40% error cuts, this only leaves one epoch with blackbody radius and bolometric luminosity data, and two epochs with blackbody temperature data.

5.7.8 AT2018dyb, AT2019ahk and AT2019azh

AT2018dyb, AT2019ahk, AT2019azh all had α values consistent with a PTDE, with $\alpha = 2.166 \pm 1.559$, 2.158 ± 2.330, and 1.878 ± 2.938 respectively. They were all bright events (with B band peaks $\sim$ 0.6 - 1 x 10^{-14} erg cm^{-2} s^{-1} $^{-1}$). This makes their status as PTDE candidates less likely, since the limited material bound to the black hole makes this class of TDE less luminous, but it is not impossible for a

PTDE to be on the brighter side if the star's mass was large in the first place, or had an efficient dM/dt[97]. In section 5.6 I obtain progenitor star mass estimates for all three of these stars. However, the method used assumes total disruption, so they cannot be used here to determine whether the masses were large enough to cause these peak luminosities.

We must also further consider their decline rates; though AT2019ahk was well described by a post-peak bolometric luminosity power-law fit with a fixed α value of 9/4, we see in Fig 14 that AT2019ahk does not have a rapid decline rate for its brightness, and so cannot be a PTDE. It seems that AT2019ahk having a more rapid decline than the expected $t^{-5/3}$ was simply the result of it being a brighter event.

Despite the large χ^2 value of 9.63, the $t^{-9/4}$ fit is describing the event well. However, in Fig 14, AT2018dyb is consistent with the expected TDE decline by 40 days post-peak, or perhaps more weakly-declining. Therefore, AT2018dyb is not consistent with a PTDE.

Meanwhile, for AT2019azh, power-law fit with $\alpha = 9/4$ was not a good description on the decline, and has a χ^2 value of 33.54. Additionally, the TDE has either a slow decline, or a typical one in Fig 14, showing that the event is not consistent with a partial disruption.

5.8 Comparison with Other Transients

In order to compare the TDE sample with other transients, I plotted a colour-peak magnitude graph for the sample, and a number of events categorised as supernova Types Ia, Ib, Ic, and IIP, shown in Fig 5.8. The B-V colour was chosen as this was the filter that I had analysed data for which was most abundantly available across the different transient types. This proved to be somewhat problematic for my own sample, as not all of the transients with peak data had B-V colours after the 20% percentage error cut introduced in the flux densities. This left only 6 TDEs

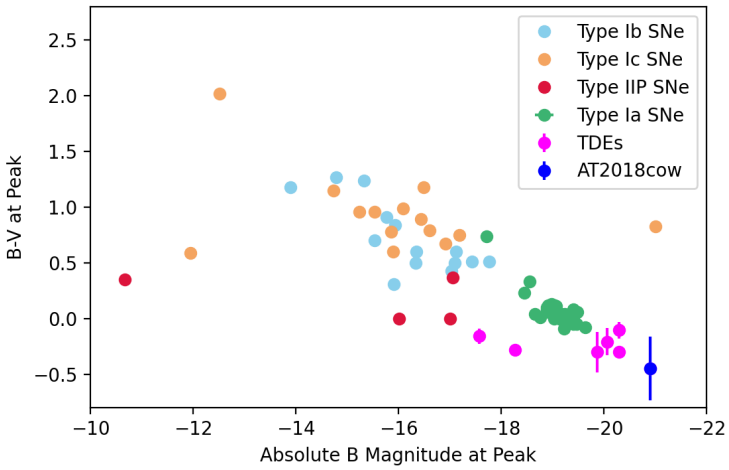

Figure 31. B-V colour at peak luminosity against absolute B band magnitude at peak for different transient types; Ia supernovae (green), Ib supernovae (light blue), Ic supernovae (orange), IIP supernovae (red), TDEs from this sample (pink) and the FBOT AT2018cow (dark blue). The TDEs in the figure are (left to right) AT2016fnl, AT2019qiz, AT2018dyb, AT2019azh, AT2018hyz (far right, upper), and AT2019ahk (far right, lower). Type Ia supernovae data were acquired from Hamuy et al. 1996[189], Ib and Ic data from Jin et al. (2023) [190]. Type IIP data was obtained via Tsvetkov et al. (2018)[191], Andrews et al .(2019)[192], Teja et. al (2023)[193] and Dong et al. (2021) [194].

and AT2018cow to compare with other transients. Despite the lack of TDEs on the graph, they are occupying a distinct region of the colour-magnitude plot; all the TDEs have blue colours, while the Ib and Ic supernovae have red colours, and the Ia and IIP supernovae may have either red or blue colours, though not as strongly blue as the TDEs. Additionally, the TDEs are brighter than almost all the Ib, Ic and IIP supernovae, with the admittedly small TDE sample spanning -17.6 to -20.3 absolute magnitude. Naturally, with such a small sample of TDEs, definitive statements about their place in the colour plot cannot be made, since we know that there are some TDEs such as AT2016fnl which are considerable dimmer, and there are likely TDEs which overlap with the SNe-Ia on the plot. That being said, SNe-Ia seem to be the only transient with a real danger of being conflated for TDEs when only photometry is available. Fortunately, spectroscopically they are very

distinct objects. TDEs often have blue, featureless continua and broad Balmer and He emission lines, as well as sometimes displaying Bowen fluorescence. Meanwhile Type Ia supernovae, can be easily identified by the intermediate mass element lines in their spectra. Since currently, most TDEs are identified spectroscopically, their shared optical properties aren't generally an issue in identification.

AT2018cow is brighter than the handful of TDEs which are available for comparison, and all but one of the supernovae. However, its colour uncertainty is large, so it is difficult to say whether it is bluer than the other TDEs, though it is certainly bluer than the comparison supernovae.

It would have been useful to compare the colour of AT2019fdr in Fig 5.8 isnce its TDE-origin is not confirmed. However, unfortunately, there is no V data near peak time, so its B-V colour cannot be obtained at peak.

This method illustrates the success of using colour-space to show TDEs' unique properties compared to other transients. With a vaster sample of TDEs, and other transients for comparison, it could be extremely useful in preemptively classifying TDEs. Additionally, TDE candidates such as AT2018cow can be compared to the TDE sample to see if their colours are consistent with a TDE.

6 Future Prospects

The Vera Rubin Observatory Legacy Survey of Space and Time (LSST) [195] promises to be a key tool in adding more TDEs to our catalogues. One of its four main goals is to observe transients, and it is estimated that it will observe tens of thousand of transients every night [196]. In recent years, optically selected TDEs have overtaken X-ray selected to become the main band in which TDEs are discovered. The LSST will observe in the optical and have the largest CCD camera in the world to date. Therefore, our optical capabilities will vastly improve when the LSST starts observing in 2024, which will certainly lead to many more discoveries of optically se-

lected TDEs. It is predicted that over 10 years of LSST's operations, 35,000-80,000 new TDEs will be observed by it[5]. However, if LSST observations are not paired with those of other missions, only 5-10% are expected be classified as TDEs [5]. Fortunately LSST will be aided by The Ultraviolet Transient Astronomy Satellite (ULTRASAT), launching in 2026[197]. ULTRASAT will have the largest field of view of any space-based telescope to date, and will be the first wide-field transient survey[197]. It will alert astronomers as to new transients within 15 minutes of detection, enabling rapid follow-up of objects by other telescopes[197], and ensuring thorough observations of important objects. Combining observations from these missions will ensure that a larger portion of detected TDEs will be identified[197].

With this influx of newly discovered TDEs, we will have vastly more data to work with and this may help answer the many unknowns surrounding the nature of TDEs, such as whether optically and X-ray selected TDEs are distinct populations, what is the UV/optical emission mechanism, and what characteristics of a TDE define the optical/X-ray emission ratio.

These new optical telescopes will discover ~ 1000 new transients per night. Currently, most TDE are classified via spectroscopy. However, it will not be feasible to spectroscopically observe as large a portion of new transients going forward due to their sheer numbers and the scientific community's limited resources. This is where methods, such as the one explored in section 5.8 will come into play; a new transient can be preemptively classified as a likely TDE based on its location within the colour diagram, which will help astronomers decide whether it is an object worth observing spectroscopically, which will confirm whether or not the object is indeed a TDE.

Currently only a handful of TDEs have been well-studied pre-peak. Since the instrumentation will be more sensitive, going forward a higher proportion of TDEs will be detected before peak light. This will help determine whether rapid early-time cooling, as in the case of AT2019ahk is a common occurrence, and whether it was indeed the result of post-trapped photons. More generally, we will have a much

greater understanding of how TDEs behave pre-peak and the processes behind this. My own thesis has been limited by the lack of peak data (e.g. only being able to infer black hole masses for 10 events, and ΔL_{40} values for 8 events), but future publications studying TDE samples will not have this same hindrance, owing to the much larger sample of TDEs observed at peak time. This will also aid in adding to colour-peak magnitude diagrams, such as the one I show in Fig 5.8.

Over the next few years we will be able to observe whether some PTDE candidates are repeating TDEs, e.g. next month (August 2023) AT2018fyk is expected to dim according to the PTDE scenario, and in 2025 a second tidal disruption is expected to occur. For TDEs in the TESS continuous viewing zone or ULTRASAT's field of view, rebrightenings will be easily identified and the possibility of repeated disruptions can be analysed. LSST will also be able to observe dimmer PTDEs than we are currently able to [5][73], which will help to better constrain the PTDE and TTDE rates, as dimmer PTDEs will be less likely to be conflated with TTDEs. Additionally the relation given in Eq 20, may be able to be separated into one for TTDEs, and PTDEs, and become better constrained.

Currently, we are aware that TDEs have a preference for E+A galaxies. Since this is known, TDE searches often focus on these galaxy types, creating a bias in calculated disruption rate for E+A galaxies. However, TDEs have also been observed in a number of other hosts including weak AGNs[166], and ultra-luminous infrared galaxies[55]. We will likely observe TDEs in a wider range of hosts going forward, and, with a much vaster sample of TDEs, the disruption rate, both in general, and for different host types will be better constrained. We will then better understand how large a contribution E+A type galaxies make in the total TDE population.

Future radio blind searches will likely reveal non-thermal TDEs which will better constrain the TDE rate since currently most TDEs are discovered in UV/optical or X-ray searches[27]. Additionally, further radio observations may enable us to study the differences in properties that jetted and non-jetted TDEs possess[27].

An additional way to constrain the TDE rate may be by future multiplexed fiber spectrographic surveys discovering ECLEs, which may provide an independent measurement of the rate[1].

7 Conclusions

I have presented UV and optical analyses of a number of TDEs, as well as TDE candidates and other nuclear transients. These were somewhat hampered by lack of Swift peak data, and the large errors arising from SED fits with few datapoints. Even so, the non-TDE objects stood out as distinct in the sample, by their post-peak decline rates and colour evolution. I showed that simply by using B-V colour, TDEs can often be easily discerned from interlopers, though Type Ia and IIP SNe may sometimes be conflated for TDEs when only photometric data is available. In the case of AT2018cow, which had been proposed to be a TDE corresponding to an IMBH, this thesis does not support this hypothesis; it is bluer and brighter than the TDEs in the sample (for which peak data was available), and its inferred black hole mass was non-physical. Its black body radius at peak was comparable to the TDEs in the sample, but it was a considerably brighter event, indicating a physically distinct phenomenon.

I used Ryu et al. (2020)'s `TDE mass inference software` [183] to infer the black hole and star masses of 9 events, which generally showed good agreement with values published in the literature, lending credence to the shock origin of the UV/optical lightcurve. However, since the method of mass inference also showed good agreement for the AGN event AT2019pev, using this software to classify TDEs based on agreement is not a method that should be undertaken. Despite the lack of inferred black hole mass obtained for the ambiguous event AT2019fdr, I tentatively agree with the TDE classification based on its luminosity decay.

Hinkle et al. (2021)'s [6] relation of more luminous TDEs decaying more rapidly

was not initially agreed with, when comparing luminosity decline power-law index α with peak luminosity, which is likely a result of the very large α uncertainties given by the power-law fits. However, by using the better-constrained quantity $\tilde{L}_{40}$, and comparing with bolometric luminosity at 40 days, I was able to show good agreement between the best fit found by Hinkle et al. (2021) [6] and my own findings. However, this is to be expected since most of the events I found $\tilde{L}_{40}$ values for had been used by Hinkle et al. (2021)[6] to obtain this fit in the first place. By comparing the $\tilde{L}_{40}$ values of TDEs in my sample with those of the probable repeating PTDE ASASSN-14ko, and the best-fit relation given by Hinkle et al. (2021)[6], I showed that only one of the 8 events was consistent with a PTDE, AT2016fnl, while the rest were consistent with TTDEs. This supports discussions in the literature proposing a PTDE origin for AT2016fnl. PTDE scenarios were also considered for a number of other events, with negative or ambiguous conclusions drawn for the remainder of the events.

8 Acknowledgements

I would like to thank my supervisors Doctor Panagiotis Charalampopoulos and Docent Rubina Kotak for their invaluable guidance and direction during this thesis. I would also like the thank Doctor Jason Hinkle for providing vast amounts of the data which this thesis was based on, and for his willingness to explain his methods during private correspondence. Additionally, my gratitude to Christian Vassalo and Wendy Collister for their kindness in advising on the thesis writing process. I acknowledge support from the University of Turku in the form of a full scholarship.

References

[1] Suvi Gezari. Tidal disruption events. *Annual Review of Astronomy and Astrophysics*, 59:21–58, 2021.

[2] Giorgos Leloudas, M Fraser, Nicholas Chamberlain Stone, S van Velzen, PG Jonker, I Arcavi, Christoffer Fremling, JR Maund, Stephen J Smartt, T Krìhler, et al. The superluminous transient asassn-15lh as a tidal disruption event from a kerr black hole. *Nature Astronomy*, 1(1):0002, 2016.

[3] Jack G Hills. Possible power source of seyfert galaxies and qsos. *Nature*, 254(5498):295–298, 1975.

[4] Jennifer L Donley, WN Brandt, Michael Eracleous, and Th Boller. Large-amplitude x-ray outbursts from galactic nuclei: a systematic survey using rosat archival data. *The Astronomical Journal*, 124(3):1308, 2002.

[5] Katja Bricman and Andreja Gomboc. The prospects of observing tidal disruption events with the large synoptic survey telescope. *The Astrophysical Journal*, 890(1):73, 2020.

[6] Jason T Hinkle, Thomas W-S Holoien, Benjamin J Shappee, and Katie Auchettl. A swift fix for nuclear outbursts. *The Astrophysical Journal*, 910(2):83, 2021.

[7] IceCube Collaboration, MAGIC, AGILE, ASAS-SN, HAWC, HESS, INTEGRAL, Kanata, Kiso, Kapteyn, et al. Multimessenger observations of a flaring blazar coincident with high-energy neutrino icecube-170922a. *Science*, 361(6398):eaat1378, 2018.

[8] Richard Abbott, TD Abbott, S Abraham, Fausto Acernese, K Ackley, C Adams, RX Adhikari, VB Adya, Christoph Affeldt, M Agathos, et al.

Gw190521: a binary black hole merger with a total mass of 150 m. *Physical review letters*, 125(10):101102, 2020.

[9] Ann Zabludoff, Iair Arcavi, Stephanie La Massa, Hagai B Perets, Benny Trakhtenbrot, B Ashley Zauderer, Katie Auchettl, Jane L Dai, K Decker French, Tiara Hung, et al. Distinguishing tidal disruption events from impostors. *Space Science Reviews*, 217(4):54, 2021.

[10] Eric C Bellm, Shrinivas R Kulkarni, Matthew J Graham, Richard Dekany, Roger M Smith, Reed Riddle, Frank J Masci, George Helou, Thomas A Prince, Scott M Adams, et al. The zwicky transient facility: system overview, performance, and first results. *Publications of the Astronomical Society of the Pacific*, 131(995):018002, 2018.

[11] Nick Kaiser, William Burgett, Ken Chambers, Larry Denneau, Jim Heasley, Robert Jedicke, Eugene Magnier, Jeff Morgan, Peter Onaka, and John Tonry. The pan-starrs wide-field optical/nir imaging survey. In *Ground-based and Airborne Telescopes III*, volume 7733, pages 159–172. SPIE, 2010.

[12] Benjamin J Shappee, JL Prieto, D Grupe, CS Kochanek, KZ Stanek, G De Rosa, S Mathur, Y Zu, BM Peterson, RW Pogge, et al. The man behind the curtain: X-rays drive the uv through nir variability in the 2013 active galactic nucleus outburst in ngc 2617. *The Astrophysical Journal*, 788(1):48, 2014.

[13] Sjoert van Velzen, Thomas W-S Holoien, Francesca Onori, Tiara Hung, and Iair Arcavi. Optical-ultraviolet tidal disruption events. *Space Science Reviews*, 216:1–33, 2020.

[14] Martin J Rees. Tidal disruption of stars by black holes of 106–108 solar masses in nearby galaxies. *Nature*, 333(6173):523–528, 1988.

[15] ES Phinney. Manifestations of a massive black hole in the galactic center. In *Symposium-International Astronomical Union*, volume 136, pages 543–553. Cambridge University Press, 1989.

[16] Charles R Evans and Christopher S Kochanek. The tidal disruption of a star by a massive black hole. *Astrophysical Journal, Part 2-Letters (ISSN 0004-637X), vol. 346, Nov. 1, 1989, p. L13-L16.*, 346:L13–L16, 1989.

[17] Tsvi Piran, Gilad Svirski, Julian Krolik, Roseanne M Cheng, and Hotaka Shiokawa. Disk formation versus disk accretion—what powers tidal disruption events? *The Astrophysical Journal*, 806(2):164, 2015.

[18] G Lodato, AR King, and JE Pringle. Stellar disruption by a supermassive black hole: is the light curve really proportional to t- 5/3? *Monthly Notices of the Royal Astronomical Society*, 392(1):332–340, 2009.

[19] Michael Kesden. Black-hole spin dependence in the light curves of tidal disruption events. *Physical Review D*, 86(6):064026, 2012.

[20] Enrico Ramirez-Ruiz and Stephan Rosswog. The star ingesting luminosity of intermediate-mass black holes in globular clusters. *The Astrophysical Journal*, 697(2):L77, 2009.

[21] Elen CA Golightly, Eric R Coughlin, and CJ Nixon. Tidal disruption events: the role of stellar spin. *The Astrophysical Journal*, 872(2):163, 2019.

[22] Emanuel Gafton and Stephan Rosswog. Tidal disruptions by rotating black holes: effects of spin and impact parameter. *Monthly Notices of the Royal Astronomical Society*, 487(4):4790–4808, 2019.

[23] Sjoert Van Velzen, Suvi Gezari, Erica Hammerstein, Nathaniel Roth, Sara Frederick, Charlotte Ward, Tiara Hung, S Bradley Cenko, Robert Stein, Daniel A Perley, et al. Seventeen tidal disruption events from the first half

of ztf survey observations: entering a new era of population studies. *The Astrophysical Journal*, 908(1):4, 2021.

[24] S Komossa. Tidal disruption of stars by supermassive black holes: Status of observations. *Journal of High Energy Astrophysics*, 7:148–157, 2015.

[25] Jo Ho Lacy, Co Ho Townes, and Do Jo Hollenbach. The nature of the central parsec of the galaxy. *Astrophysical Journal, Part 1, vol. 262, Nov. 1, 1982, p. 120-134. Research supported by the University of California*, 262:120–134, 1982.

[26] Nadia Blagorodnova, S Gezari, T Hung, SR Kulkarni, SB Cenko, DR Pasham, L Yan, Iair Arcavi, Sagi Ben-Ami, BD Bue, et al. iptf16fnl: a faint and fast tidal disruption event in an e+ a galaxy. *The Astrophysical Journal*, 844(1):46, 2017.

[27] Kate D Alexander, Sjoert van Velzen, Assaf Horesh, and B Ashley Zauderer. Radio properties of tidal disruption events. *Space Science Reviews*, 216(5):81, 2020.

[28] Jon M Miller, Jelle S Kaastra, M Coleman Miller, Mark T Reynolds, Gregory Brown, S Bradley Cenko, Jeremy J Drake, Suvi Gezari, James Guillochon, Kayhan Gultekin, et al. Flows of x-ray gas reveal the disruption of a star by a massive black hole. *Nature*, 526(7574):542–545, 2015.

[29] Tiara Hung, Ryan J Foley, Enrico Ramirez-Ruiz, Jane L Dai, Katie Auchettl, Charles D Kilpatrick, Brenna Mockler, Jonathan S Brown, David A Coulter, Georgios Dimitriadis, et al. Double-peaked balmer emission indicating prompt accretion disk formation in an x-ray faint tidal disruption event. *The Astrophysical Journal*, 903(1):31, 2020.

[30] R Saxton, S Komossa, K Auchettl, and PG Jonker. X-ray properties of tdes. *Space Science Reviews*, 216:1–45, 2020.

[31] James Guillochon and Enrico Ramirez-Ruiz. Hydrodynamical simulations to determine the feeding rate of black holes by the tidal disruption of stars: the importance of the impact parameter and stellar structure. *The Astrophysical Journal*, 767(1):25, 2013.

[32] Giuseppe Lodato and Elena M Rossi. Multiband light curves of tidal disruption events. *Monthly Notices of the Royal Astronomical Society*, 410(1):359–367, 2011.

[33] Nathaniel Roth, Daniel Kasen, James Guillochon, and Enrico Ramirez-Ruiz. The x-ray through optical fluxes and line strengths of tidal disruption events. *The Astrophysical Journal*, 827(1):3, 2016.

[34] Brenna Mockler and Enrico Ramirez-Ruiz. An energy inventory of tidal disruption events. *The Astrophysical Journal*, 906(2):101, 2021.

[35] Brian D Metzger and Nicholas C Stone. A bright year for tidal disruptions. *Monthly Notices of the Royal Astronomical Society*, 461(1):948–966, 2016.

[36] Abraham Loeb and Andrew Ulmer. Optical appearance of the debris of a star disrupted by a massive black hole. *The Astrophysical Journal*, 489(2):573, 1997.

[37] M Coleman Miller. Disk winds as an explanation for slowly evolving temperatures in tidal disruption events. *The Astrophysical Journal*, 805(1):83, 2015.

[38] Tatsuya Matsumoto and Tsvi Piran. Limits on mass outflow from optical tidal disruption events. *Monthly Notices of the Royal Astronomical Society*, 502(3):3385–3393, 2021.

[39] Sjoert Van Velzen, Glennys R Farrar, Suvi Gezari, Nidia Morrell, Dennis Zaritsky, Linda Östman, Mathew Smith, Joseph Gelfand, and Andrew J Drake. Optical discovery of probable stellar tidal disruption flares. *The Astrophysical Journal*, 741(2):73, 2011.

[40] Tiara Hung, Ryan J Foley, S Veilleux, SB Cenko, Jane L Dai, Katie Auchettl, Thomas G Brink, Georgios Dimitriadis, Alexei V Filippenko, S Gezari, et al. Discovery of a fast iron low-ionization outflow in the early evolution of the nearby tidal disruption event at 2019qiz. *The Astrophysical Journal*, 917(1):9, 2021.

[41] PG Jonker, NC Stone, A Generozov, S van Velzen, and B Metzger. Implications from late-time x-ray detections of optically selected tidal disruption events: state changes, unification, and detection rates. *The Astrophysical Journal*, 889(2):166, 2020.

[42] Kimitake Hayasaki, Nicholas Stone, and Abraham Loeb. Circularization of tidally disrupted stars around spinning supermassive black holes. *Monthly Notices of the Royal Astronomical Society*, 461(4):3760–3780, 2016.

[43] TW-S Holoien, CS Kochanek, JL Prieto, KZ Stanek, Subo Dong, BJ Shappee, D Grupe, JS Brown, U Basu, JF Beacom, et al. Six months of multiwavelength follow-up of the tidal disruption candidate asassn-14li and implied tde rates from asas-sn. *Monthly Notices of the Royal Astronomical Society*, 455(3):2918–2935, 2016.

[44] Lixin Dai, Jonathan C McKinney, Nathaniel Roth, Enrico Ramirez-Ruiz, and M Coleman Miller. A unified model for tidal disruption events. *The Astrophysical Journal Letters*, 859(2):L20, 2018.

[45] Iair Arcavi, Avishay Gal-Yam, Mark Sullivan, Yen-Chen Pan, S Bradley Cenko, Assaf Horesh, Eran O Ofek, Annalisa De Cia, Lin Yan, Chen-Wei

Yang, et al. A continuum of h-to he-rich tidal disruption candidates with a preference for e+ a galaxies. *The Astrophysical Journal*, 793(1):38, 2014.

[46] Kaiyou Chen, Jules P Halpern, and Alexei V Filippenko. Kinematic evidence for a relativistic keplerian disk-arp 102b. *The Astrophysical Journal*, 339:742–751, 1989.

[47] IS Bowen. The spectrum and composition of the gaseous nebulae. *The Astrophysical Journal*, 81:1, 1935.

[48] S Gezari, R Chornock, A Rest, ME Huber, K Forster, Edo Berger, Peter J Challis, JD Neill, DC Martin, T Heckman, et al. An ultraviolet–optical flare from the tidal disruption of a helium-rich stellar core. *Nature*, 485(7397):217–220, 2012.

[49] James Guillochon, Haik Manukian, and Enrico Ramirez-Ruiz. Ps1-10jh: the disruption of a main-sequence star of near-solar composition. *The Astrophysical Journal*, 783(1):23, 2014.

[50] Nathaniel Roth, Daniel Kasen, James Guillochon, and Enrico Ramirez-Ruiz. Radiative transfer models of tidal disruption events: What sets their emission line strengths and total optical flux? In *American Astronomical Society Meeting Abstracts# 227*, volume 227, pages 203–04, 2016.

[51] Thomas Wevers, DR Pasham, S van Velzen, G Leloudas, S Schulze, JCA Miller-Jones, PG Jonker, M Gromadzki, E Kankare, ST Hodgkin, et al. Evidence for rapid disc formation and reprocessing in the x-ray bright tidal disruption event candidate at 2018fyk. *Monthly Notices of the Royal Astronomical Society*, 488(4):4816–4830, 2019.

[52] M Nicholl, PK Blanchard, E Berger, S Gomez, R Margutti, KD Alexander, J Guillochon, J Leja, R Chornock, B Snios, et al. The tidal disruption event

at2017eqx: spectroscopic evolution from hydrogen rich to poor suggests an atmosphere and outflow. *Monthly Notices of the Royal Astronomical Society*, 488(2):1878–1893, 2019.

[53] Sjoert Van Velzen, Alexander J Mendez, Julian H Krolik, and Varoujan Gorjian. Discovery of transient infrared emission from dust heated by stellar tidal disruption flares. *The Astrophysical Journal*, 829(1):19, 2016.

[54] Richard Barvainis. Hot dust and the near-infrared bump in the continuum spectra of quasars and active galactic nuclei. *Astrophysical Journal, Part 1 (ISSN 0004-637X), vol. 320, Sept. 15, 1987, p. 537-544.*, 320:537–544, 1987.

[55] S Mattila, M Pérez-Torres, Andreas Efstathiou, Petar Mimica, Morgan Fraser, Erkki Kankare, Antxón Alberdi, Miguel Ángel Aloy, T Heikkilä, Peter G Jonker, et al. A dust-enshrouded tidal disruption event with a resolved radio jet in a galaxy merger. *Science*, 361(6401):482–485, 2018.

[56] Sara Frederick, Suvi Gezari, Matthew J Graham, S Bradley Cenko, Sjoert Van Velzen, Daniel Stern, Nadejda Blagorodnova, Shrinivas R Kulkarni, Lin Yan, Kishalay De, et al. A new class of changing-look liners. *The Astrophysical Journal*, 883(1):31, 2019.

[57] Stephanie M LaMassa, Sabrina Cales, Edward C Moran, Adam D Myers, Gordon T Richards, Michael Eracleous, Timothy M Heckman, Luigi Gallo, and C Megan Urry. The discovery of the first "changing look" quasar: new insights into the physics and phenomenology of active galactic nuclei. *The Astrophysical Journal*, 800(2):144, 2015.

[58] S Komossa, H Zhou, T Wang, M Ajello, J Ge, J Greiner, H Lu, M Salvato, R Saxton, H Shan, et al. Discovery of superstrong, fading, iron line emission and double-peaked balmer lines of the galaxy sdss j095209. 56+ 214313.3: the light echo of a huge flare. *The Astrophysical Journal*, 678(1):L13, 2008.

[59] Liming Dou, Ting-gui Wang, Ning Jiang, Chenwei Yang, Jianwei Lyu, and Hongyan Zhou. Long fading mid-infrared emission in transient coronal line emitters: Dust echo of a tidal disruption flare. *The Astrophysical Journal*, 832(2):188, 2016.

[60] Dimitrios Giannios and Brian D Metzger. Radio transients from stellar tidal disruption by massive black holes. *Monthly Notices of the Royal Astronomical Society*, 416(3):2102–2107, 2011.

[61] Nicholas C Stone, Eugene Vasiliev, Michael Kesden, Elena M Rossi, Hagai B Perets, and Pau Amaro-Seoane. Rates of stellar tidal disruption. *Space Science Reviews*, 216:1–48, 2020.

[62] GB Taylor, DA Frail, E Berger, and SR Kulkarni. The angular size and proper motion of the afterglow of grb 030329. *The Astrophysical Journal*, 609(1):L1, 2004.

[63] Samantha Wu, Eric R Coughlin, and Chris Nixon. Super-eddington accretion in tidal disruption events: the impactof realistic fallback rates on accretion rates. *Monthly Notices of the Royal Astronomical Society*, 478(3):3016–3024, 2018.

[64] Linda E Strubbe and Eliot Quataert. Spectroscopic signatures of the tidal disruption of stars by massive black holes. *Monthly Notices of the Royal Astronomical Society*, 415(1):168–180, 2011.

[65] Igor Andreoni, Michael W Coughlin, Daniel A Perley, Yuhan Yao, Wenbin Lu, S Bradley Cenko, Harsh Kumar, Shreya Anand, Anna YQ Ho, Mansi M Kasliwal, et al. A very luminous jet from the disruption of a star by a massive black hole. *Nature*, 612(7940):430–434, 2022.

[66] Gregory C Brown, Andrew J Levan, Elizabeth R Stanway, NR Tanvir, SB Cenko, Edo Berger, R Chornock, and A Cucchiaria. Swift j1112. 2- 8238: a candidate relativistic tidal disruption flare. *Monthly Notices of the Royal Astronomical Society*, 452(4):4297–4306, 2015.

[67] Robert Stein, Sjoert van Velzen, Marek Kowalski, Anna Franckowiak, Suvi Gezari, James CA Miller-Jones, Sara Frederick, Itai Sfaradi, Michael F Bietenholz, Assaf Horesh, et al. A tidal disruption event coincident with a high-energy neutrino. *Nature Astronomy*, 5(5):510–518, 2021.

[68] Simeon Reusch, Robert Stein, Marek Kowalski, Sjoert Van Velzen, Anna Franckowiak, Cecilia Lunardini, Kohta Murase, Walter Winter, James CA Miller-Jones, Mansi M Kasliwal, et al. Candidate tidal disruption event at2019fdr coincident with a high-energy neutrino. *Physical review letters*, 128(22):221101, 2022.

[69] Walter Winter and Cecilia Lunardini. Interpretation of the observed neutrino emission from three tidal disruption events. *The Astrophysical Journal*, 948(1):42, 2023.

[70] Kimitake Hayasaki and Ryo Yamazaki. Neutrino emissions from tidal disruption remnants. *The Astrophysical Journal*, 886(2):114, 2019.

[71] Walter Winter and Cecilia Lunardini. A concordance scenario for the observation of a neutrino from the tidal disruption event at2019dsg. Technical report, Deutsches Elektronen-Synchrotron (DESY), 2020.

[72] PK Blanchard, M Nicholl, E Berger, J Guillochon, R Margutti, R Chornock, KD Alexander, J Leja, and MR Drout. Ps16dtm: a tidal disruption event in a narrow-line seyfert 1 galaxy. *The Astrophysical Journal*, 843(2):106, 2017.

[73] Elisa Bortolas, Taeho Ryu, Luca Broggi, and Alberto Sesana. Partial stellar tidal disruption events and their rates. *arXiv preprint arXiv:2303.03408*, 2023.

[74] Shiyan Zhong, Shuo Li, Peter Berczik, and Rainer Spurzem. Revisit the rate of tidal disruption events: the role of the partial tidal disruption event. *The Astrophysical Journal*, 933(1):96, 2022.

[75] Taeho Ryu, Julian Krolik, Tsvi Piran, and Scott C Noble. Tidal disruptions of main-sequence stars. iii. stellar mass dependence of the character of partial disruptions. *The Astrophysical Journal*, 904(2):100, 2020.

[76] Jin-Hong Chen and Rong-Feng Shen. Light curves of partial tidal disruption events. *The Astrophysical Journal*, 914(1):69, 2021.

[77] Anna V Payne, Benjamin J Shappee, Jason T Hinkle, Patrick J Vallely, Christopher S Kochanek, Thomas W-S Holoien, Katie Auchettl, KZ Stanek, Todd A Thompson, Jack MM Neustadt, et al. Asassn-14ko is a periodic nuclear transient in eso 253-g003. *The Astrophysical Journal*, 910(2):125, 2021.

[78] Jason T Hinkle, Thomas W-S Holoien, Benjamin J Shappee, Katie Auchettl, Christopher S Kochanek, KZ Stanek, Anna V Payne, and Todd A Thompson. Examining a peak-luminosity/decline-rate relationship for tidal disruption events. *The Astrophysical Journal Letters*, 894(1):L10, 2020.

[79] Julian Krolik, Tsvi Piran, and Taeho Ryu. Tidal disruptions of main-sequence stars. v. the varieties of disruptions. *The Astrophysical Journal*, 904(1):68, 2020.

[80] James Guillochon and Enrico Ramirez-Ruiz. A dark year for tidal disruption events. *The Astrophysical Journal*, 809(2):166, 2015.

[81] Jianxiang Wang and David Merritt. Revised rates of stellar disruption in galactic nuclei. *The Astrophysical Journal*, 600(1):149, 2004.

[82] Marco Tinyeung Xue and Fuguo Xie. A numerical investigation of tidal disruption rate enhancement in post-starburst galaxies. In *Journal of Physics: Conference Series*, volume 2441, page 012037. IOP Publishing, 2023.

[83] John Magorrian and Scott Tremaine. Rates of tidal disruption of stars by massive central black holes. *Monthly Notices of the Royal Astronomical Society*, 309(2):447–460, 1999.

[84] Jamie Law-Smith, Enrico Ramirez-Ruiz, Sara L Ellison, and Ryan J Foley. Tidal disruption event host galaxies in the context of the local galaxy population. *The Astrophysical Journal*, 850(1):22, 2017.

[85] K Decker French, Iair Arcavi, and Ann Zabludoff. Tidal disruption events prefer unusual host galaxies. *The Astrophysical Journal Letters*, 818(1):L21, 2016.

[86] Jason T Hinkle, Christopher S Kochanek, Benjamin J Shappee, Patrick J Vallely, Katie Auchettl, Michael Fausnaugh, Thomas WS Holoien, Helena P Treiber, Anna V Payne, B Scott Gaudi, et al. Tess shines light on the origin of the ambiguous nuclear transient asassn-18el. *Monthly Notices of the Royal Astronomical Society*, 521(3):3517–3526, 2023.

[87] Giorgos Leloudas, Lixin Dai, Iair Arcavi, Paul M Vreeswijk, Brenna Mockler, Rupak Roy, Daniele B Malesani, Steve Schulze, Thomas Wevers, Morgan Fraser, et al. The spectral evolution of at 2018dyb and the presence of metal lines in tidal disruption events. *The Astrophysical Journal*, 887(2):218, 2019.

[88] Sebastian Gomez, Matt Nicholl, Philip Short, Raffaella Margutti, Kate D Alexander, Peter K Blanchard, Edo Berger, Tarraneh Eftekhari, Steve Schulze, Joseph Anderson, et al. The tidal disruption event at 2018hyz ii: Light-curve modelling of a partially disrupted star. *Monthly Notices of the Royal Astronomical Society*, 497(2):1925–1934, 2020.

[89] Thomas W-S Holoien, Patrick J Vallely, Katie Auchettl, KZ Stanek, Christopher S Kochanek, K Decker French, Jose L Prieto, Benjamin J Shappee, Jonathan S Brown, Michael M Fausnaugh, et al. Discovery and early evolution of asassn-19bt, the first tde detected by tess. *The Astrophysical Journal*, 883(2):111, 2019.

[90] Xiao-Long Liu, Li-Ming Dou, Jin-Hong Chen, and Rong-Feng Shen. The uv/optical peak and x-ray brightening in tde candidate at 2019azh: A case of stream–stream collision and delayed accretion. *The Astrophysical Journal*, 925(1):67, 2022.

[91] SJ Prentice, Kate Maguire, SJ Smartt, MR Magee, P Schady, Stuart Sim, T-W Chen, Peter Clark, Christelle Colin, M Fulton, et al. The cow: discovery of a luminous, hot, and rapidly evolving transient. *The Astrophysical Journal Letters*, 865(1):L3, 2018.

[92] Tanja Petrushevska, G Leloudas, D Ilic, M Bronikowski, P Charalampopoulos, GK Jaisawal, E Paraskeva, M Pursiainen, N Rakic, Steve Schulze, et al. The rise and fall of the iron-strong nuclear transient ps16dtm. *Astronomy and Astrophysics*, 669:A140, 2023.

[93] Sjoert Van Velzen, Suvi Gezari, S Bradley Cenko, Erin Kara, James CA Miller-Jones, Tiara Hung, Joe Bright, Nathaniel Roth, Nadejda Blagorodnova, Daniela Huppenkothen, et al. The first tidal disruption flare in ztf: from photometric selection to multi-wavelength characterization. *The Astrophysical Journal*, 872(2):198, 2019.

[94] Tetyana Pitik, Irene Tamborra, Charlotte R Angus, and Katie Auchettl. Is the high-energy neutrino event icecube-200530a associated with a hydrogen-rich superluminous supernova? *The Astrophysical Journal*, 929(2):163, 2022.

[95] Zhefu Yu, CS Kochanek, S Mathur, K Auchettl, D Grupe, and T WS Holoien. An x-ray view of the ambiguous nuclear transient at2019pev. *Monthly Notices of the Royal Astronomical Society*, 515(4):5198–5210, 2022.

[96] M Nicholl, T Wevers, SR Oates, KD Alexander, G Leloudas, F Onori, Anders Jerkstrand, S Gomez, S Campana, I Arcavi, et al. An outflow powers the optical rise of the nearby, fast-evolving tidal disruption event at2019qiz. *Monthly Notices of the Royal Astronomical Society*, 499(1):482–504, 2020.

[97] N Blagorodnova, SB Cenko, SR Kulkarni, I Arcavi, JS Bloom, G Duggan, AV Filippenko, C Fremling, A Horesh, G Hosseinzadeh, et al. The broad absorption line tidal disruption event iptf15af: optical and ultraviolet evolution. *The Astrophysical Journal*, 873(1):92, 2019.

[98] Jari JE Kajava, Margherita Giustini, Richard D Saxton, and Giovanni Miniutti. Rapid late-time x-ray brightening of the tidal disruption event ogle16aaa. *Astronomy & Astrophysics*, 639:A100, 2020.

[99] Mariusz Gromadzki, Aleksandra Hamanowicz, Lukasz Wyrzykowski, Kirill V Sokolovsky, Morgan Fraser, Sz Kozłowski, James Guillochon, Iair Arcavi, Benjamin Trakhtenbrot, Peter G Jonker, et al. Discovery and follow-up of the unusual nuclear transient ogle17aaj. *Astronomy & Astrophysics*, 622:L2, 2019.

[100] S Kiyota, J Brimacombe, RA Koff, RS Post, JS Brown, KZ Stanek, TW-S Holoien, CS Kochanek, J Shields, TA Thompson, et al. Asassn-17cu and asassn-17cv: discovery of two probable supernovae. *The Astronomer's Telegram*, 10113:1, 2017.

[101] Benny Trakhtenbrot, Iair Arcavi, Claudio Ricci, Sandro Tacchella, Daniel Stern, Hagai Netzer, Peter G Jonker, Assaf Horesh, Julián Esteban Mejía-Restrepo, Griffin Hosseinzadeh, et al. A new class of flares from accreting supermassive black holes. *Nature Astronomy*, 3(3):242–250, 2019.

[102] Daniel E Vanden Berk, Gordon T Richards, Amanda Bauer, Michael A Strauss, Donald P Schneider, Timothy M Heckman, Donald G York, Patrick B Hall, Xiaohui Fan, GR Knapp, et al. Composite quasar spectra from the sloan digital sky survey. *The Astronomical Journal*, 122(2):549, 2001.

[103] E Lusso and G Risaliti. The tight relation between x-ray and ultraviolet luminosity of quasars. *The Astrophysical Journal*, 819(2):154, 2016.

[104] S Gezari, R Chornock, Andy Lawrence, A Rest, DO Jones, Edo Berger, PM Challis, and G Narayan. Ps1-10jh continues to follow the fallback accretion rate of a tidally disrupted star. *The Astrophysical Journal Letters*, 815(1):L5, 2015.

[105] JS Brown, CS Kochanek, TW-S Holoien, KZ Stanek, K Auchettl, BJ Shappee, JL Prieto, N Morrell, E Falco, J Strader, et al. The ultraviolet spectroscopic evolution of the low-luminosity tidal disruption event iptf16fnl. *Monthly Notices of the Royal Astronomical Society*, 473(1):1130–1144, 2018.

[106] JS Brown, TW-S Holoien, K Auchettl, KZ Stanek, CS Kochanek, BJ Shappee, JL Prieto, and D Grupe. The-long term evolution of asassn-14li. *Monthly Notices of the Royal Astronomical Society*, 466(4):4904–4916, 2017.

[107] JL Tonry, L Denneau, AN Heinze, B Stalder, KW Smith, SJ Smartt, CW Stubbs, HJ Weiland, and A Rest. Atlas: a high-cadence all-sky survey system. *Publications of the Astronomical Society of the Pacific*, 130(988):064505, 2018.

[108] Benny Trakhtenbrot, Iair Arcavi, Chelsea L MacLeod, Claudio Ricci, Erin Kara, Melissa L Graham, Daniel Stern, Fiona A Harrison, Jamison Burke, Daichi Hiramatsu, et al. 1es 1927+ 654: an agn caught changing look on a timescale of months. *The Astrophysical Journal*, 883(1):94, 2019.

[109] A Merloni, T Dwelly, M Salvato, A Georgakakis, J Greiner, M Krumpe, K Nandra, G Ponti, and A Rau. A tidal disruption flare in a massive galaxy? implications for the fuelling mechanisms of nuclear black holes. *Monthly Notices of the Royal Astronomical Society*, 452(1):69–87, 2015.

[110] C Ricci, E Kara, M Loewenstein, B Trakhtenbrot, I Arcavi, R Remillard, AC Fabian, KC Gendreau, Z Arzoumanian, R Li, et al. The destruction and recreation of the x-ray corona in a changing-look active galactic nucleus. *The Astrophysical Journal Letters*, 898(1):L1, 2020.

[111] K. Z. Stanek J Brimacombe, R Cornect. Asas-sn transient discovery report for 2018-07-15. *Transient Name Server Discovery Report*, 2018:1, 2018.

[112] Y-C Pan, RJ Foley, SW Jha, A Rest, and D Scolnic. Spectroscopic classifications of optical transients with soar. *The Astronomer's Telegram*, 11557:1, 2018.

[113] Thomas W-S Holoien, Katie Auchettl, Michael A Tucker, Benjamin J Shappee, Shannon G Patel, James CA Miller-Jones, Brenna Mockler, Danièl N Groenewald, Jason T Hinkle, Jonathan S Brown, et al. The rise and fall of asassn-18pg: following a tde from early to late times. *The Astrophysical Journal*, 898(2):161, 2020.

[114] Katie Auchettl, James Guillochon, and Enrico Ramirez-Ruiz. New physical insights about tidal disruption events from a comprehensive observational inventory at x-ray wavelengths. *The Astrophysical Journal*, 838(2):149, 2017.

[115] Dheeraj R Pasham, Thomas Wevers, Ann Zabuldoff, Sixiang Wen, Peter Jonker, Eric Coughlin, Zheng Cao, and Dacheng Lin. X-ray and uv awakening of a years old stellar tidal disruption event candidate at2018fyk/asassn-18ul: an accretion instability, repeating partial disruption, or supermassive black hole binary? *The Astronomer's Telegram*, 15333:1, 2022.

[116] Subo Dong, Subhash Bose, Ping Chen, TG Brink, Thomas de Jaeger, AV Filippenko, and W Zheng. Spectroscopic classification of asassn-18zj with the lick 3-m shane telescope. *The Astronomer's Telegram*, 12198:1, 2018.

[117] T WS Holoien, JS Brown, K Auchettl, CS Kochanek, JL Prieto, BJ Shappee, and J Van Saders. The unusual late-time evolution of the tidal disruption event asassn-15oi. *Monthly Notices of the Royal Astronomical Society*, 480(4):5689–5703, 2018.

[118] Daniel A Perley, Paolo A Mazzali, Lin Yan, S Bradley Cenko, Suvi Gezari, Kirsty Taggart, Nadia Blagorodnova, Christoffer Fremling, Brenna Mockler, Avinash Singh, et al. The fast, luminous ultraviolet transient at2018cow: extreme supernova, or disruption of a star by an intermediate-mass black hole? *Monthly Notices of the Royal Astronomical Society*, 484(1):1031–1049, 2019.

[119] H Corbett, N Law, E Goeke, J Ratzloff, W Howard, O Fors, D del Ser, and RM Quimby. The astronomer's telegram. 2018.

[120] Dougal Dobie, Vikram Ravi, Anna Ho, Mansi Kasliwal, and Tara Murphy. Atca observations of at2018cow. *The Astronomer's Telegram*, 11795:1, 2018.

[121] IA Smith, NR Tanvir, and DA Perley. At2018cow: Jcmt scuba-2 sub-mm detection. *The Astronomer's Telegram*, 11781:1, 2018.

[122] Dong Xu, Jing Wang, Liping Xin, Junbo Zhang, Zipei Zhu, Sarah Antier, Jirong Mao, Damien Turpin, Chao Wu, Weikang Zheng, et al. Emergence of spectroscopic features of at2018cow/atlas18qqn with the xinglong-2.16 m spectroscopy. *The Astronomer's Telegram*, 11740:1, 2018.

[123] L Izzo, A de Ugarte Postigo, DA Kann, CC Thoene, G Leloudas, M Blazek, K Bensch, R Sanchez-Ramirez, S Schulze, NR Tanvir, et al. At2018cow: de-

tection of an underlying broad-line sn ic. *The Astronomer's Telegram*, 11753:1, 2018.

[124] DA Perley, N Blagorodnova, JD Neill, and R Walters. At2018cow: Continued optical fading and weakening of spectral features. *The Astronomer's Telegram*, 11776:1, 2018.

[125] Jin-Hong Chen and Rong-Feng Shen. Tidal disruption of a main-sequence star by an intermediate-mass black hole: A bright decade. *The Astrophysical Journal*, 867(1):20, 2018.

[126] Miika Pursiainen, Michael Childress, Matthew Smith, Szymon Prajs, M Sullivan, TM Davis, Ryan J Foley, Jacob Asorey, Josh Calcino, Daniela Carollo, et al. Rapidly evolving transients in the dark energy survey. *Monthly Notices of the Royal Astronomical Society*, 481(1):894–917, 2018.

[127] Maria R Drout, Ryan Chornock, Alicia M Soderberg, Nathan Edward Sanders, R McKinnon, A Rest, Ryan J Foley, Danny Milisavljevic, R Margutti, Edo Berger, et al. Rapidly evolving and luminous transients from pan-starrs1. *The Astrophysical Journal*, 794(1):23, 2014.

[128] Cosimo Inserra. Observational properties of extreme supernovae. *Nature Astronomy*, 3(8):697–705, 2019.

[129] Anna YQ Ho, Daniel A Perley, Avishay Gal-Yam, Ragnhild Lunnan, Jesper Sollerman, Steve Schulze, Kaustav K Das, Dougal Dobie, Yuhan Yao, Christoffer Fremling, et al. A search for extragalactic fast blue optical transients in ztf and the rate of at2018cow-like transients. *The Astrophysical Journal*, 949(2):120, 2023.

[130] S van Velzen, S Gezari, SB Cenko, A Ho, Y Yao, SR Kulkarni, K De, MM Kasliwal, C Fremling, MJ Graham, et al. Classification of at2018hco

(atlas18way/ztf18abxftqm) as a tidal disruption flare. *The Astronomer's Telegram*, 12263:1, 2018.

[131] TM Reynolds, I Arcavi, MB Stone, P Nurmi, S Mattila, M Hanski, M Taskula, K Rasanen, R Meller, and V Vepsalainen. Optical spectrum of the tde at2018hco. *The Astronomer's Telegram*, 12281:1, 2018.

[132] L. ; Heinze A. ; Weiland H. ; Flewelling H. ; Stalder B. ; Rest A. ; Stubbs C. ; Smith K. W. ; Smartt S. J. ; Young D. R. ; Maguire K. ; Prentice S. J. ; McBrien O. ; O'Neill D. ; Clark P. ; Magee M. ; Fulton M. ; Mccormack A. ; Wright D. E. Tonry, J. ; Denneau. Atlas transient discovery report for 2018-11-11. *Transient Name Server Discovery Report*, 2018:1, 2018.

[133] L. ; Heinze A. ; Weiland H. ; Flewelling H. ; Stalder B. ; Rest A. ; Stubbs C. ; Smith K. W. ; Smartt S. J. ; Young D. R. ; Srivastav S. ; McBrien O. ; O'Neill D. ; Clark P. ; Fulton M. ; Gillanders J. ; Dobson M. ; Chen T. W. ; Wright D. E. Tonry, J. ; Denneau. Atlas transient discovery report for 2019-08-02. *Transient Name Server Discovery Report*, 2019:1, 2019.

[134] M. E. ; Flewelling H. ; Magnier E. A. ; Primak N. ; Schultz A. ; Smartt S. J. ; Smith K. W. ; Tonry J. ; Waters C. ; Wright D. E. ; Young D. R. Chambers, K. C.; Huber. Pan-starrs1 transient discovery report for 2016-08-14. *Transient Name Server Discovery Report*, 2016:1, 2016.

[135] G Terreran, M Berton, S Benetti, E Cappellaro, N Elias-Rosa, P Ochner, A Pastorello, L Tomasella, and M Turatto. Asiago spectroscopic classification of 2 sne and one agn. *The Astronomer's Telegram*, 9417:1, 2016.

[136] Subo Dong, Ping Chen, S Bose, KZ Stanek, CS Kochanek, TW-S Holoien, BJ Shappee, JL Prieto, Peter J Brown, and P Milne. Optical and uv re-brightening of hydrogen-rich super-luminous supernova ps16dtm/sn 2016ezh. *The Astronomer's Telegram*, 9843:1, 2016.

[137] Chelsea L MacLeod, Nicholas P Ross, Andy Lawrence, Mike Goad, Keith Horne, William Burgett, Ken C Chambers, Heather Flewelling, Klaus Hodapp, Nick Kaiser, et al. A systematic search for changing-look quasars in sdss. *Monthly Notices of the Royal Astronomical Society*, 457(1):389–404, 2016.

[138] Kenneth C Chambers, EA Magnier, N Metcalfe, HA Flewelling, ME Huber, CZ Waters, L Denneau, PW Draper, D Farrow, DP Finkbeiner, et al. The pan-starrs1 surveys. *arXiv preprint arXiv:1612.05560*, 2016.

[139] TWS Holoien, ME Huber, BJ Shappee, M Eracleous, K Auchettl, JS Brown, MA Tucker, KC Chambers, CS Kochanek, KZ Stanek, et al. Ps18kh: a new tidal disruption event with a non-axisymmetric accretion disk (2018). *arXiv preprint arXiv:1808.02890*.

[140] Sara Frederick, Suvi Gezari, Matthew J Graham, Jesper Sollerman, Sjoert van Velzen, Daniel A Perley, Daniel Stern, Charlotte Ward, Erica Hammerstein, Tiara Hung, et al. A family tree of optical transients from narrow-line seyfert 1 galaxies. *The Astrophysical Journal*, 920(1):56, 2021.

[141] D. ; Zabludoff A. ; Valenti S. Hosseinzadeh, I. A. J. B. D. H. C. M. A. H. G. ; French. Transient classification report for 2018-08-15. *Transient Name Server Classification Report*, 2018:1, 2018.

[142] S van Velzen, S Gezari, T Hung, P Gatkine, SB Cenko, A Ho, SR Kulkarni, and A Mahabal. Classification of at2019azh as an eddington-limited tidal disruption flare. *The Astronomer's Telegram*, 12568:1, 2019.

[143] B Trakhtenbrot, I Arcavi, C Ricci, and J Burke. At 2019avd shows strong bowen fluorescence emission lines. *Transient Name Server AstroNote*, 105:1, 2020.

[144] A Malyali, A Rau, A Merloni, K Nandra, J Buchner, Z Liu, S Gezari, Jesper Sollerman, B Shappee, B Trakhtenbrot, et al. At 2019avd: a novel addition to the diverse population of nuclear transients. *Astronomy & Astrophysics*, 647:A9, 2021.

[145] Clément Bonnerot and Elena M Rossi. Streams collision as possible precursor of double tidal disruption events. *Monthly Notices of the Royal Astronomical Society*, 484(1):1301–1316, 2019.

[146] FK Liu, S Li, and Xian Chen. Interruption of tidal-disruption flares by supermassive black hole binaries. *The Astrophysical Journal*, 706(1):L133, 2009.

[147] Th Boller, William Nielsen Brandt, and Henner Fink. Soft x-ray properties of" narrow-line" seyfert 1 galaxies. *arXiv preprint astro-ph/9504093*, 1995.

[148] Suvendu Rakshit, CS Stalin, Hum Chand, and Xue-Guang Zhang. A catalog of narrow line seyfert 1 galaxies from the sloan digital sky survey data release 12. *The Astrophysical Journal Supplement Series*, 229(2):39, 2017.

[149] EO Ofek, D Fox, Stephen B Cenko, M Sullivan, O Gnat, DA Frail, Assaf Horesh, A Corsi, RM Quimby, N Gehrels, et al. X-ray emission from supernovae in dense circumstellar matter environments: a search for collisionless shocks. *The Astrophysical Journal*, 763(1):42, 2013.

[150] Ulrich Feindt, Jakob Nordin, Mickael Rigault, Valéry Brinnel, Suhail Dhawan, Ariel Goobar, and Marek Kowalski. simsurvey: estimating transient discovery rates for the zwicky transient facility. *Journal of Cosmology and Astroparticle Physics*, 2019(10):005, 2019.

[151] C Fremling. Ztf transient discovery report for 2019-02-28. *Transient Name Server Discovery Report No.*, 299:1, 2019.

[152] A Dahiwale and C Fremling. Ztf transient classification report for 2020-07-23. *Transient Name Server Classification Report*, 2020:1, 2020.

[153] SJ Smartt, KW Smith, O McBrien, S Srivastav, J Gillanders, L Denneau, H Flewelling, A Heinze, J Tonry, H Weiland, et al. Long rise and bump feature in the lightcurve of at2019fdr-spectroscopy requested. *Transient Name Server AstroNote*, 33:1, 2019.

[154] MRS Hawkins. Caustic crossings in quasar light curves? *arXiv preprint astro-ph/9810337*, 1998.

[155] Raffaella Margutti, R Chornock, BD Metzger, DL Coppejans, C Guidorzi, G Migliori, D Milisavljevic, E Berger, M Nicholl, BA Zauderer, et al. Results from a systematic survey of x-ray emission from hydrogen-poor superluminous sne. *The Astrophysical Journal*, 864(1):45, 2018.

[156] R Chornock, PK Blanchard, S Gomez, G Hosseinzadeh, and E Berger. Transient classification report for 2019-06-15. *Transient Name Server Classification Report*, 2019:1, 2019.

[157] Daniel Khazov, Ofer Yaron, Avishay Gal-Yam, Ilan Manulis, Alon Rubin, SR Kulkarni, Iair Arcavi, MM Kasliwal, EO Ofek, Y Cao, et al. Flash spectroscopy: emission lines from the ionized circumstellar material around$<$ 10-day-old type ii supernovae. *The Astrophysical Journal*, 818(1):3, 2016.

[158] AJ Drake, SG Djorgovski, A Mahabal, E Beshore, S Larson, MJ Graham, R Williams, E Christensen, M Catelan, A Boattini, et al. First results from the catalina real-time transient survey. *The Astrophysical Journal*, 696(1):870, 2009.

[159] Mark G Aartsen, M Ackermann, J Adams, JA Aguilar, M Ahlers, M Ahrens, D Altmann, K Andeen, T Anderson, I Ansseau, et al. The icecube neutrino

observatory: instrumentation and online systems. *Journal of Instrumentation*, 12(03):P03012, 2017.

[160] J. Nordin. Ztf transient discovery report for 2019-07-31. *Transient Name Server Discovery Report*, 2019, 1378.

[161] SV Velzen, S Gezari, C Ward, S Frederick, E Hammerstein, and SB Cenko. Classification of at2019meg as a tidal disruption event, evidence for an increasing temperature. *Transient Name Server AstroNote*, 88:1, 2019.

[162] M Gromadzki, N Ihanec, E Callis, S Brennan, MT Botticella, H Kuncarayakti, J Anderson, TM Bravo, TW Chen, C Inserra, et al. epessto+ spectroscopic classification of at 2019lwu as a tde. *Transient Name Server AstroNote*, 80:1, 2019.

[163] Rachel J Bruch, Avishay Gal-Yam, Steve Schulze, Ofer Yaron, Yi Yang, Maayane Soumagnac, Mickael Rigault, Nora L Strotjohann, Eran Ofek, Jesper Sollerman, et al. A large fraction of hydrogen-rich supernova progenitors experience elevated mass loss shortly prior to explosion. *The Astrophysical Journal*, 912(1):46, 2021.

[164] JMM Neustadt, T WS Holoien, CS Kochanek, K Auchettl, JS Brown, BJ Shappee, RW Pogge, Subo Dong, KZ Stanek, MA Tucker, et al. To tde or not to tde: the luminous transient asassn-18jd with tde-like and agn-like qualities. *Monthly Notices of the Royal Astronomical Society*, 494(2):2538–2560, 2020.

[165] Andrew O'Brien, David Kaplan, Tara Murphy, Wenfei Yu, and Wenda Zhang. Rising radio emission from tde at2019qiz. *The Astronomer's Telegram*, 13334:1, 2019.

[166] Łukasz Wyrzykowski, M Zieliński, Z Kostrzewa-Rutkowska, A Hamanowicz, PG Jonker, I Arcavi, J Guillochon, PJ Brown, S Kozłowski, A Udalski, et al. Ogle16aaa-a signature of a hungry super massive black hole. *Monthly Notices of the Royal Astronomical Society: Letters*, page slw213, 2016.

[167] Sixiang Wen, Peter G Jonker, Nicholas C Stone, Ann I Zabludoff, and Dimitrios Psaltis. Continuum-fitting the x-ray spectra of tidal disruption events. *The Astrophysical Journal*, 897(1):80, 2020.

[168] Nada Ihanec, Mariusz Gromadzki, and Lukasz Wyrzykowski. A new class of transient flares in super massive black holes. In *XXXIX Polish Astronomical Society Meeting*, volume 10, pages 226–230, 2020.

[169] Carlos Rodrigo, Enrique Solano, Amelia Bayo, and C Rodrigo. Svo filter profile service version 1.0. *IVOA Working Draft*, 15, 2012.

[170] TMC Abbott, FB Abdalla, S Allam, A Amara, J Annis, J Asorey, S Avila, Otger Ballester, Manda Banerji, W Barkhouse, et al. The dark energy survey: Data release 1. *The Astrophysical Journal Supplement Series*, 239(2):18, 2018.

[171] Arne A Henden, DL Welch, D Terrell, and SE Levine. The aavso photometric all-sky survey (apass). In *American Astronomical Society Meeting Abstracts# 214*, volume 214, pages 407–02, 2009.

[172] Mariska Kriek, Pieter G van Dokkum, Ivo Labbé, Marijn Franx, Garth D Illingworth, Danilo Marchesini, Ryan F Quadri, James Aird, Alison L Coil, and Antonis Georgakakis. Fast: Fitting and assessment of synthetic templates. *Astrophysics Source Code Library*, pages ascl–1803, 2018.

[173] D Christopher Martin, James Fanson, David Schiminovich, Patrick Morrissey, Peter G Friedman, Tom A Barlow, Tim Conrow, Robert Grange, Patrick N

Jelinsky, Bruno Milliard, et al. The galaxy evolution explorer: a space ultraviolet survey mission. *The Astrophysical Journal*, 619(1):L1, 2005.

[174] Edward L Wright, Peter RM Eisenhardt, Amy K Mainzer, Michael E Ressler, Roc M Cutri, Thomas Jarrett, J Davy Kirkpatrick, Deborah Padgett, Robert S McMillan, Michael Skrutskie, et al. The wide-field infrared survey explorer (wise): mission description and initial on-orbit performance. *The Astronomical Journal*, 140(6):1868, 2010.

[175] JB Oke and JE Gunn. Secondary standard stars for absolute spectrophotometry. *Astrophysical Journal, Part 1, vol. 266, Mar. 15, 1983, p. 713-717.*, 266:713–717, 1983.

[176] Jason A Cardelli, Geoffrey C Clayton, and John S Mathis. The relationship between infrared, optical, and ultraviolet extinction. *Astrophysical Journal, Part 1 (ISSN 0004-637X), vol. 345, Oct. 1, 1989, p. 245-256.*, 345:245–256, 1989.

[177] Kyle Barbary. Extinction v0. 3.0. *Zenodo*, 2016.

[178] Max Planck. *The theory of heat radiation*. Blakiston, 1914.

[179] Edward L Wright. A cosmology calculator for the world wide web. *Publications of the Astronomical Society of the Pacific*, 118(850):1711, 2006.

[180] Pauli Virtanen, Ralf Gommers, Travis E Oliphant, Matt Haberland, Tyler Reddy, David Cournapeau, Evgeni Burovski, Pearu Peterson, Warren Weckesser, Jonathan Bright, et al. Scipy 1.0: fundamental algorithms for scientific computing in python. *Nature methods*, 17(3):261–272, 2020.

[181] Rene Andrae, Tim Schulze-Hartung, and Peter Melchior. Dos and don'ts of reduced chi-squared. *arXiv preprint arXiv:1012.3754*, 2010.

[182] J Stefan. Uber die beziehung zwischen der warmestrahlung und der temperatur, sitzungsberichte der mathematisch-naturwissenschaftlichen classe der kaiserlichen (on the relationship between heat radiation and temperature). *Akademie der Wissenschaften*, 79:S–391, 1879.

[183] Taeho Ryu, Julian Krolik, and Tsvi Piran. Measuring stellar and black hole masses of tidal disruption events. *The Astrophysical Journal*, 904(1):73, 2020.

[184] Jason T Hinkle, T WS Holoien, K Auchettl, BJ Shappee, JMM Neustadt, AV Payne, JS Brown, CS Kochanek, KZ Stanek, MJ Graham, et al. Discovery and follow-up of asassn-19dj: an x-ray and uv luminous tde in an extreme post-starburst galaxy. *Monthly Notices of the Royal Astronomical Society*, 500(2):1673–1696, 2021.

[185] JM Miller, A Zoghbi, M Reynolds, JJ Drake, S Gezari, C Miller, R Mushotzky, J Irwin, PG Jonker, JS Kaastra, et al. Early chandra x-ray spectroscopy of the nuclear transient at2019pev. 2019.

[186] James Guillochon, Matt Nicholl, V Ashley Villar, Brenna Mockler, Gautham Narayan, Kaisey S Mandel, Edo Berger, and Peter KG Williams. Mosfit: modular open source fitter for transients. *The Astrophysical Journal Supplement Series*, 236(1):6, 2018.

[187] Sjoert van Velzen. On the mass and luminosity functions of tidal disruption flares: rate suppression due to black hole event horizons. *The Astrophysical Journal*, 852(2):72, 2018.

[188] T Wevers, ER Coughlin, DR Pasham, M Guolo, Y Sun, S Wen, PG Jonker, A Zabludoff, A Malyali, R Arcodia, et al. Live to die another day: The rebrightening of at 2018fyk as a repeating partial tidal disruption event. *The Astrophysical Journal Letters*, 942(2):L33, 2023.

[189] Mario Hamuy, MM Phillips, Robert A Schommer, Nicholas B Suntzeff, Jose Maza, and R Aviles. The absolute luminosities of the calan/tololo type ia supernovae. *arXiv preprint astro-ph/9609059*, 1996.

[190] Harim Jin, Sung-Chul Yoon, and Sergei Blinnikov. Optical color of type ib and ic supernovae and implications for their progenitors. *The Astrophysical Journal*, 950(1):44, 2023.

[191] D Yu Tsvetkov, S Yu Shugarov, IM Volkov, NN Pavlyuk, OV Vozyakova, NI Shatsky, AA Nikiforova, IS Troitsky, Yu V Troitskaya, and PV Baklanov. Light curves of the type ii-p supernova sn 2017eaw: The first 200 days. *Astronomy Letters*, 44:315–323, 2018.

[192] Jennifer E Andrews, DJ Sand, S Valenti, Nathan Smith, Raya Dastidar, DK Sahu, Kuntal Misra, Avinash Singh, D Hiramatsu, PJ Brown, et al. Sn 2017gmr: An energetic type ii-p supernova with asymmetries. *The Astrophysical Journal*, 885(1):43, 2019.

[193] Rishabh Singh Teja, Avinash Singh, DK Sahu, GC Anupama, Brajesh Kumar, Tatsuya Nakaoka, Koji S Kawabata, Masayuki Yamanaka, Takey Ali, and Miho Kawabata. Sn 2018gj: A short-plateau type ii supernova with persistent blue-shifted h-alpha emission. *arXiv preprint arXiv:2306.10136*, 2023.

[194] Yize Dong, Stefano Valenti, KA Bostroem, DJ Sand, Jennifer E Andrews, Lluís Galbany, Saurabh W Jha, Youssef Eweis, Lindsey Kwok, Eric Y Hsiao, et al. Supernova 2018cuf: A type iip supernova with a slow fall from plateau. *The Astrophysical Journal*, 906(1):56, 2021.

[195] J Anthony Tyson. Large synoptic survey telescope: overview. *Survey and Other Telescope Technologies and Discoveries*, 4836:10–20, 2002.

[196] Marina Kisley, Yu-Jing Qin, Ann Zabludoff, Kobus Barnard, and Chia-Lin Ko. Classifying astronomical transients using only host galaxy photometry. *The Astrophysical Journal*, 942(1):29, 2023.

[197] Y Shvartzvald, E Waxman, A Gal-Yam, EO Ofek, S Ben-Ami, D Berge, M Kowalski, R Bühler, S Worm, JE Rhoads, et al. Ultrasat: A wide-field time-domain uv space telescope. *arXiv preprint arXiv:2304.14482*, 2023.

Appendix A: Host Galaxy Magnitudes Provided by Jason Hinkle Through Private Correspondence

Object Name	Filter	Host Magnitude	Host Magnitude Error
AT2017bgt	UVW2	19.654	0.282
AT2017bgt	UVM2	19.608	0.278
AT2017bgt	UVW1	19.362	0.254
AT2017bgt	U	18.764	0.107
AT2017bgt	B	17.754	0.043
AT2017bgt	V	16.937	0.009
AT2018dyk	UVW2	20.208	0.241
AT2018dyk	UVM2	20.115	0.216
AT2018dyk	UVW1	19.564	0.123
AT2018dyk	U	17.954	0.087
AT2018dyk	B	16.637	0.064
AT2018dyk	V	15.770	0.038
AT2019avd	UVW2	20.716	0.047
AT2019avd	UVM2	20.607	0.050
AT2019avd	UVW1	20.036	0.046
AT2019avd	U	18.449	0.043
AT2019avd	B	17.143	0.031
AT2019avd	V	16.320	0.027
AT2019qiz	UVW2	22.637	0.049
AT2019qiz	UVM2	22.200	0.072
AT2019qiz	UVW1	20.682	0.040
AT2019qiz	U	18.444	0.022
AT2019qiz	B	17.025	0.015
AT2019qiz	V	16.177	0.008

Appendix B: Supplementary Figures

Multi-filter lightcurves for individual events.

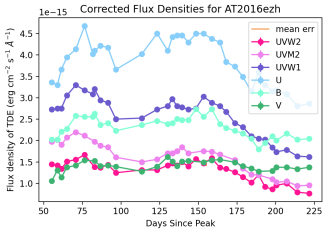

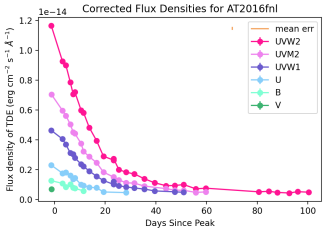

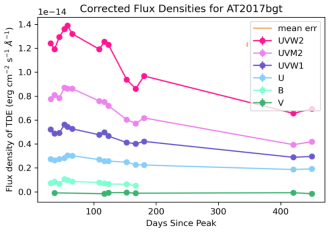

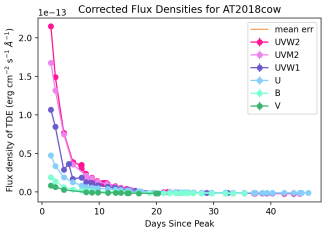

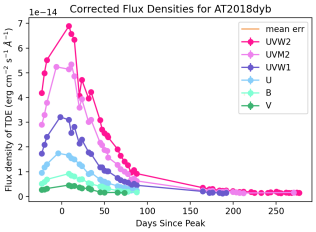

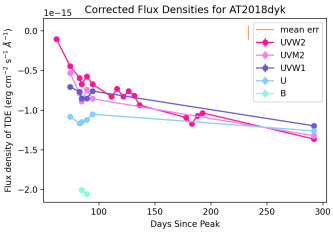

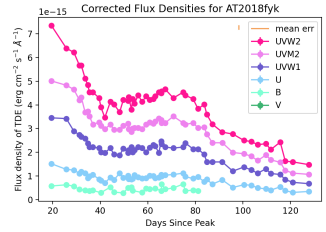

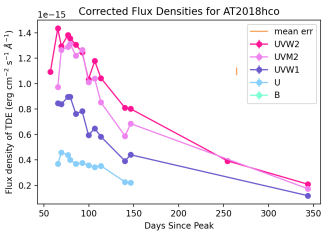

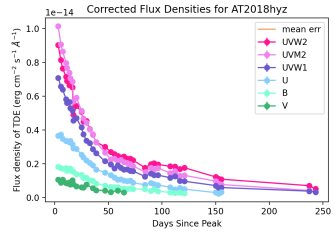

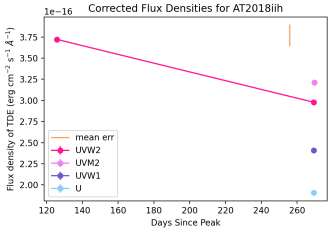

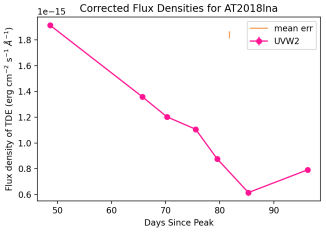

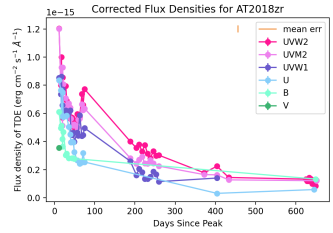

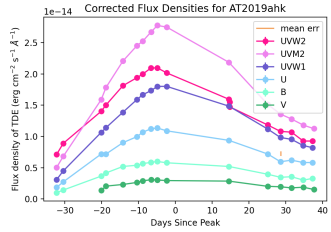

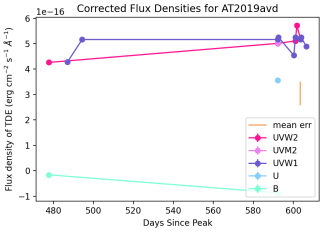

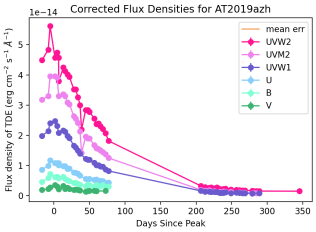

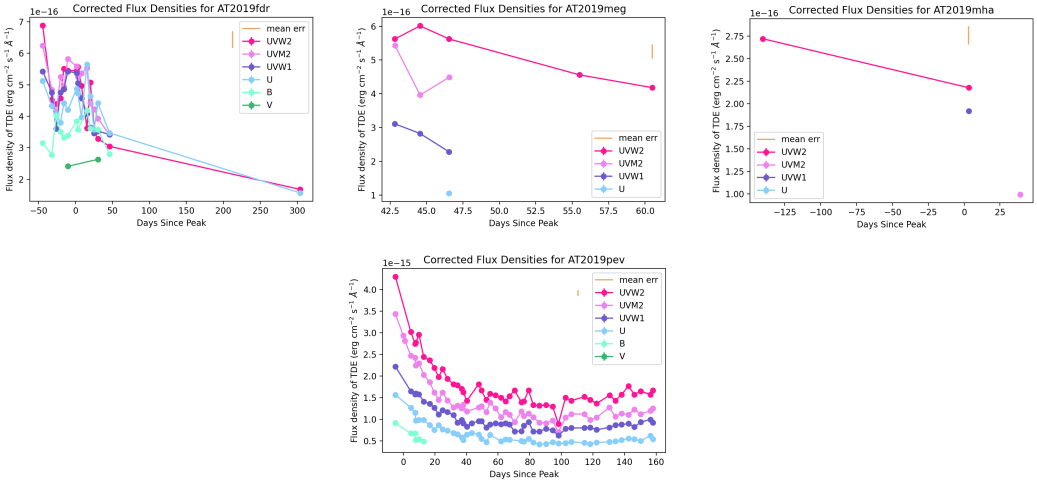

Flux density and magnitude lightcurves comparing multiple events, with the zero date being the peak.

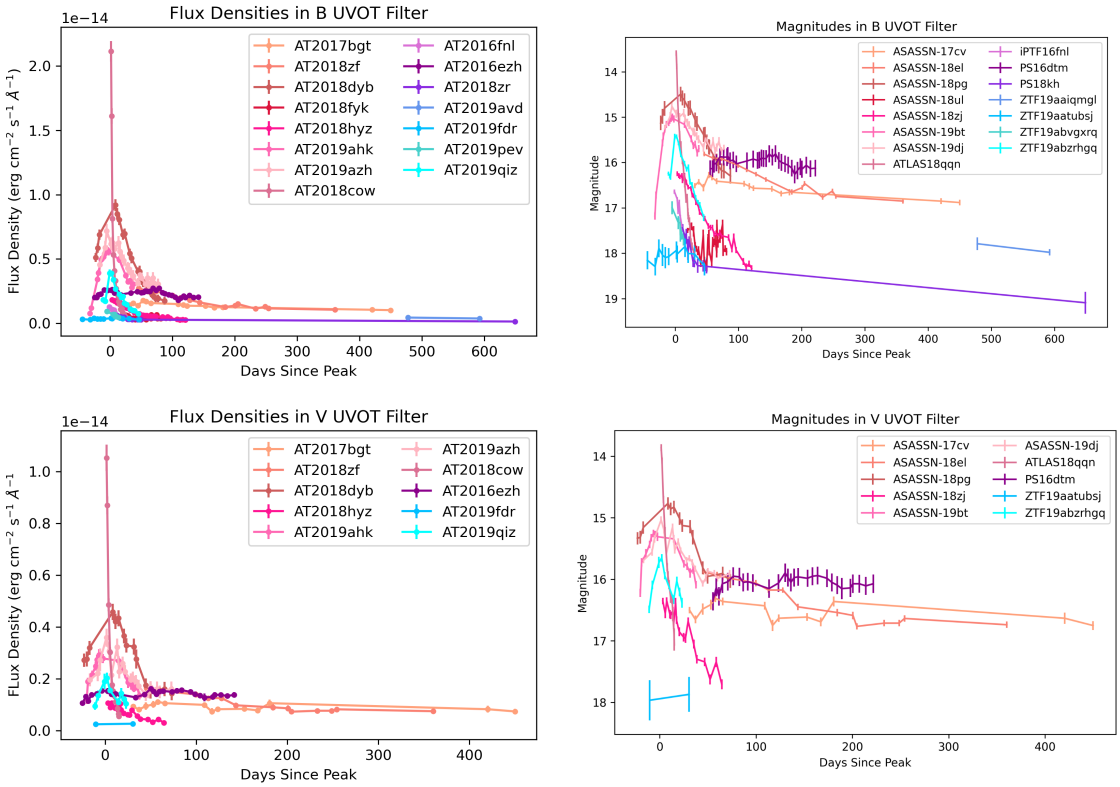

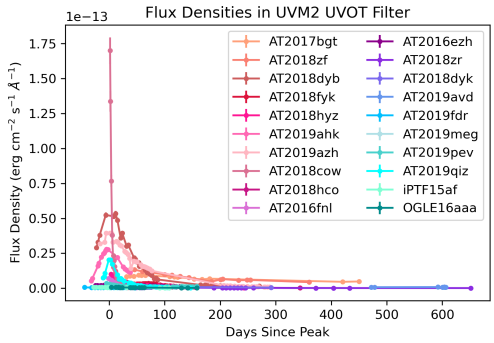
Flux Densities in UVM2 UVOT Filter
1e−13
Flux Density (erg cm^{-2} s^{-1} Å^{-1})
Days Since Peak
AT2017bgt
AT2018zf
AT2018dyb
AT2018fyk
AT2018hyz
AT2019ahk
AT2019azh
AT2018cow
AT2018hco
AT2016fnl
AT2016ezh
AT2018zr
AT2018dyk
AT2019avd
AT2019fdr
AT2019meg
AT2019pev
AT2019qiz
iPTF15af
OGLE16aaa

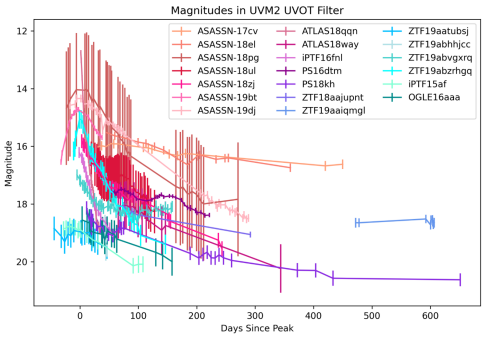
Magnitudes in UVM2 UVOT Filter
Magnitude
Days Since Peak
ASASSN-17cv
ASASSN-18el
ASASSN-18pg
ASASSN-18ul
ASASSN-18zj
ASASSN-19bt
ASASSN-19dj
ATLAS18qqn
ATLAS18way
iPTF16fnl
PS16dtm
PS18kh
ZTF18aajupnt
ZTF19aaiqmgl
ZTF19aatubsj
ZTF19abhhjcc
ZTF19abvgxrq
ZTF19abzrhgq
iPTF15af
OGLE16aaa

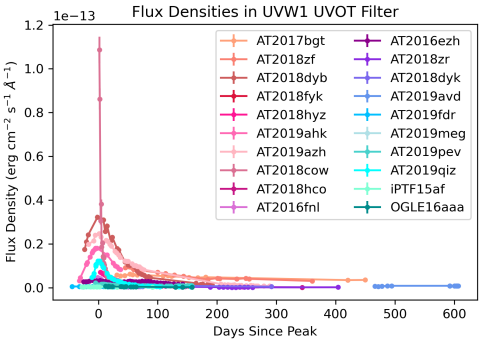
Flux Densities in UVW1 UVOT Filter
1e−13
Flux Density (erg cm^{-2} s^{-1} Å^{-1})
Days Since Peak
AT2017bgt
AT2018zf
AT2018dyb
AT2018fyk
AT2018hyz
AT2019ahk
AT2019azh
AT2018cow
AT2018hco
AT2016fnl
AT2016ezh
AT2018zr
AT2018dyk
AT2019avd
AT2019fdr
AT2019meg
AT2019pev
AT2019qiz
iPTF15af
OGLE16aaa

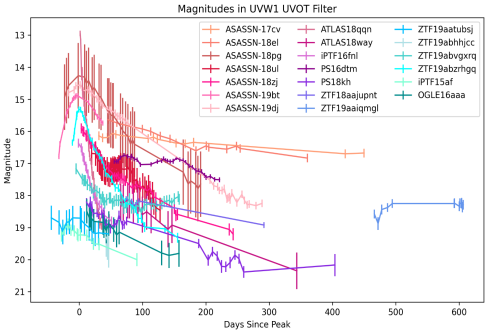
Magnitudes in UVW1 UVOT Filter
Magnitude
Days Since Peak
ASASSN-17cv
ASASSN-18el
ASASSN-18pg
ASASSN-18ul
ASASSN-18zj
ASASSN-19bt
ASASSN-19dj
ATLAS18qqn
ATLAS18way
iPTF16fnl
PS16dtm
PS18kh
ZTF18aajupnt
ZTF19aaiqmgl
ZTF19aatubsj
ZTF19abhhjcc
ZTF19abvgxrq
ZTF19abzrhgq
iPTF15af
OGLE16aaa

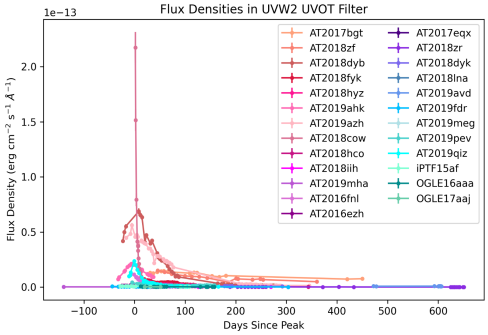
Flux Densities in UVW2 UVOT Filter
1e−13
Flux Density (erg cm^{-2} s^{-1} Å^{-1})
Days Since Peak
AT2017bgt
AT2018zf
AT2018dyb
AT2018fyk
AT2018hyz
AT2019ahk
AT2019azh
AT2018cow
AT2018hco
AT2018iih
AT2019mha
AT2016fnl
AT2016ezh
AT2017eqx
AT2018zr
AT2018dyk
AT2018lna
AT2019avd
AT2019fdr
AT2019meg
AT2019pev
AT2019qiz
iPTF15af
OGLE16aaa
OGLE17aaj

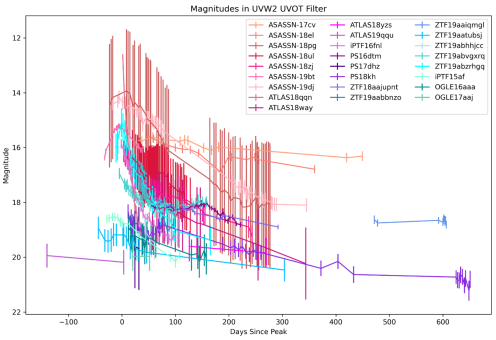
Magnitudes in UVW2 UVOT Filter
Magnitude
Days Since Peak
ASASSN-17cv
ASASSN-18el
ASASSN-18pg
ASASSN-18ul
ASASSN-18zj
ASASSN-19bt
ASASSN-19dj
ATLAS18qqn
ATLAS18way
ATLAS18yzs
ATLAS19qqu
iPTF16fnl
PS16dtm
PS17dhz
PS18kh
ZTF18aajupnt
ZTF18aabbnzo
ZTF19aaiqmgl
ZTF19aatubsj
ZTF19abhhjcc
ZTF19abvgxrq
ZTF19abzrhgq
iPTF15af
OGLE16aaa
OGLE17aaj

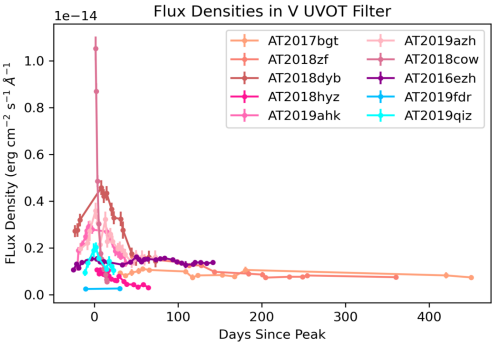
Flux Densities in V UVOT Filter
1e−14
FLux Density (erg cm^{-2} s^{-1} Å^{-1})
Days Since Peak
AT2017bgt
AT2018zf
AT2018dyb
AT2018hyz
AT2019ahk
AT2019azh
AT2018cow
AT2016ezh
AT2019fdr
AT2019qiz

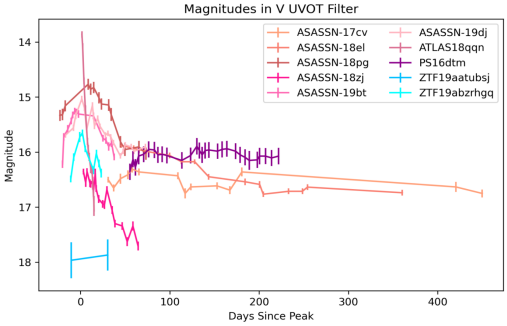
Magnitudes in V UVOT Filter
Magnitude
Days Since Peak
ASASSN-17cv
ASASSN-18el
ASASSN-18pg
ASASSN-18zj
ASASSN-19bt
ASASSN-19dj
ATLAS18qqn
PS16dtm
ZTF19aatubsj
ZTF19abzrhgq

Blackbody temperature, blackbody radius and bolometric luminosity evolution for events in the sample.

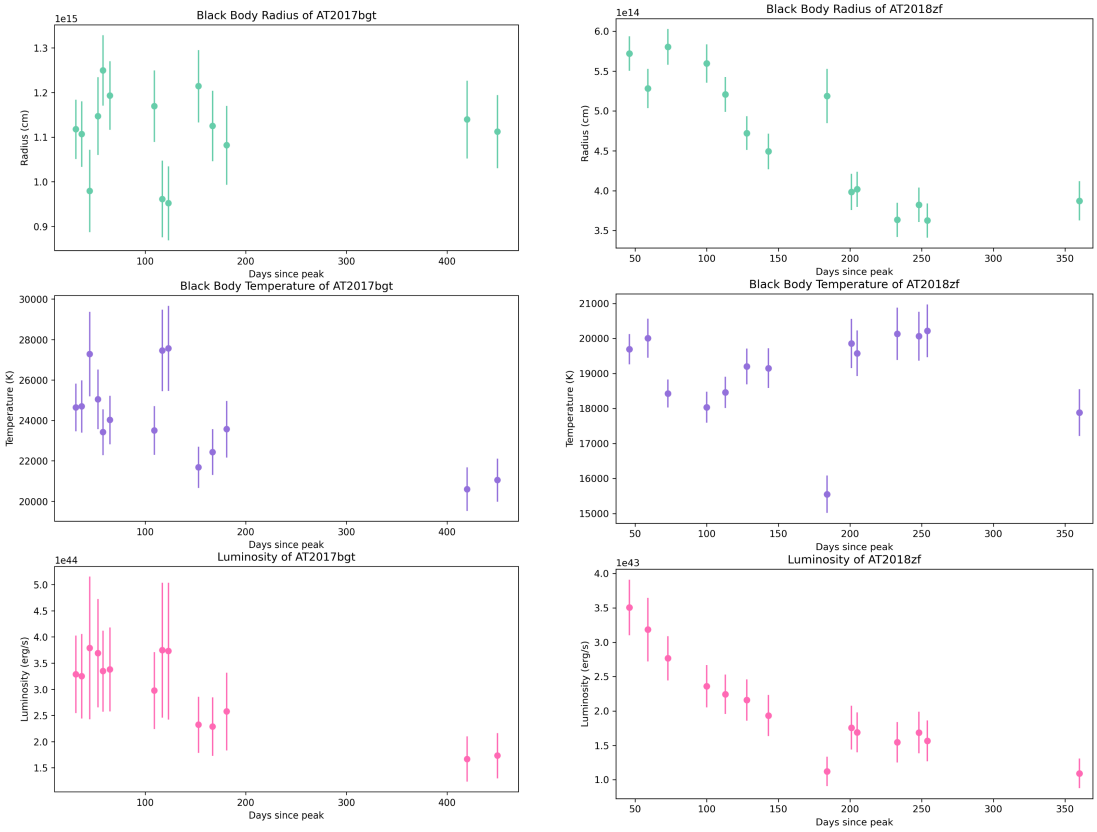

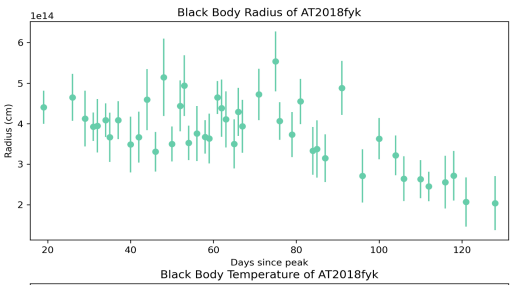
Black Body Radius of AT2018fyk
1e14
Radius (cm)
Days since peak

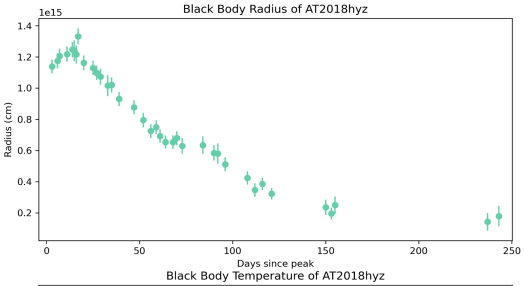
Black Body Radius of AT2018hyz
1e15
Radius (cm)
Days since peak

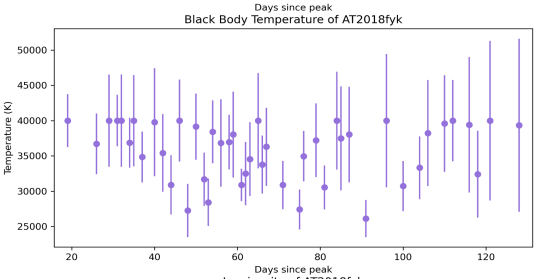
Black Body Temperature of AT2018fyk
Temperature (K)
Days since peak

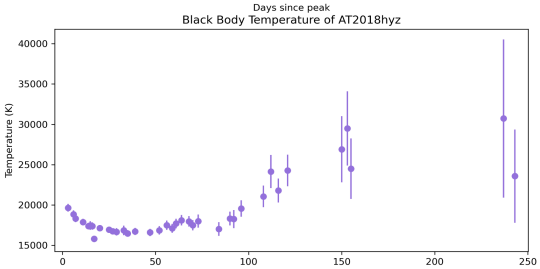
Black Body Temperature of AT2018hyz
Temperature (K)
Days since peak

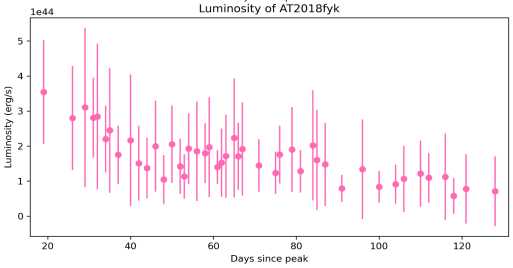
Luminosity of AT2018fyk
1e44
Luminosity (erg/s)
Days since peak

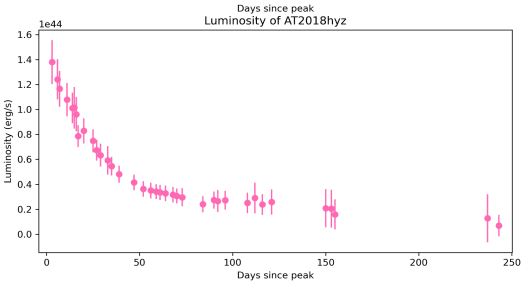
Luminosity of AT2018hyz
1e44
Luminosity (erg/s)
Days since peak

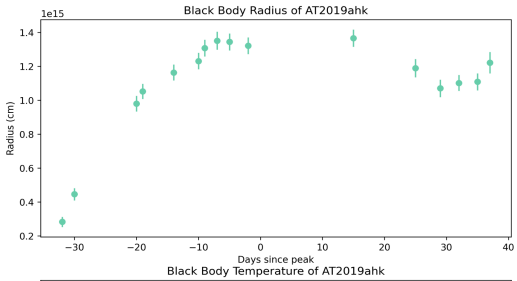
Black Body Radius of AT2019ahk
1e15
Radius (cm)
Days since peak

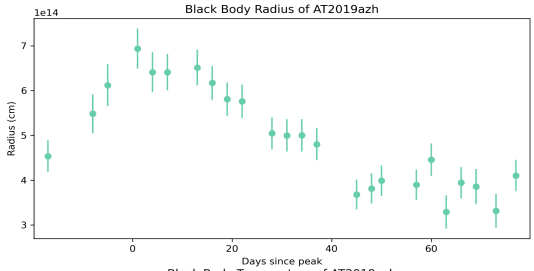
Black Body Radius of AT2019azh
1e14
Radius (cm)
Days since peak

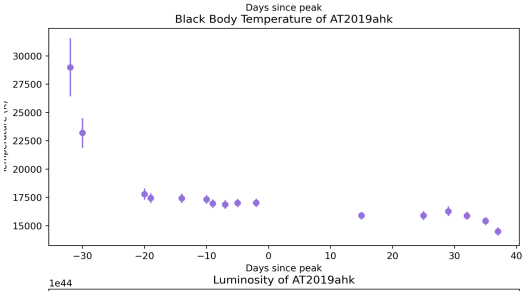
Black Body Temperature of AT2019ahk
Days since peak

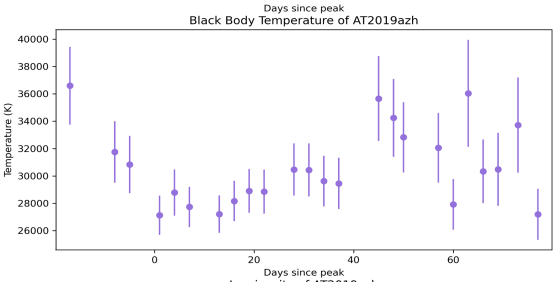
Black Body Temperature of AT2019azh
Temperature (K)
Days since peak

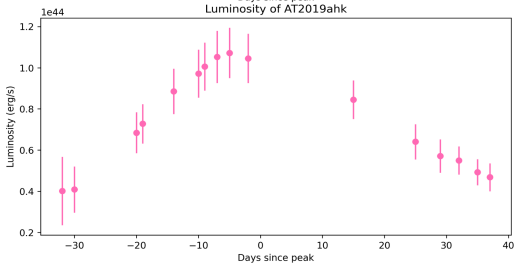
Luminosity of AT2019ahk
1e44
Luminosity (erg/s)
Days since peak

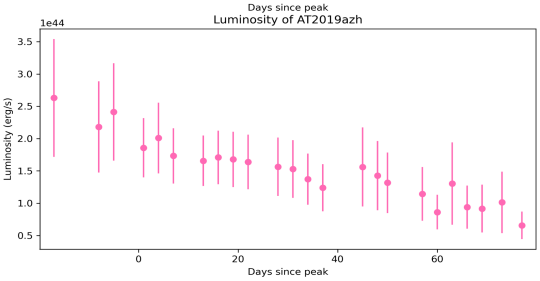
Luminosity of AT2019azh
1e44
Luminosity (erg/s)
Days since peak

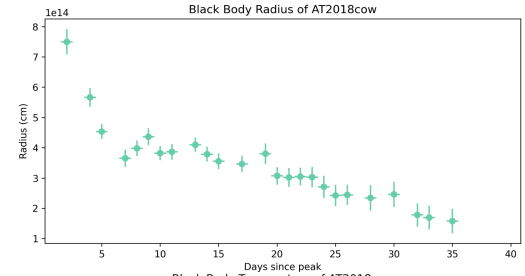
Black Body Radius of AT2018cow
1e14
Radius (cm)
Days since peak

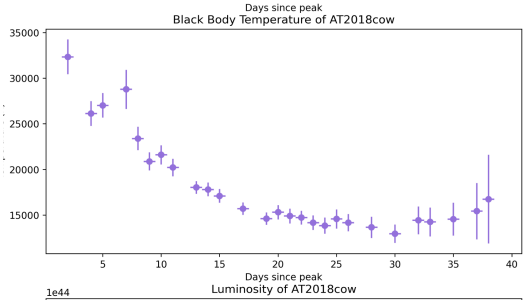
Black Body Temperature of AT2018cow
Temperature (K)
Days since peak

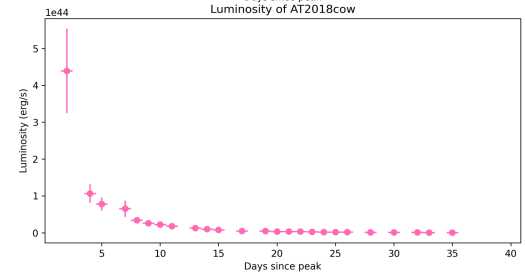
Luminosity of AT2018cow
1e44
Luminosity (erg/s)
Days since peak

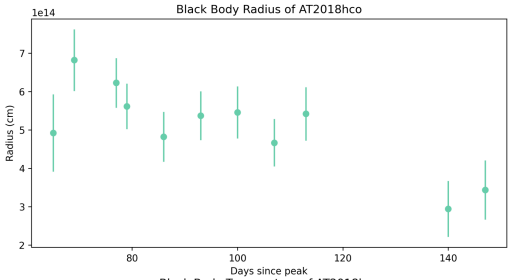
Black Body Radius of AT2018hco
1e14
Radius (cm)
Days since peak

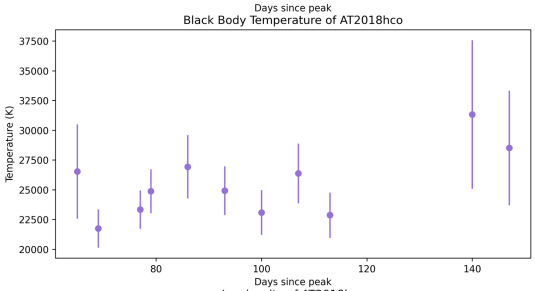
Black Body Temperature of AT2018hco
Temperature (K)
Days since peak

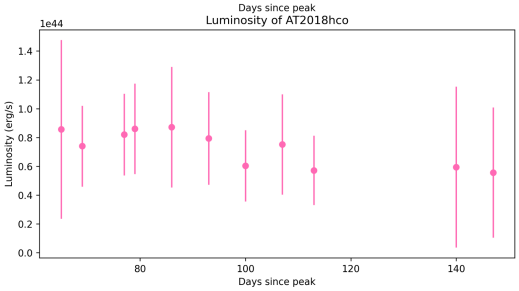
Luminosity of AT2018hco
1e44
Luminosity (erg/s)
Days since peak

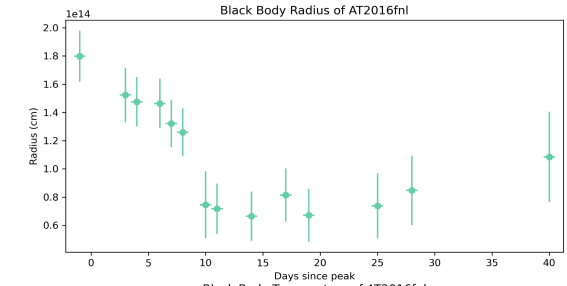
Black Body Radius of AT2016fnl
1e14
Radius (cm)
Days since peak

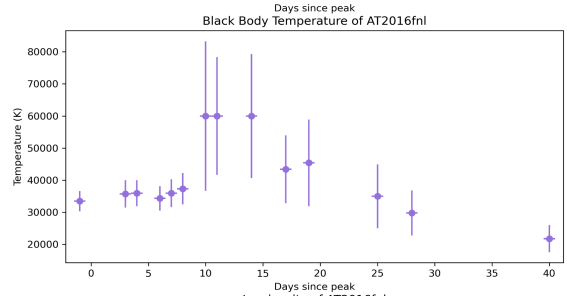
Black Body Temperature of AT2016fnl
Temperature (K)
Days since peak

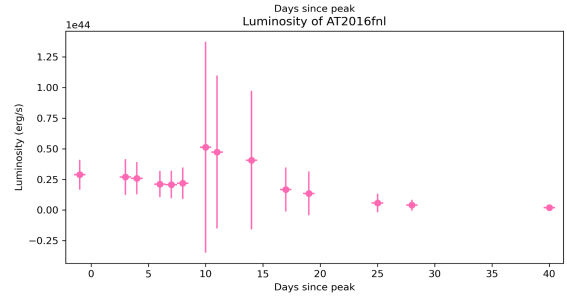
Luminosity of AT2016fnl
1e44
Luminosity (erg/s)
Days since peak

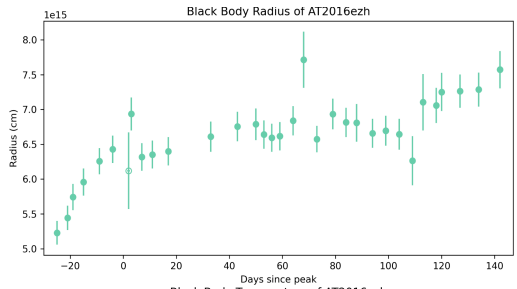
Black Body Radius of AT2016ezh
1e15
Radius (cm)
Days since peak

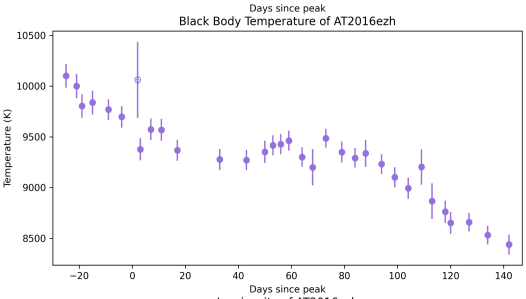
Black Body Temperature of AT2016ezh
Temperature (K)
Days since peak

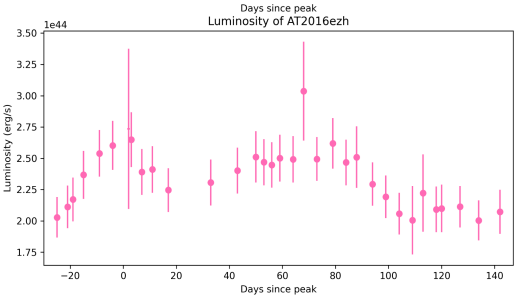
Luminosity of AT2016ezh
1e44
Luminosity (erg/s)
Days since peak

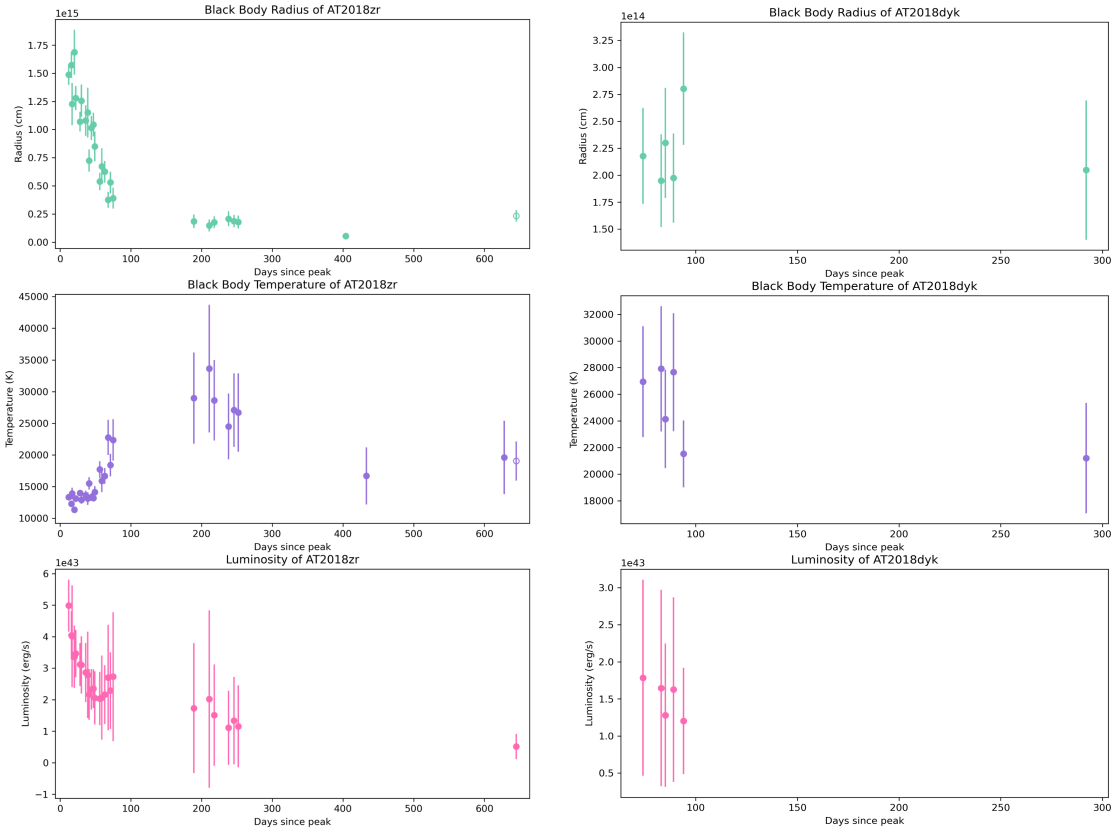
Black Body Radius of AT2018zr
1e15
Radius (cm)
Days since peak
Black Body Radius of AT2018dyk
1e14
Radius (cm)
Days since peak
Black Body Temperature of AT2018zr
Temperature (K)
Days since peak
Black Body Temperature of AT2018dyk
Temperature (K)
Days since peak
Luminosity of AT2018zr
1e43
Luminosity (erg/s)
Days since peak
Luminosity of AT2018dyk
1e43
Luminosity (erg/s)
Days since peak

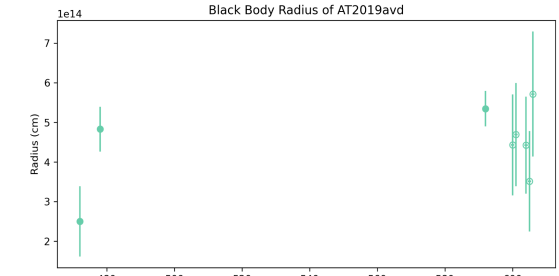
Black Body Radius of AT2019avd
1e14
Radius (cm)
Days since peak

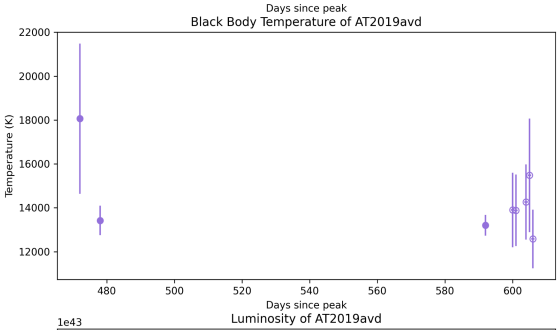
Black Body Temperature of AT2019avd
Temperature (K)
Days since peak

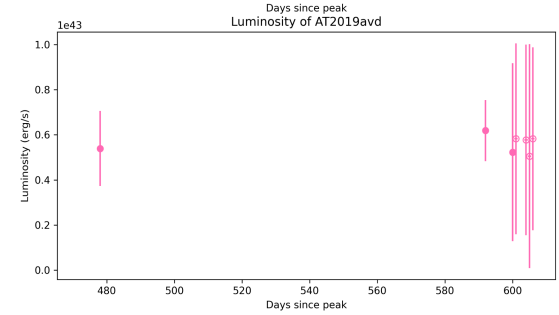
Luminosity of AT2019avd
1e43
Luminosity (erg/s)
Days since peak

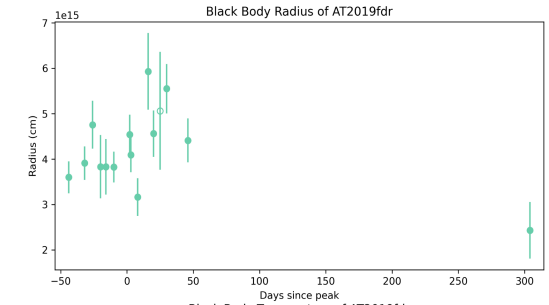
Black Body Radius of AT2019fdr
1e15
Radius (cm)
Days since peak

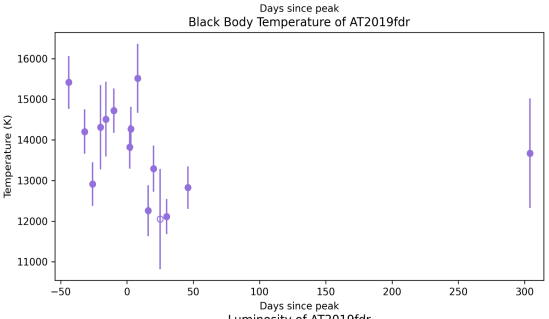
Black Body Temperature of AT2019fdr
Temperature (K)
Days since peak

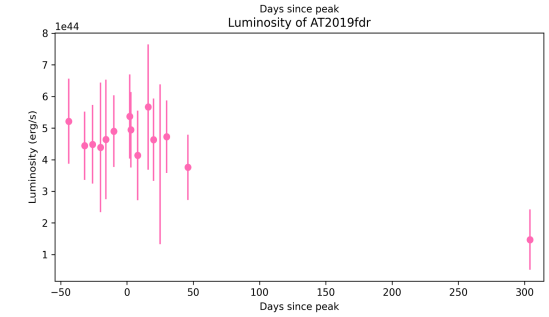
Luminosity of AT2019fdr
1e44
Luminosity (erg/s)
Days since peak

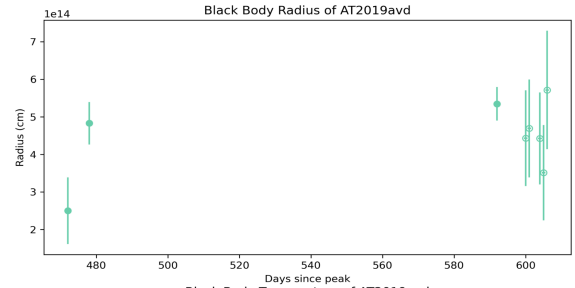
Black Body Radius of AT2019avd
1e14
Radius (cm)
Days since peak

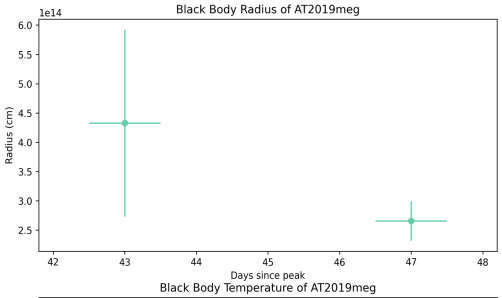
Black Body Radius of AT2019meg
1e14
Radius (cm)
Days since peak

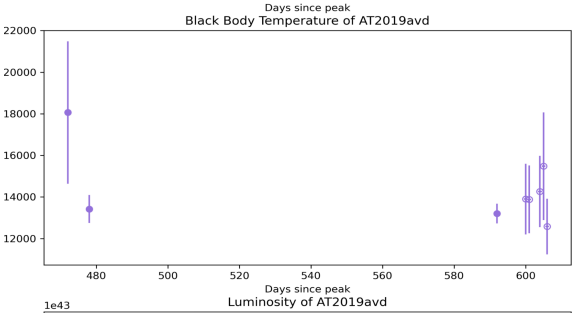
Black Body Temperature of AT2019avd
Days since peak

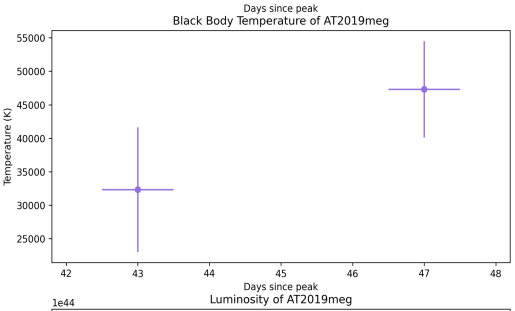
Black Body Temperature of AT2019meg
Temperature (K)
Days since peak

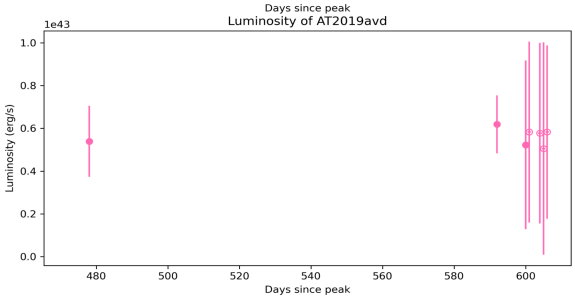
Luminosity of AT2019avd
1e43
Luminosity (erg/s)
Days since peak

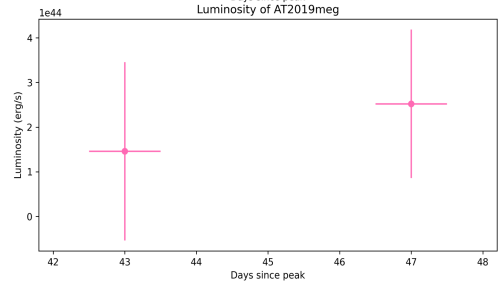
Luminosity of AT2019meg
1e44
Luminosity (erg/s)
Days since peak

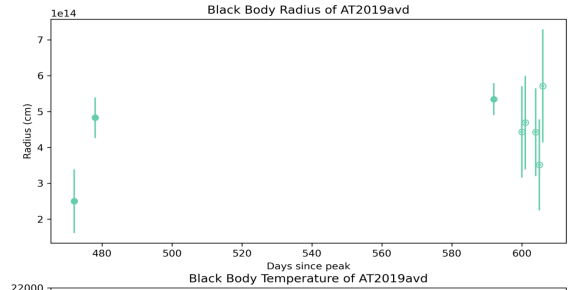
Black Body Radius of AT2019avd
1e14
Radius (cm)
Days since peak

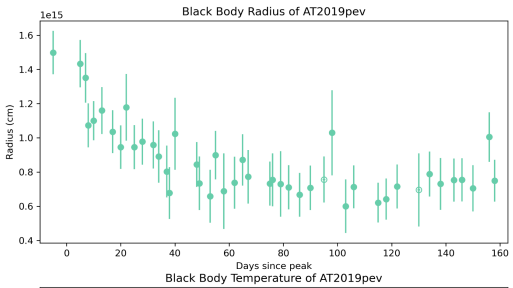
Black Body Radius of AT2019pev
1e15
Radius (cm)
Days since peak

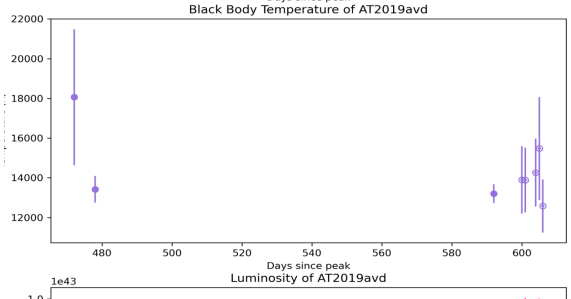
Black Body Temperature of AT2019avd
Days since peak

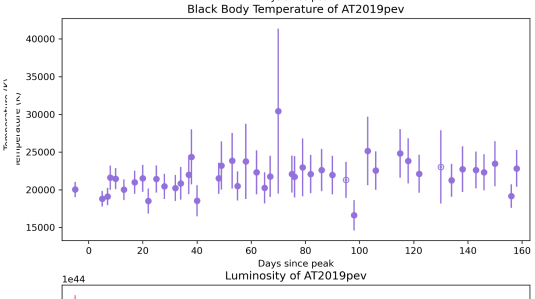
Black Body Temperature of AT2019pev
Days since peak

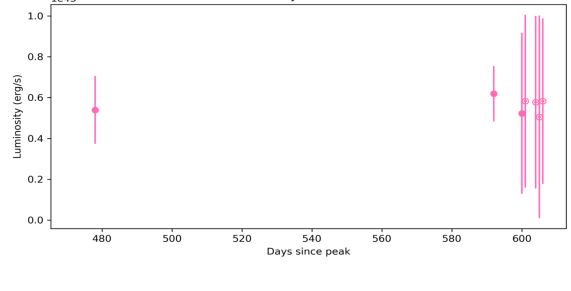
Luminosity of AT2019avd
1e43
Luminosity (erg/s)
Days since peak

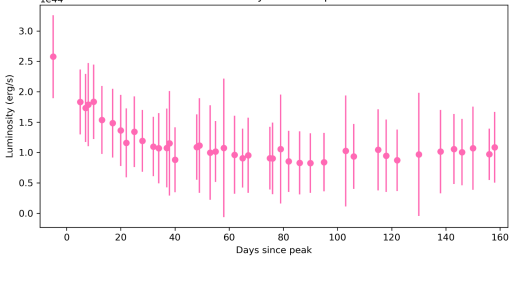
Luminosity of AT2019pev
1e44
Luminosity (erg/s)
Days since peak

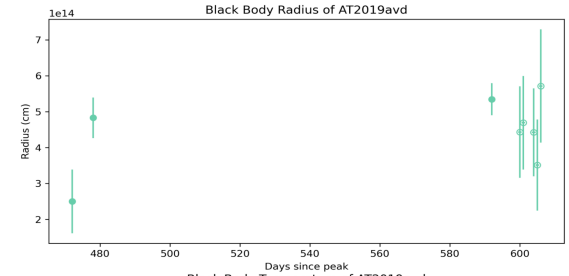
Black Body Radius of AT2019avd
1e14
Radius (cm)
Days since peak

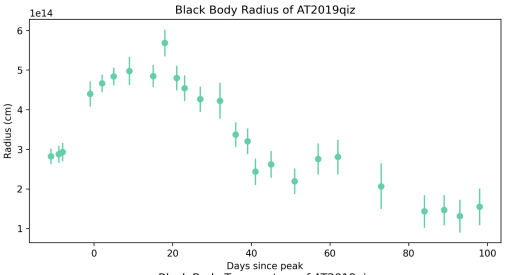
Black Body Radius of AT2019qiz
1e14
Radius (cm)
Days since peak

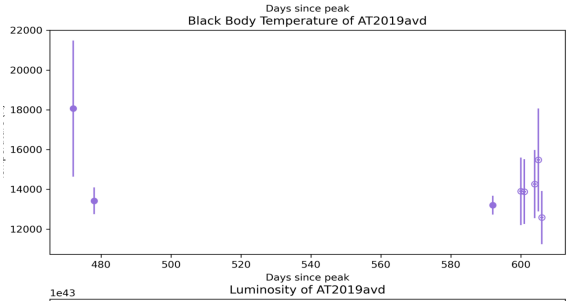
Black Body Temperature of AT2019avd
Days since peak

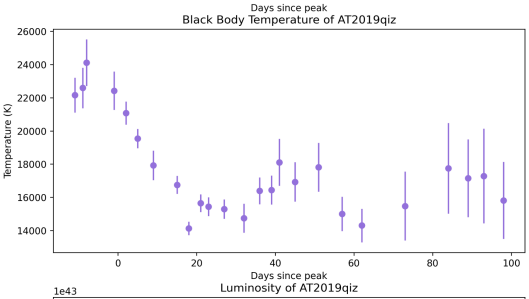
Black Body Temperature of AT2019qiz
Temperature (K)
Days since peak

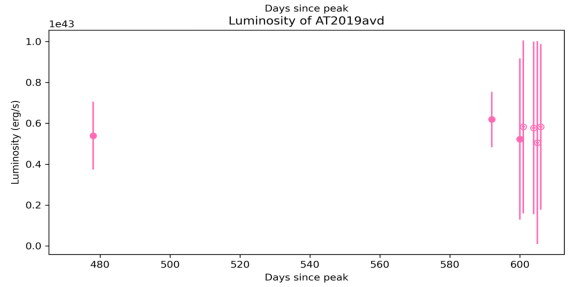
Luminosity of AT2019avd
1e43
Luminosity (erg/s)
Days since peak

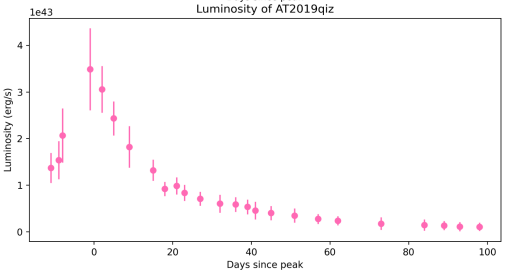
Luminosity of AT2019qiz
1e43
Luminosity (erg/s)
Days since peak

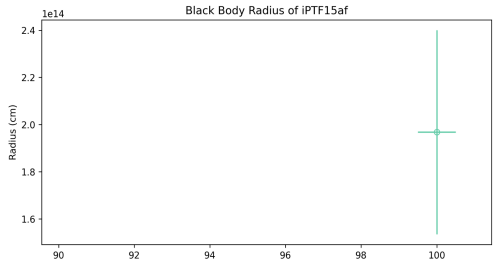
Black Body Radius of iPTF15af
1e14
Radius (cm)
Days since peak

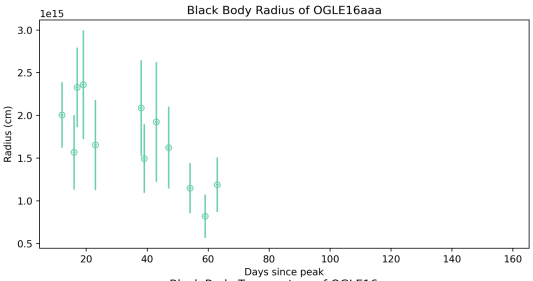
Black Body Radius of OGLE16aaa
1e15
Radius (cm)
Days since peak

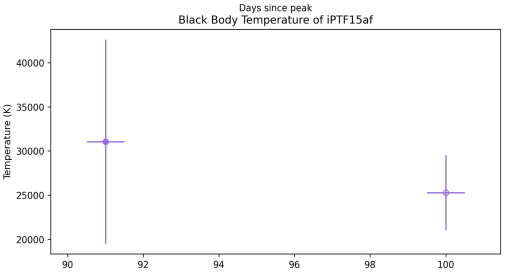
Black Body Temperature of iPTF15af
Temperature (K)
Days since peak

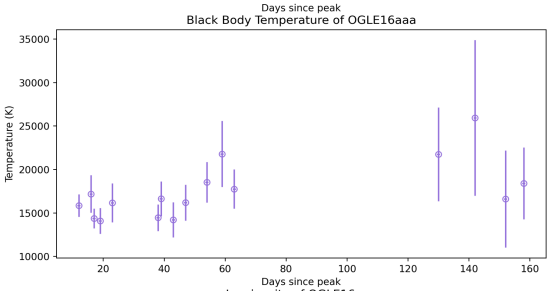
Black Body Temperature of OGLE16aaa
Temperature (K)
Days since peak

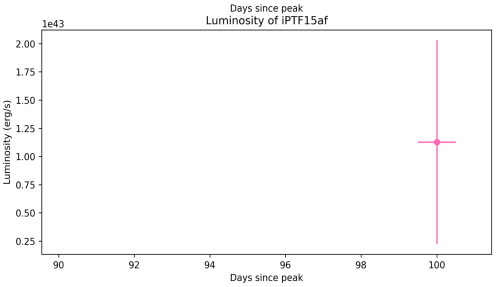
Luminosity of iPTF15af
1e43
Luminosity (erg/s)
Days since peak

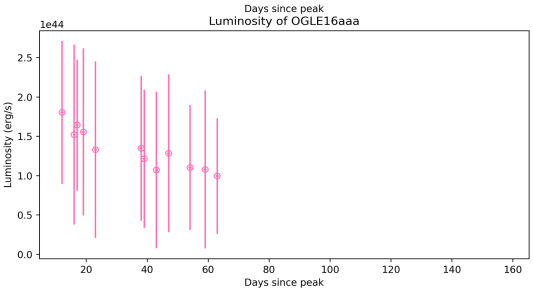
Luminosity of OGLE16aaa
1e44
Luminosity (erg/s)
Days since peak

Post-peak bolometric luminosity power-law index fits, with the index α as a free parameter on the left hand side in each figure, and $\alpha = 5/3$ on the right. Below, the residuals for the respective fits are shown.

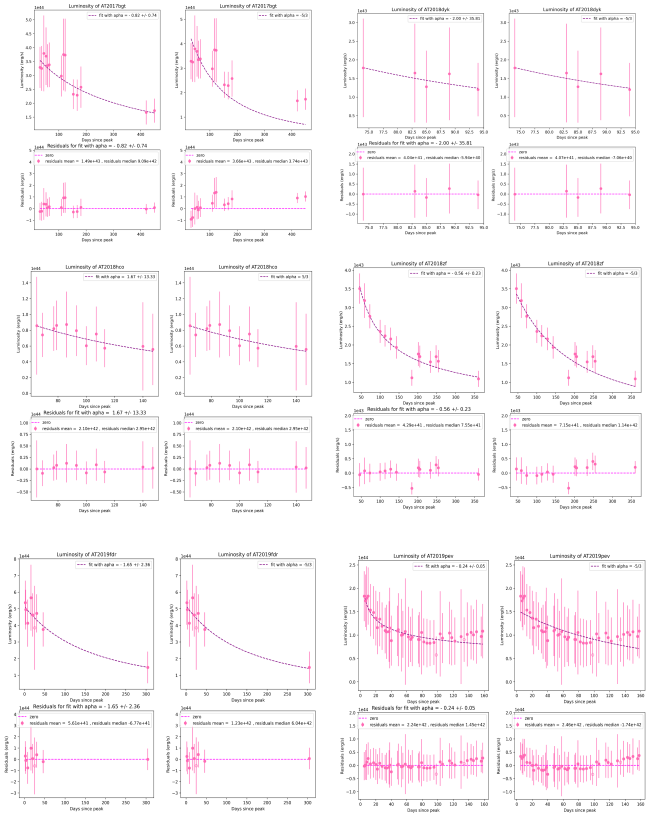

Post-peak bolometric luminosity free α fits (left), $\alpha = 5/3$ fits (centre), and $\alpha = 9/4$ fits (right). Below each fit, the residuals are shown.

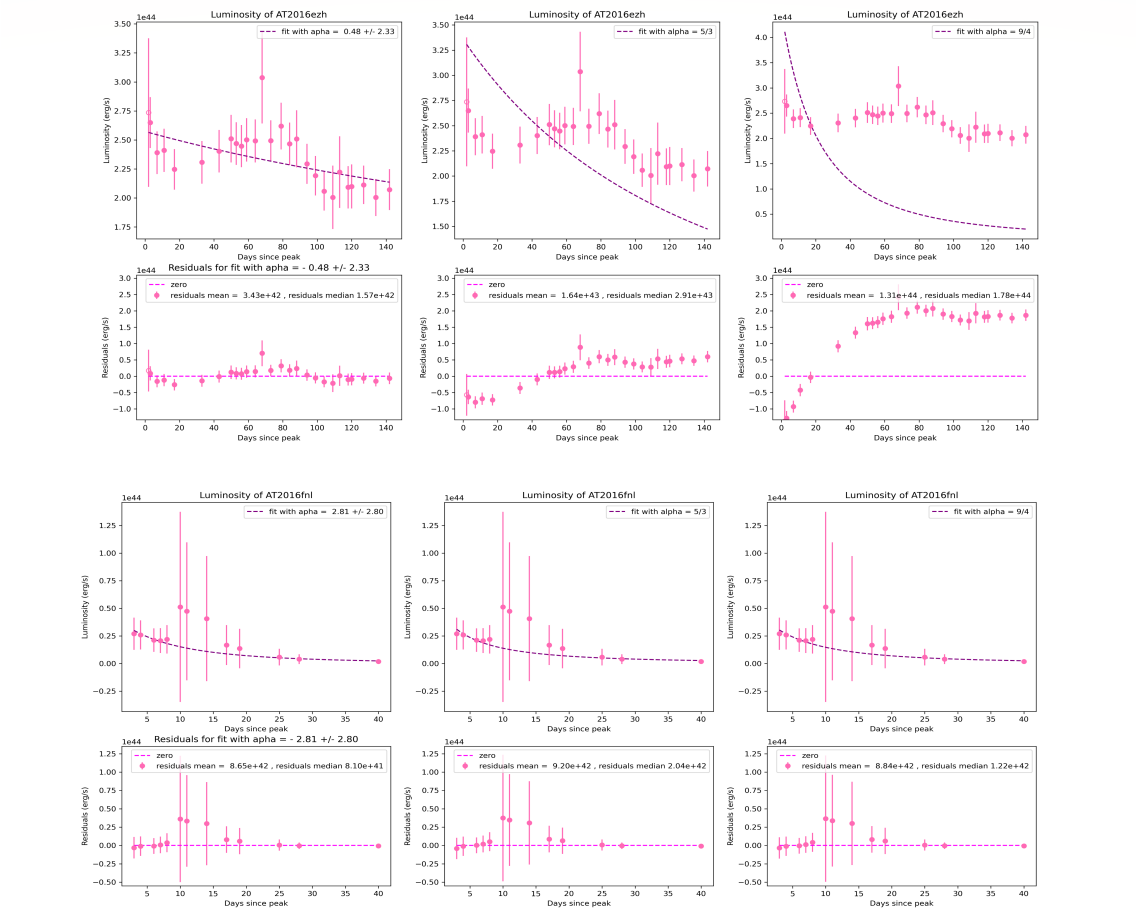

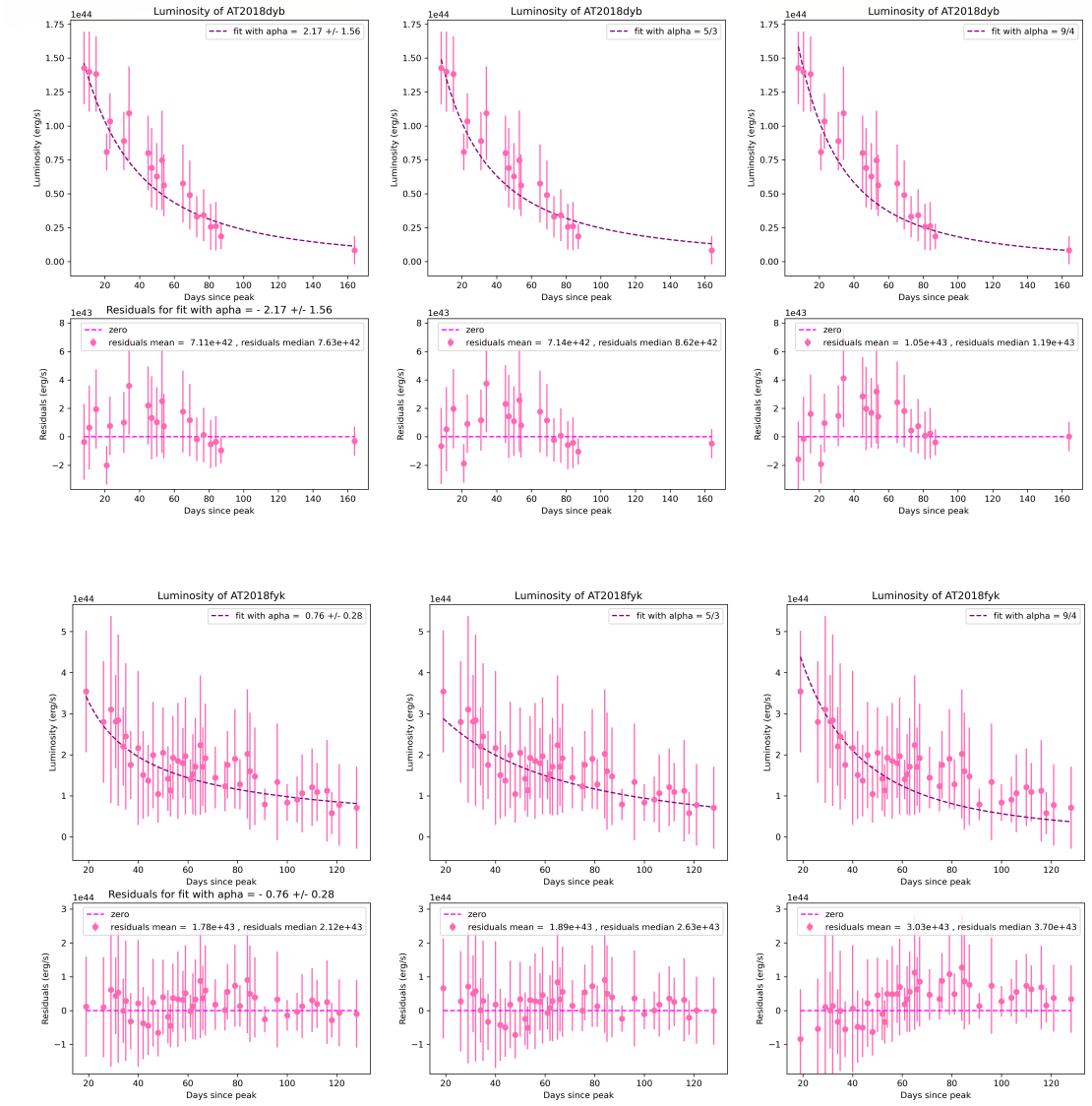
Luminosity of AT2018dyb
fit with apha = 2.17 +/- 1.56
Luminosity (erg/s)
Days since peak
Residuals for fit with apha = - 2.17 +/- 1.56
zero
residuals mean = 7.11e+42 , residuals median 7.63e+42
Residuals (erg/s)
Luminosity of AT2018dyb
fit with alpha = 5/3
Luminosity (erg/s)
Days since peak
zero
residuals mean = 7.14e+42 , residuals median 8.62e+42
Residuals (erg/s)
Luminosity of AT2018dyb
fit with alpha = 9/4
Luminosity (erg/s)
Days since peak
zero
residuals mean = 1.05e+43 , residuals median 1.19e+43
Residuals (erg/s)
Luminosity of AT2018fyk
fit with apha = 0.76 +/- 0.28
Luminosity (erg/s)
Days since peak
Residuals for fit with apha = - 0.76 +/- 0.28
zero
residuals mean = 1.78e+43 , residuals median 2.12e+43
Residuals (erg/s)
Luminosity of AT2018fyk
fit with alpha = 5/3
Luminosity (erg/s)
Days since peak
zero
residuals mean = 1.89e+43 , residuals median 2.63e+43
Residuals (erg/s)
Luminosity of AT2018fyk
fit with alpha = 9/4
Luminosity (erg/s)
Days since peak
zero
residuals mean = 3.03e+43 , residuals median 3.70e+43
Residuals (erg/s)

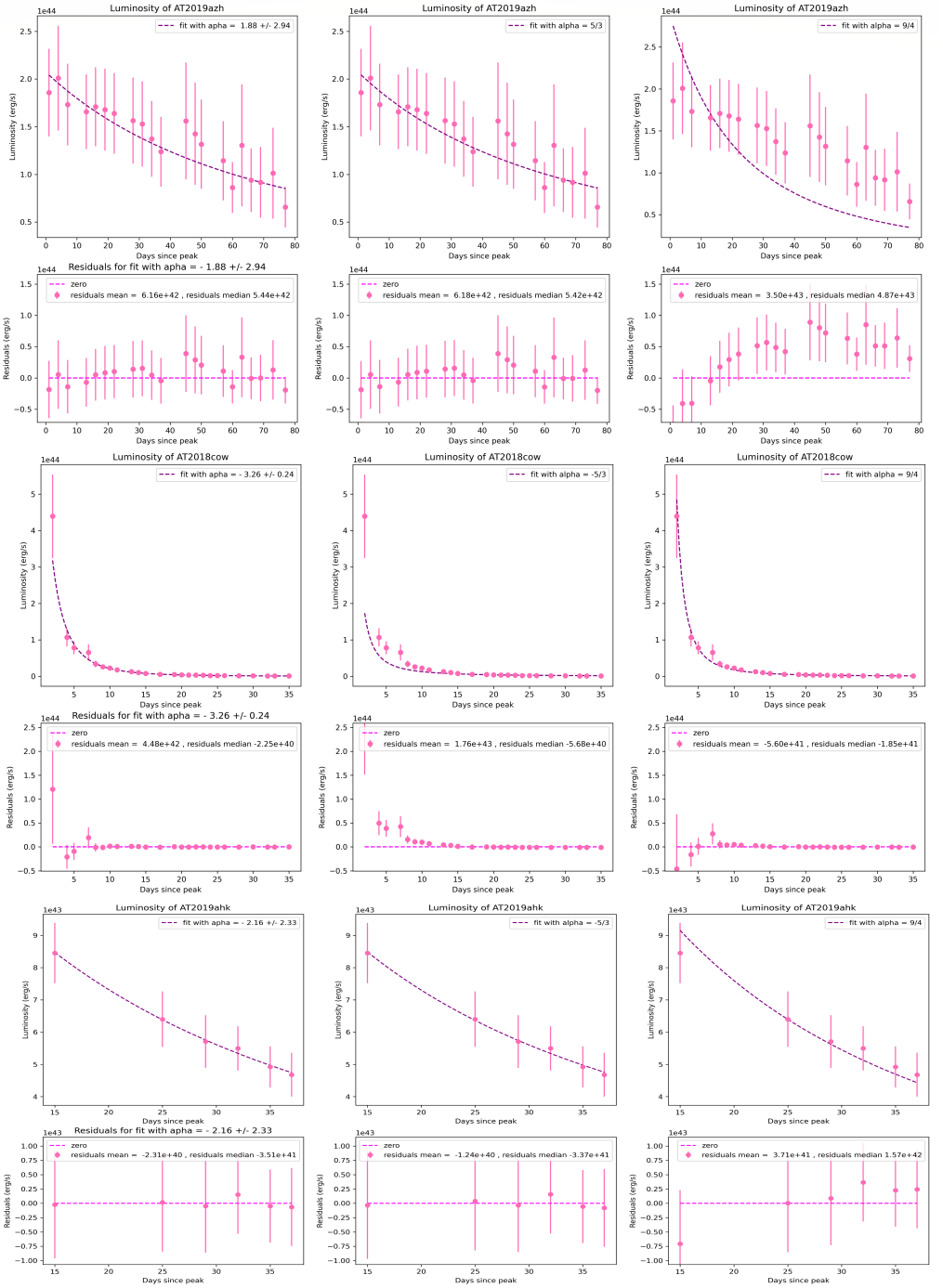
Luminosity of AT2019azh
fit with apha = 1.88 +/- 2.94
fit with alpha = 5/3
fit with alpha = 9/4
Residuals for fit with apha = - 1.88 +/- 2.94
zero
residuals mean = 6.16e+42 , residuals median 5.44e+42
residuals mean = 6.18e+42 , residuals median 5.42e+42
residuals mean = 3.50e+43 , residuals median 4.87e+43
Luminosity of AT2018cow
fit with apha = - 3.26 +/- 0.24
fit with alpha = -5/3
fit with alpha = 9/4
Residuals for fit with apha = - 3.26 +/- 0.24
residuals mean = 4.48e+42 , residuals median -2.25e+40
residuals mean = 1.76e+43 , residuals median -5.68e+40
residuals mean = -5.60e+41 , residuals median -1.85e+41
Luminosity of AT2019ahk
fit with apha = - 2.16 +/- 2.33
fit with alpha = -5/3
fit with alpha = 9/4
Residuals for fit with apha = - 2.16 +/- 2.33
residuals mean = -2.31e+40 , residuals median -3.51e+41
residuals mean = -1.24e+40 , residuals median -3.37e+41
residuals mean = 3.71e+41 , residuals median 1.57e+42
Luminosity (erg/s)
Residuals (erg/s)
Days since peak

Colour evolutions for events in the sample, with B-V (left), U-B (centre) and UVW2-UVW1 (right). In some cases no data remained after percentage error cuts, leaving blank figures

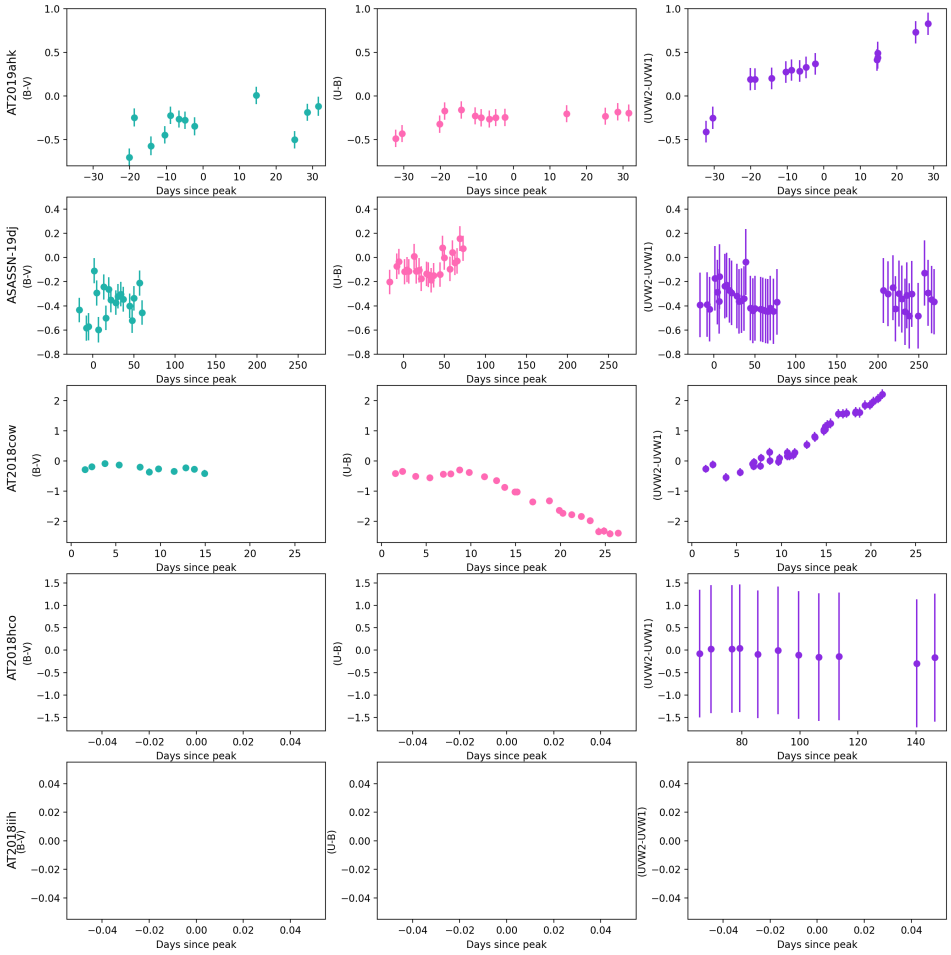

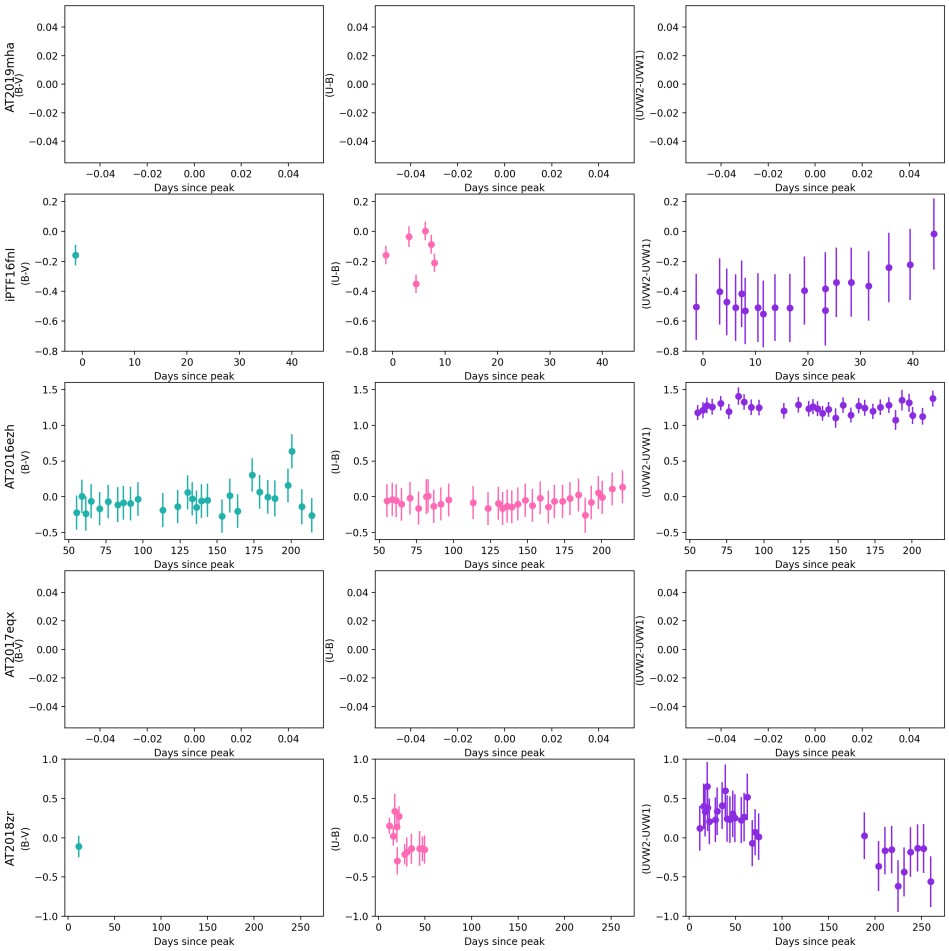
AT2019mha
iPTF16fnl
AT2016ezh
AT2017eqx
AT2018zr
(B-V)
(U-B)
(UVW2-UVW1)
Days since peak

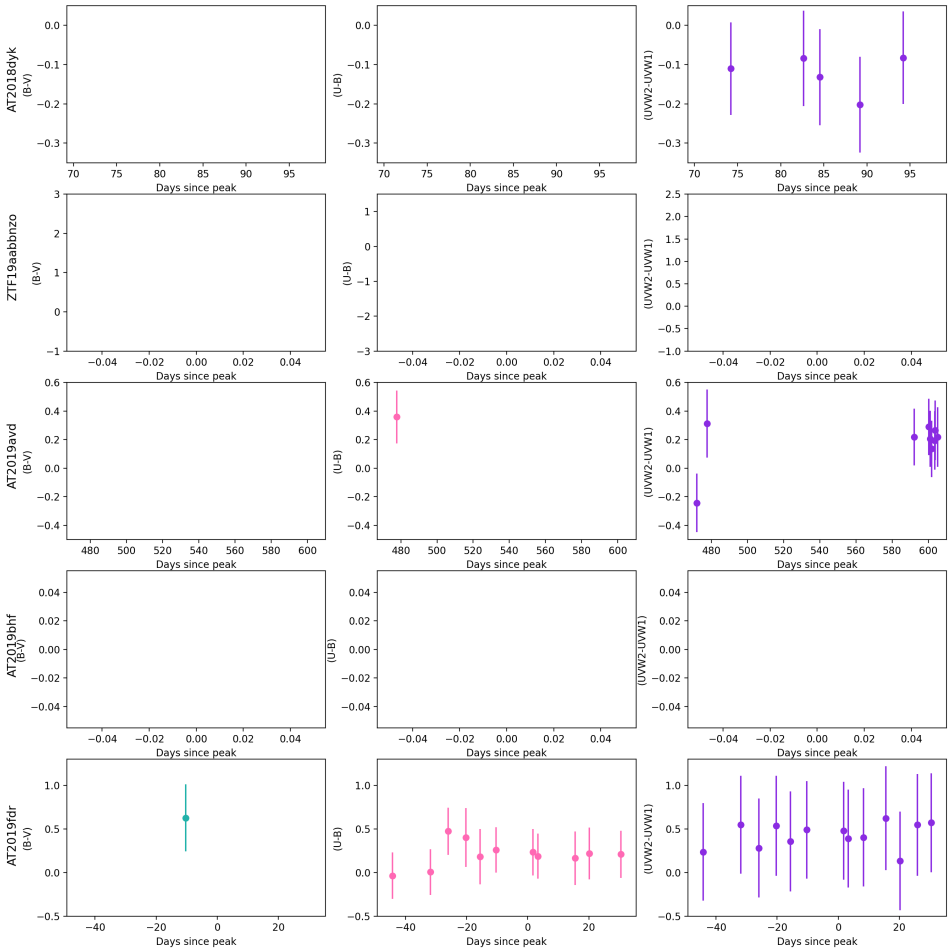
AT2018dyk
ZTF19aabbnzo
AT2019avd
AT2019bhf
AT2019fdr
(B-V)
(U-B)
(UVW2-UVW1)
Days since peak

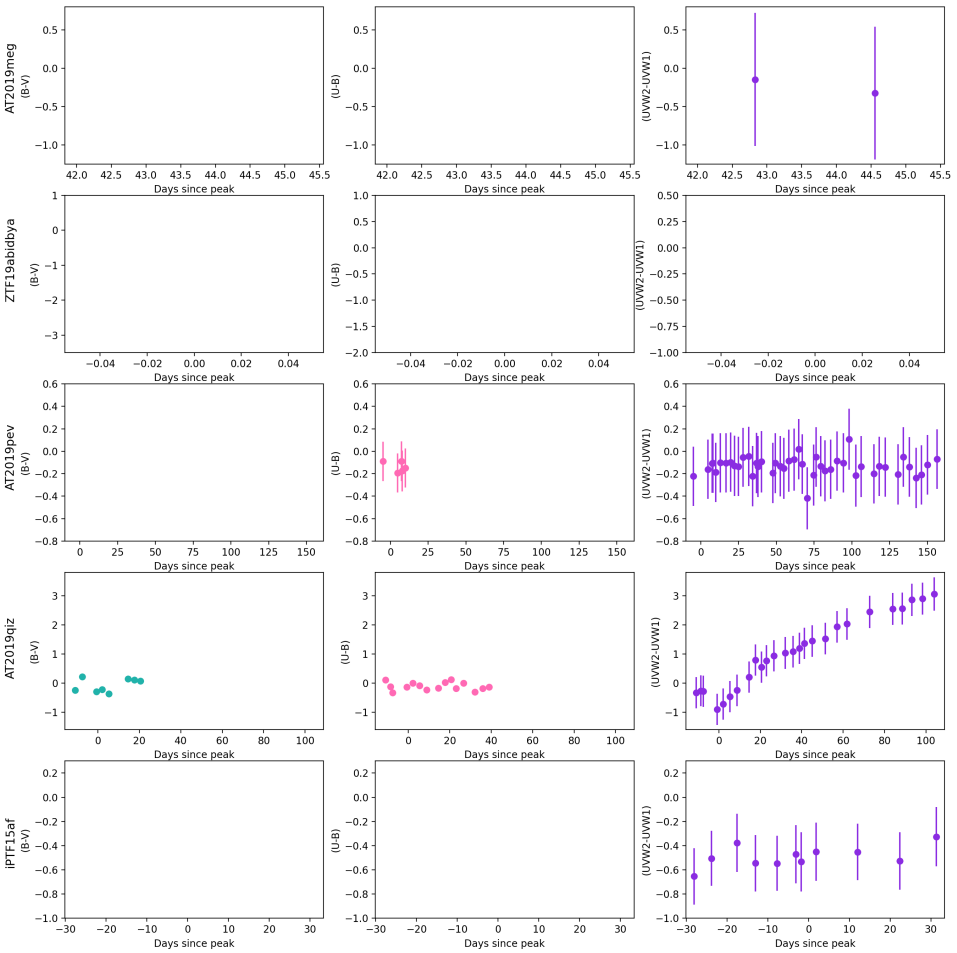
AT2019meg
ZTF19abidbya
AT2019pev
AT2019qiz
iPTF15af
(B-V)
(U-B)
(UVW2-UVW1)
Days since peak

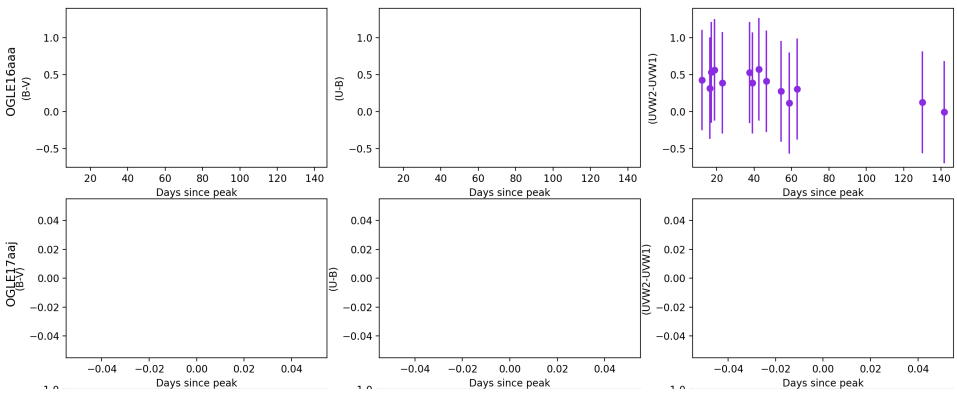
OGLE16aaa
OGLE17aaj
(B-V)
(U-B)
(UVW2-UVW1)
Days since peak

Colour evolution (top) compared with blackbody temperature evolution (bottom) for events in the sample.

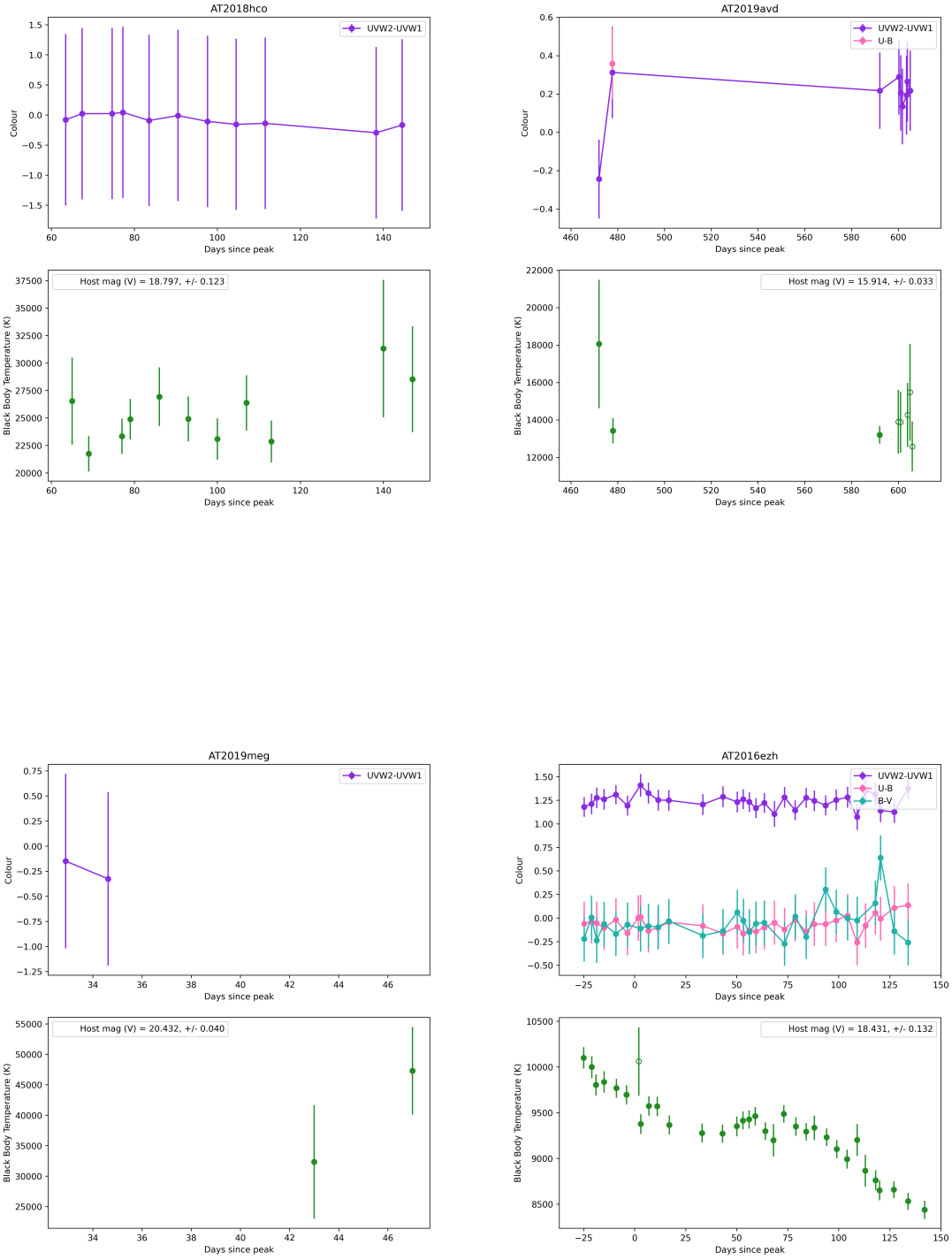

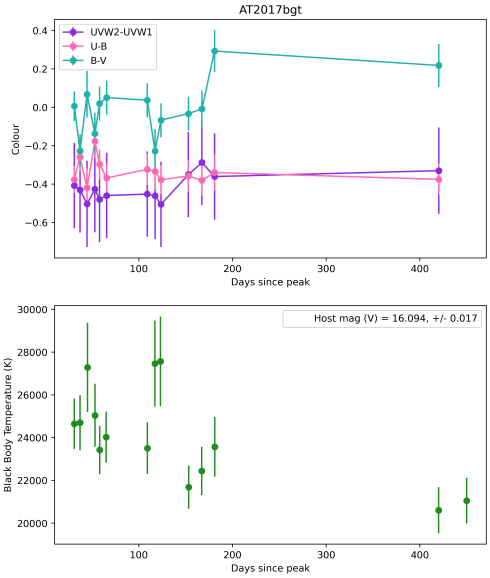
AT2017bgt
UVW2-UVW1
U-B
B-V
Colour
Days since peak
Host mag (V) = 16.094, +/- 0.017
Black Body Temperature (K)
Days since peak

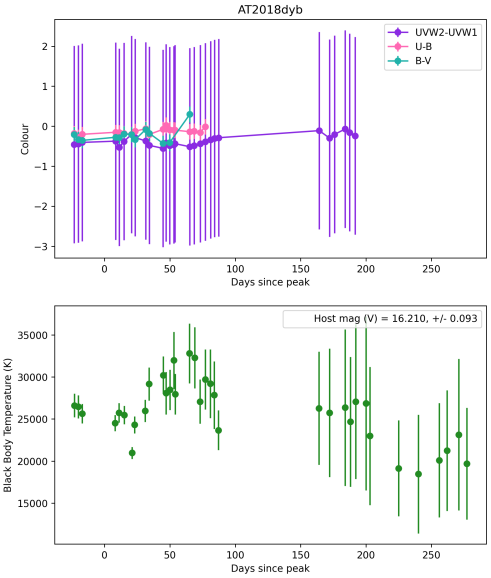
AT2018dyb
UVW2-UVW1
U-B
B-V
Colour
Days since peak
Host mag (V) = 16.210, +/- 0.093
Black Body Temperature (K)
Days since peak

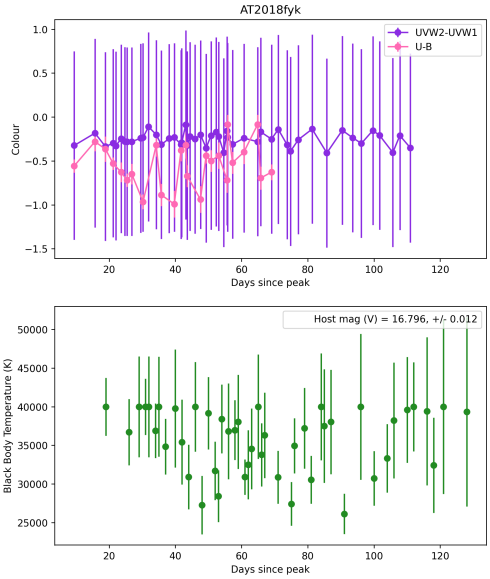
AT2018fyk
UVW2-UVW1
U-B
Colour
Days since peak
Host mag (V) = 16.796, +/- 0.012
Black Body Temperature (K)
Days since peak

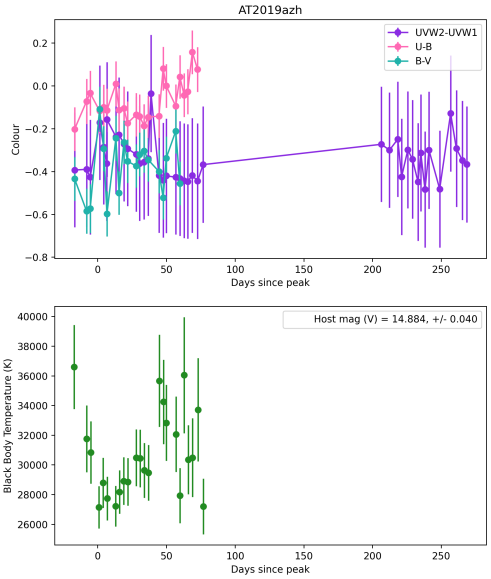
AT2019azh
UVW2-UVW1
U-B
B-V
Colour
Days since peak
Host mag (V) = 14.884, +/- 0.040
Black Body Temperature (K)
Days since peak

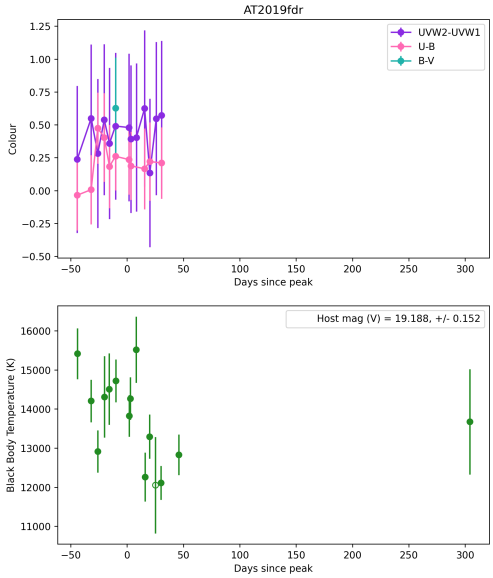
AT2019fdr
UVW2-UVW1
U-B
B-V
Colour
Days since peak
Host mag (V) = 19.188, +/- 0.152
Black Body Temperature (K)
Days since peak

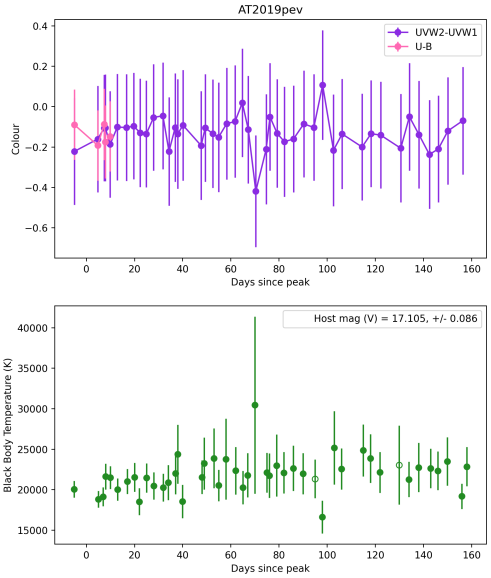
AT2019pev
UVW2-UVW1
U-B
Colour
Days since peak
Host mag (V) = 17.105, +/- 0.086
Black Body Temperature (K)
Days since peak

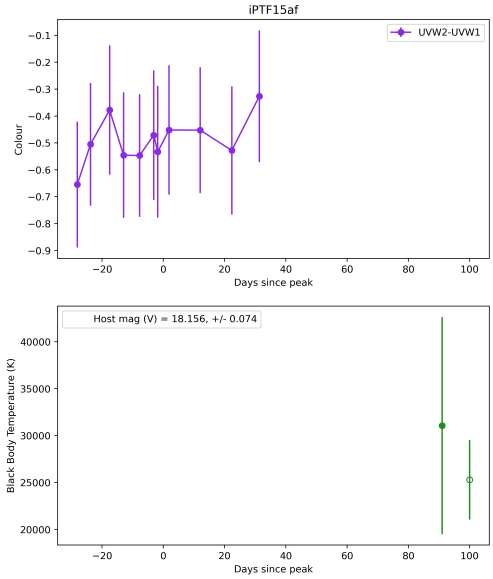
iPTF15af
UVW2-UVW1
Colour
Days since peak
Host mag (V) = 18.156, +/- 0.074
Black Body Temperature (K)
Days since peak

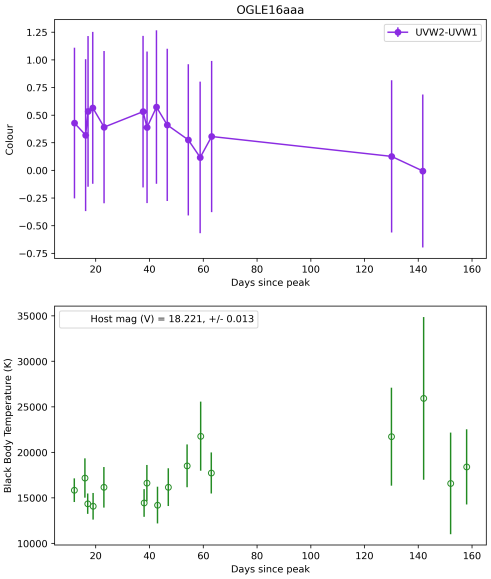
OGLE16aaa
UVW2-UVW1
Colour
Days since peak
Host mag (V) = 18.221, +/- 0.013
Black Body Temperature (K)
Days since peak